A Diagrammatic Theory of Random Knots

by

Harrison Chapman

(Under the Direction of Jason Cantarella)

Abstract

We study random knotting by considering knot and link diagrams as decorated, (rooted) topological maps on spheres and pulling them uniformly from among sets of a given number of vertices n. This model is an exciting new model which captures both the random geometry of space curve models of knotting as well as the ease of computing invariants from diagrams. This model of random knotting is similar to those studied by Diao et al., and Dunfield et al.

We prove that unknot diagrams are asymptotically exponentially rare, an analogue of Sumners and Whittington's result for self-avoiding walks. Our proof uses the same idea: We first show that knot diagrams obey a pattern theorem and exhibit fractal structure. We use a rejection sampling method to present experimental data showing that these asymptotic results occur quickly, and compare parallels to other models of random knots.

We finish by providing a number of extensions to the diagram model. The diagram model can be used to study embedded graph theory, open knot theory, virtual knot theory, and even random knots of fixed type. In this latter scenario, we prove a result still unproven for other models of random knotting. We additionally discuss an alternative method for randomly sampling diagrams via a Markov chain Monte Carlo method.

Index words: Random knots, Knot theory, Random maps, Low dimensional topology, Quantum field theory, Statistical mechanics

A Diagrammatic Theory of Random Knots

by

Harrison Chapman

B.A., Bowdoin College, 2011

M.A., University of Georgia, 2015

A Dissertation Submitted to the Graduate Faculty

of The University of Georgia in Partial Fulfillment

of the

Requirements for the Degree

Doctor of Philosophy

Athens, Georgia

2017

A Diagrammatic Theory of Random Knots

by

Harrison Chapman

Approved:

Major Professor: Jason Cantarella

Committee: David Gay
Daniel Krashen
Michael Usher

Electronic Version Approved:

Suzanne Barbour
Dean of the Graduate School
The University of Georgia
May 2017

Dedication

To Rachel, who brightens each of my days.

Acknowledgements

I am grateful to my advisor Jason Cantarella, for his support and advice throughout my tenure as a graduate student. The quality of this thesis is a direct result of him introducing me to the knot tabulation project and suggesting that I prove the Frisch-Wasserman-Delbrück conjecture. I am extremely fortunate that I have had the opportunity to work with such a wonderful advisor, brilliant mathematician, and exceptional person.

I am also grateful to the summer school on applied combinatorics at the University of Saskatchewan and CanaDAM thereafter, where I was able to meet many experts in combinatorics and random knotting models. I am grateful to Andrew Rechnitzer and his expertise, and his collaboration on the results in Chapter 9.

Throughout my graduate career I have been very fortunate to receive funding from the NSF, PIMS (CRG in Analytic Combinatorics), the Simons Center, and the AMS through which I was able to collaborate with many brilliant mathematicians.

I would like to thank Gary Iliev greatly to alerting me to reference [87], which greatly simplified a number of proofs. I am grateful for conversations with Julien Courtiel, Elizabeth Denne, Chris Soteros, Chaim Even-Zohar, Éric Fusy, Rafał Komendarczyk, Matt Mastin, Neal Madras, Kenneth Millett, Marni Mishna, Erik Panzer, Jason Parsley, Eric Rawdon, Gilles Schaeffer, Paul Zinn-Justin, Chris Manon, Clayton Shonkwiler, Karen Yeats, and Chris Duffy which have aided or otherwise improved the quality of this manuscript. I am grateful to the anonymous referees of my papers who have greatly improved the clarity and correctness of the language therein, and hence here as well.

I owe a great debt to all of my friends—in particular Bret and Hans—thanks to whom these years went by *too* quickly. Lastly, I must thank my family—my sister Kimberly and

parents Craig and Karen—for everything; I owe so much to the love and encouragement which they have provided me throughout my entire life.

Table of Contents

List of Figures

List of Tables

Chapter 1

Overview

The study of *random* knotting arises in numerous areas, principal among which is polymer physics: Polymers (such as DNA or proteins) are considered to be strings in space and in many cases their function (or lack thereof) depends on any "knots" that appear within [98, 85]. The *random diagram model* of random knotting is briefly: Given a number n of crossings, sample uniformly an unlabeled knot diagram with n crossings and return its knot type. It is similar to models of [37] and [39], but these models do not sample from any well-understood measure on spaces of knot diagrams.

In the context of chemistry and bioligy, Frisch and Wasserman [49] and Delbrück [34] independently conjectured;

Conjecture 1.1 (Frisch-Wasserman 1962, Delbrück 1961)**.** *As the size n of a randomly sampled knot grows large, the probability that it is knotted tends to 1.*

The first proof of the conjecture was for n-step self-avoiding lattice polygons, a landmark result by Sumners and Whittington [99] and Pippenger [84]:

Theorem 1.2 (Sumners-Whittington 1988, Pippenger 1989)**.** *As the number of steps n of a self-avoiding lattice polygon grows large, the probability that the polygon is knotted tends to 1 exponentially quickly.*

Shortly thereafter the conjecture was proved in view of other models of space curves: Gaussian random polygons [59], and equilateral random polygons [36]. As new models of random knotting are developed, such as the new Petaluma [41] model of Even-Zohar et al., it is typically a primary goal to prove the analogous result.

The driving goal of the research presented in this manuscript was to show that the Frisch-Wasserman-Delbrück (FWD) conjecture holds in the random diagram model;

Theorem 1.3. *As the number of crossings n of a randomly sampled knot diagram grows large, the probability that the diagram is knotted tends to 1 exponentially quickly.*

We prove this result in Chapter 4. This will follow from a Pattern theorem that expresses the fractal structure of random knot diagrams.

We begin in Chapter 2 with preliminaries on knot theory, random knotting, and relevant combinatorial models. In Chapter 3 we explicitly define knot diagrams and the knot diagram model, and we describe the findings of a census of all such objects of up to 10 crossings from work together with Cantarella and Mastin.

In Chapter 4, we prove a Pattern theorem for knot diagrams. This is done with generality sufficient to extend to many different types of objects. There are two core ingredients for this theorem: 1) A method of "attaching" patterns and 2) some control over the asymptotic number of diagrams involved. This Pattern theorem allows us to confirm the above FWD conjecture for a number of random diagram models. In Chapter 5 we provide experimental data gathered using rejection sampling for the random diagram model and compare numerical results to other models of random knotting.

In the following chapters we examine a variety of different classes of diagrams relating to different aspects of knot theory: Chapter 6 discusses extensions to embedded spatial graph theory, Chapter 7 discusses applications to open knot theory and random knots of fixed type, and Chapter 8 explores generalizations to virtual knot theory. We examine when Pattern theorem results continue to hold—or when they might not, any potential obstructions. In Chapter 9 we present work done together with Rechnitzer on developing a new method of sampling knot diagrams randomly using a Metropolis style Markov chain Monte Carlo algorithm. We prove that this sampler converges to a desired distribution, and examine extensions to varied classes of diagrams.

Chapter 2

Introduction

2.1 Knot Theory

We briefly outline the important concepts of knot theory below. For a more thorough presentation of the theory, see for instance Colin Adams's *The Knot Book* [1].

2.1.1 Basics of Knot Theory

A *knot* is an embedding $K : S^1 \hookrightarrow S^3$ of the circle into the 3-sphere. A *link* is an embedding $L : (S^1)^k \hookrightarrow S^3$ of k circles into the 3-sphere. Each circle in the domain is called a *link component*; knots are simply links with a single component. A knot or link is *oriented* if there is a designated direction around each link component. This definition by itself does not capture the motif that a mathematical knot or link should be analogous physical string or rope. This is resolved through the definition of ambient isotopy.

Definition 2.1. Let N and M be manifolds and let g_0 and g_1 both be embeddings of N into M. An *ambient isotopy* is a smooth map $g : [0,1] \times N \to M$ with the property that,

1. $g|_0 = g_0$,
2. $g|_1 = g_1$, and
3. $g|_t$ is an embedding of N into M for all $t \in [0,1]$.

In knot theory, the notion of equivalence for knots and links is that of ambient isotopy. A *knot type* $[K]$ is the equivalence class of all other knots which are ambient-isotopic to the knot K. Similarly, a *link type* $[L]$ is the equivalence class of all other links who are

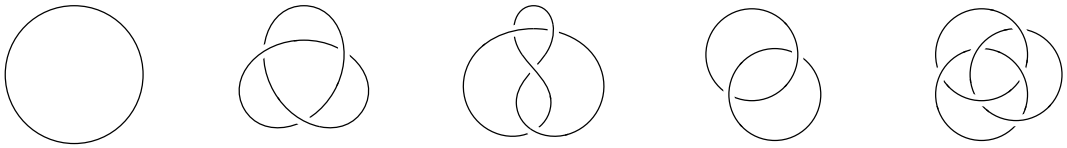

Figure 2.1: Small knots and links. From left to right: Unknot, Trefoil, Figure-Eight Knot, Hopf Link, Boromean Link

ambient-isotopic to L. In this manuscript we will always refer to embeddings K as knots or links and equivalence classes $[K]$ as knot types or link types. For the remainder of this discussion, we will discuss the case of knots. The analogous results and definitions follow for links as well, except where explicitly mentioned.

So far our definitions permit *wild knots*; knots with infinitesimal behavior whose embedding cannot be thickened to an embedded tube. As wild knots are both more difficult to work with and less physically relevant, we will require additionally that all of our knots, links, and ambient isotopies are *smooth* (*i.e.* differentiable maps). The smooth ambient isotopy equivalence essentially says then that two knots are equivalent if one can be moved around in space *without cutting and splicing* and transformed into the other. We will henceforth omit the descriptor "smooth" in these cases, and it should be taken as implied.

Knots which are not wild are *tame*; this descriptor is usually omitted. The field of knot and link types is still vast and varied; the most simple knot type, the *unknot*, is the equivalence class of knots containing a great circle of the ambient S^3. If a knot represents the unknot, it is *trivial*; otherwise, it is *knotted*. Some small knots and links, including the unknot, are given in Figure 2.1.

A beautiful theorem of Reidemester [86] relates the theory of knotting in space to a study of artistic representations of knots called *diagrams*. Informally (we will be far more precise in a following section), a diagram for the knot or link L is a generic projection of L onto

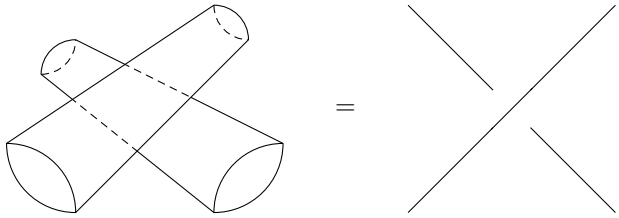

Figure 2.2: A crossing. The solid piece passes over the broken piece, although both portions represent a continuous interval of a larger knot.

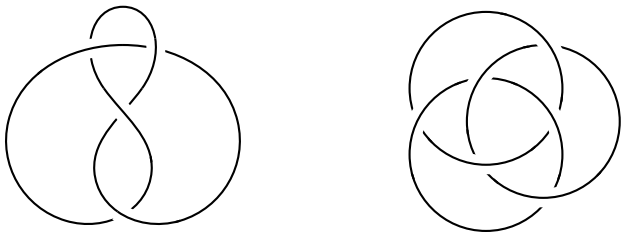

Figure 2.3: A knot diagram (left) and a link diagram (right).

a sphere, except that each double point is drawn as a *crossing* as shown in Figure 2.2 in order to demarcate which piece of the knot is closer to the viewer. Examples of both a knot diagram and a link diagram are given in Figure 2.3.

The embedding of a diagram is insignificant—two diagrams which are related by perturbations which do not introduce new double points or change the local embedding of crossings are equivalent. Reidemeister defined three local moves which act on diagrams called *Reidemeister moves* and are depicted in Figure 2.4. We then have an alternate definition of knot and link type: The *knot* or *link type* of a diagram D is the equivalence class $[D]$ of the diagram under the Reidemeister moves. Reidemeister's theorem says that there is a one-to-one correspondence between types of knots and links in space and types of knot and

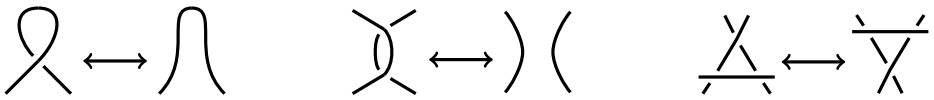

Figure 2.4: The three Reidemeister moves.

link diagrams which is natural in the sense that two knots or links have the same type if and only if any of their diagrams are equivalent up to Reidemeister moves.

The *split link* of two links L_1 and L_2 with ℓ_1 and ℓ_2 respective link components is an embedding $L_1 \cup L_2 : (S^1)^{\ell_1} \times (S^1)^{\ell_2} \hookrightarrow S^3$, so that there exist disjoint balls B_1^3 and $B_2^3 \subset S^3$ so that the image of $L_1 \cup L_2$ contained in B_1^3 is the image of L_1 and the image inside of B_2^3 is L_2. The link type of a split link is independent of the choice of embedding.

Knots have the important composition operation of connect summation. Let K_1, K_2 be two knots in space. Consider their split link $K_1 \cup K_2$. Let $\gamma : [0,1] \times [0,1] \hookrightarrow S^3$ be the embedding of a rectangle whose left side $\gamma|_{x=0}$ maps to a small portion of K_1 and whose right side $\gamma|_{x=1}$ maps to a small portion of K_2. Then the *connect sum* of K_1 and K_2, denoted $K_1 \# K_2$, is the new knot formed by smoothing the curve which starts at $\gamma(0,0)$, traverses $K_1 \setminus \gamma|_{x=0}$ until $\gamma(0,1)$, follows $\gamma|_{y=1}$, traverses $K_2 \setminus \gamma_{x=1}$ until $\gamma(1,0)$, and follows $\gamma|_{y=0}$ to close. The knot type of a connect sum is independent of the choice of rectangle γ.

The connect sum extends to oriented knots (the new curve's orientation must preserve the original orientations of both components), and to links (although the connect summation happens to designated link components of either link). Importantly, connect sum *has no inverses*; there are no two knots (or links) whose connect sum is trivial. Connect sum is associative on knot types, and for knot types connect sum is transitive, *i.e.* $[(K_1 \# K_2) \# K_3] = [K_1 \# (K_2 \# K_3)]$, although this is not necessarily true in the case of links. The connect sum of two links with ℓ_1 and ℓ_2 respective components produces a new link of $\ell_1 + \ell_2 - 1$ components; namely, the connect sum of two knots is always a knot.

It is important for our purposes to consider how knots and links may decompose into pieces. A *k-tangle* is a generic embedding of k closed intervals and any number of closed circles into B^3 so that precisely the $2k$ interval ends all lie in the boundary. A *k-tangle diagram* T is a generic immersion (generic in the same way as knot diagrams above) of k intervals and any number of circles into S^2 together with over-under information at each double point. We will primarily discuss tangle diagrams in which all $2k$ ends of the intervals are all adjacent across some connected component of $S^2 \setminus T$, so that the k-tangle diagram may be viewed as being an immersion into the disk D^2 with exactly the $2k$ interval ends lying in the boundary circle. An *open strand* of a tangle is any one interval; a *closed strand* of a tangle is any one circle.

2.1.2 Identification and Invariants

An important and incredibly difficult problem in knot theory is that of *identification*: How can one determine if two knot types $[K_1]$ and $[K_2]$ are the same? Of course, one could prove this by providing an explicit ambient isotopy equating $[K_1]$ and $[K_2]$. Writing out such an isotopy is often exceedingly tedious, and finding such an isotopy computationally difficult. Rather than find such an isotopy explicitly, the mantra of the knot theorist is to use *knot* or *link invariants*—properties of knots and links which are invariant under ambient isotopy—to identify and distinguish knot types.

A simple and important invariant is the minimal crossing number. Let $[L]$ be a knot or link type and let D be a diagram in $[L]$. Then the *crossing number* $\mathrm{cr}(D)$ of the diagram D is the number of crossings in D. The *minimal crossing number* (sometimes just *crossing number* when it is unambiguous) $\mathrm{cr}([L])$ of $[L]$ is the minimum $\min_{[D]=[L]} \mathrm{cr}(D)$ over all diagrams D for the type $[L]$.

The minimal crossing number is difficult to compute (there are an infinite number of diagrams for any given knot or link type to minimize over) but plays an important role in the naming of small knots and links. Rolfsen's Knots and Links [90] contains a table of all

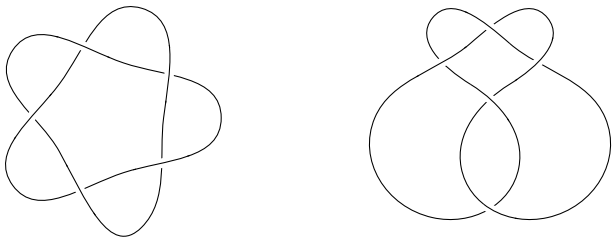

Figure 2.5: The knots 5_1 and 5_2 are different but have the same minimal crossing number.

knots[1] named in the format,

$$[\text{minimal crossing number}]_{[\text{index}]},$$

where for each minimal crossing number, the index starts from 1. Links and knots of higher minimal crossing number have been tabulated similarly by Thistlethwaite [100] and later by others including Hoste et al. [54].

Under this convention, the unknot has name 0_1, the trefoil has name 3_1, and the figure-eight knot has name 4_1. As there are two different knots with minimal crossing number 5, 5_1 and 5_2 shown in Figure 2.5, minimal crossing number alone is insufficient to uniquely identify the type of a knot or link. Typically, knot and link tables only list knot and link types $[L]$ which are *prime* in that there are no two types $[L_1]$ and $[L_2]$ for which $[L] = [L_1 \# L_2]$. Knots and links which are not prime are *composite*. All knot types have a unique *prime decomposition* into prime knot types under connect sum.

An invariant which is both better (although not perfect) at identifying knots as well as easier to compute is the HOMFLY polynomial [48]. The *HOMFLY polynomial* $\mathrm{H}([L])$ of an *oriented* knot or link type $[L]$ is a Laurent polynomial in variables a, z defined recursively by

[1]Rolfsen's table actually double-counts: Perko [83] noticed that Rolfsen's knots 10_{161} and 10_{162} are actually equivalent. Some tables omit 10_{162} entirely, while others downshift the index for knots 10_{163}–10_{166}.

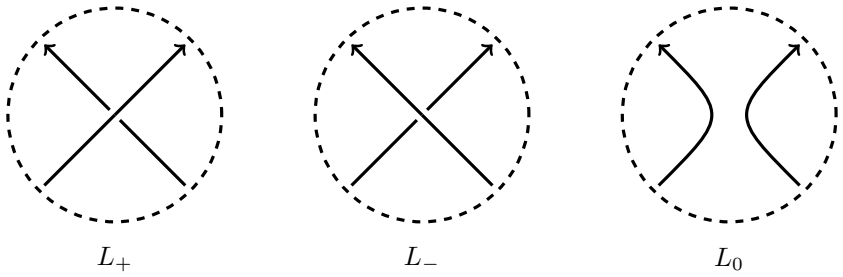

Figure 2.6: Definitions of terms in the HOMFLY skein relation equation.

base case

$$\mathrm{H}(0_1) = 1,$$

and the *skein relation*,

$$a\,\mathrm{H}(L_+) - a^{-1}\,\mathrm{H}(L_-) = \mathrm{H}(L_0),$$

where L_+, L_-, and L_0 are diagrams which differ from a diagram L of $[L]$ locally with some designated crossing either signed positively, negatively, or smoothed as defined in Figure 2.6.

Although the HOMFLY polynomial is defined for oriented links, this is immaterial in the case of unoriented knots; either orientation of a knot type $[K]$ produces the same HOMFLY polynomial. This is not the case for unoriented links, and by considering all orientations of link components of an unoriented link type $[L]$, one can find a spectrum of different HOMFLY polynomials for $[L]$.

It is incredibly useful that, unlike invariants like the minimal crossing number, the HOMFLY polynomial can be computed from a single diagram representation of a knot or link. As a result, it is possible to compute HOMFLY polynomials for knots and links with relative ease through software [42]. The HOMFLY polynomial is not alone in this computational convenience. In fact, it generalizes two other polynomials—the Alexander polynomial [4] and the Jones polynomial [62]—which can be computed similarly using a recursive skein relation.

The HOMFLY polynomial cannot alone distinguish knots. For instance, $\mathrm{H}(5_1) = \mathrm{H}(10_{132})$ and $\mathrm{H}(10_{25}) = \mathrm{H}(10_{56})$. However, it is yet an open question of whether the unknot the

only knot with trivial (*i.e.*, 1) HOMFLY polynomial. The conjecture to the affirmative is a generalization of the *Jones Conjecture*. Recently, the conjecture has been confirmed for all knot types up to 22 crossings by Sikora et al. [106]. The Jones Conjecture is *false* in the case of links: There exist relatively small nontrivial links with HOMFLY polynomial 1.

2.2 Combinatorial Classes and Generating Functions

We will use some of the language and tools of combinatorics in formalizing the material of this manuscript. Further information and numerous examples can be found in, for example, Flajolet and Sedgewick's *Analytic Combinatorics* [44].

Definition 2.2. A *(combinatorial) class* $\mathcal{A}$ is a finite or countable set of objects on which a size function is defined, so that

1. The size of any object is non-negative, and
2. The number of objects of any fixed size is finite.

There are some conventions for notation when dealing with classes. If $\mathcal{A}$ is a class, then $\mathcal{A}_n$ denotes the objects in $\mathcal{A}$ of size n. The number of objects of size n, $|\mathcal{A}_n|$, is denoted in lower case, as a_n. The size function is denoted as $|\cdot|$.

A critical tool for working with combinatorial classes is the generating function:

Definition 2.3. The *(ordinary) generating function* (OGF) for a class $\mathcal{A}$ is the formal power series,

$$A(z) = \sum_{n=0}^{\infty} a_n z^n.$$

Equivalently, the ordinary generating function for a class $\mathcal{A}$ can be expressed,

$$A(z) = \sum_{a \in \mathcal{A}} z^{|a|}.$$

The standard notation for generating functions is that, for calligraphic- or script-named classes $\mathcal{A}$, the generating function is denoted by the roman A. Generating functions contain

all the information of a sequence (in this case, the sequence of counts $\{a_n\}$) in the form of a function. This has many advantages, but most important to this manuscript is the close relationship between the *asymptotic growth* of a class and the *radius of convergence* of its generating function:

Theorem 2.1 (Cauchy 1821 [23], Hadamard 1888 [50])**.** *The radius of convergence ρ of a series $A(z) = \sum_n a_n z^n$ is given by,*

$$\frac{1}{\rho} = \limsup_{n\to\infty} |a_n|^{1/n}.$$

The generating function has an important connection to the *partition function* in statistical mechanics [67]. If for $a \in |\mathcal{A}|$ we view the size $|a|$ as the total energy E_a of the object a, and if we make the substitution $z = e^{-\beta}$ (where β corresponds in some manner to thermodynamic energy), then we recover an expression for a partition function;

$$A(e^{-\beta}) = \sum_{a\in\mathcal{A}} e^{-\beta E_a}.$$

2.3 Random knotting

Knots and links arise naturally in biology, chemistry, and physics. There are many interesting applications [61], although perhaps the most obvious application is whenever something acts like a rope or string. A critical recurring example of this are *polymers*, long molecular chains built as a sequence of small pieces called *monomers*.

Example. *Deoxyribonucleic acid* or *DNA* is a long, double-helical polymer formed out of base pairs of nucleotides—cytosine (C) and guanine (G), and adenine (A) and thymine (T). In most organisms and some viruses, DNA carries genetic data which is *transcribed* (read) during the synthesis of materials by biological machines called enzymes.

In bacteria, DNA takes the shape of a closed topological circle which can exhibit true topological knotting. In more complicated organisms, DNA is a long open strand. In either case, any "knotting" [18, 8, 31, 92, 101] which occurs may disrupt or otherwise affect DNA's primary duties or its duplication during *cellular division*.

Example. A *protein* is a long polymer formed out of amino acids. Proteins serve an array of purposes in living organisms, including working as machines called *enzymes* which manipulate molecules and catalyze reactions inside cells. After creation, proteins are carefully folded into different shapes (potentially even "knotted" [85, 57, 79, 33, 70]) which are essential to their functionality.

Example. There are a large number of polymers which arise elsewhere in chemistry. This includes natural polymers—such as silk, shellac, rubber, amber, and cotton—and synthetic polymers—such as nylon, neoprene, and polystyrene [77]. Knotting or lack thereof can affect the configuration space or structural integrity of any such polymers.

As knotting is integral to our understanding of polymers and similar objects, mathematicians have devised models for the study of such *physical knots*. A key theme throughout all models is that these knots have some *geometry* in addition to their topology. Indeed, one cannot necessarily presume that a molecule is "infinitely flexible" or "infinitesimally thin;" introducing geometry provides an access point for incorporating these properties. The geometry then induces a *probability distribution* on knots and knot types, so we call this scenario *random knot theory*.

There are many such models for studying random knots, including random Grassmannian space polygons [22, 21], random Chebychev polynomials [27], random braid words [80], and Even-Zohar et al.'s *Petaluma* [41] model. A classical, simple, and highly relevant such model is that of self-avoiding polygons, which we now define.

2.3.1 Self-avoiding polygons

Let Λ be a lattice with a basepoint O and a set S of nonzero vectors in Λ. We will primarily consider the hypercubic lattices $\mathbb{Z}^d$ (specifically $d = 2, 3$) with basepoint the origin $O = \vec{0}$ and S the set of unit vectors $\pm e_i$). A *random walk* [71] on Λ of n steps in S is a sequence of $n+1$ points $W = (\omega_0, \omega_1, \ldots, \omega_n)$ such that $\omega_0 = O$, and $\omega_{i-1} - \omega_i \in S$ for all $1 \leq i \leq n$. A random walk is *self-avoiding* if furthermore $\omega_i \neq \omega_j$ for all $i \neq j$. When the lattice is $\mathbb{Z}^d$ and

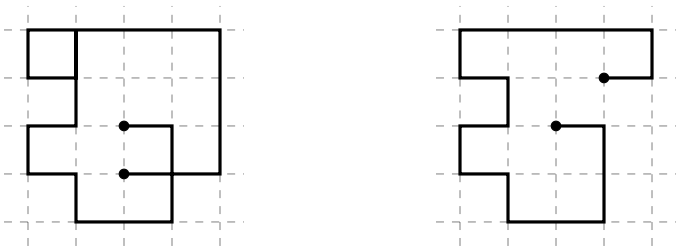

Figure 2.7: An example of a random walk and a self-avoiding walk on $\mathbb{Z}^2$.

S is the set of unit vectors, we will call these objects *random walks on the integer lattice* or *self-avoiding walks on the integer lattice* respectively. An example of a random walk and a self-avoiding walk on $\mathbb{Z}^2$ is given in Figure 2.7.

Although it is a combinatorial object defined rather simply, there are neither *closed formulas* nor *precise asymptotic growth rates* for the counts of self-avoiding walks on the lattices $\mathbb{Z}^d$ for $d = 2, 3$. It is simple to work with self-avoiding walks on computers, but the "long-term memory" condition of self-avoidingness and the exponential rate at which the number of self-avoiding walks grows makes exact enumeration and even computational tabulation difficult or space-intensive. Nevertheless, it is conjectured that the asymptotic growth behavior of the number of self avoiding walks of n steps, c_n, behaves like,

$$c_n \underset{n\to\infty}{\sim} A\mu^n n^{\gamma-1}. \tag{2.1}$$

This is a type of behavior which is exhibited by a large number of combinatorial models [44], including some which are solved exactly. The number μ is called the *connective constant* for the lattice Λ, and γ is a *critical exponent*. Although this behavior is unproven, it *is* known that the connective constant

$$\mu = \lim_{n\to\infty} (c_n)^{1/n}$$

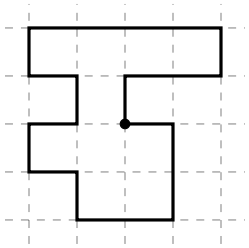

Figure 2.8: An example of a self-avoiding polygon on $\mathbb{Z}^2$.

exists for the hypercubic lattices $\mathbb{Z}^d$, and estimates are known numerically. Existence of μ is important to a number of results on self-avoiding walks; we will have a similar requirement for random diagrams.

Points in self-avoiding walks are referred to as *sites*, and edges between points *(nearest-neighbor) bonds*. It is easy to see how self-avoiding walks model polymers: Each site corresponds to a monomer in the larger chain, and each bond corresponds to a (chemical) bond between monomers in the molecule. That polymers are not infinitely flexible is represented in that all bonds are of unit (or otherwise bounded) length. That polymers are not infinitesimally thin is modeled in that the walk cannot intersect with itself, much like a physical piece of rope.

A self-avoiding walk in $\mathbb{Z}^3$ may be viewed as a specific embedding of an interval into S^3; to arrive at knot theory proper, we need the notion of a closed loop. This is a self-avoiding polygon. A *self-avoiding polygon* in a lattice Λ with n steps in S is a self-avoiding walk $P = (p_0, p_1, \ldots, p_n)$ which is self-avoiding *except* for that $p_n = p_0$ (the degenerate case where $n = 2$ and the polygon steps out and backtracks is forbidden). An example of a self-avoiding polygon on $\mathbb{Z}^2$ is given in Figure 2.8. Hence, a self-avoiding polygon has the topology of a circle rather than an interval. Notice that in the case of $\mathbb{Z}^d$, a self-avoiding polygon necessarily has an even number of steps.

Much like the case of self-avoiding walks, it is conjectured but unproven that the asymptotic behavior of the counts g_n of self-avoiding polygons of n steps is

$$g_n \underset{n\to\infty}{\sim} B\mu^n n^{\alpha-1}. \tag{2.2}$$

It is known that the connective constant μ exists; in fact, it is a result of Hammersley [51] that for the (hyper-)cubic lattices the connective constant is identical to that of self avoiding walks.

A self-avoiding polygon in $\mathbb{Z}^3$ has the topology of a circle S^1 in the space S^3. Hence, we can associate to any self-avoiding polygon P a knot type $[P]$. Let $g_n([K])$ be the number of self-avoiding polygons of n steps representing the knot type $[K]$. For every fixed n this defines a probability distribution on knot types $[K]$:

$$\mathbb{P}([K]) = \frac{g_n([K])}{g_n}.$$

This is the *self-avoiding polygon model of random knotting.*

2.3.2 Pattern theorems and the Frisch-Wasserman-Delbrück Conjecture

In the context of chemical and DNA topology, Frisch and Wasserman [49] and Delbrück [34] independently conjectured;

Conjecture 2.2 (Frisch-Wasserman 1962, Delbrück 1961)**.** *As the number of steps n of a random self-avoiding polygon grows large, the probability that it is knotted (that is, does not represent the knot type 0_1) tends to 1. Conversely,*

$$\lim_{n\to\infty} \frac{g_n(0_1)}{g_n} = 0.$$

This conjecture remained unproven for nearly three decades until 1988 when Sumners and Whittington [99] and Pippenger [84] independently proved it as a theorem. Their proofs rely on a key tool: A pattern theorem for self-avoiding polygons, which dictates that self-avoiding polygons exhibit fractal structure, and contain desired sub-patterns often with high probability.

A *pattern* is a finite sub-walk inside of a self-avoiding walk or polygon [87]. A pattern $S = (s_0, s_1, \ldots, s_k)$ occurs at the i-th vertex of a walk $W = (\omega_0, \omega_1, \ldots, \omega_n)$ if there exists some vector $\vec{v} \in \Lambda$ so that $\omega_{i+\ell} - s_\ell = \vec{v}$ for all $0 \leq \ell \leq k$. A pattern occurs m times in W if there exist m distinct indices i and vectors $\vec{v}$ at which S occurs in W.

Not every pattern can occur in certain walks, and some patterns which can occur still cannot occur multiple times. For a class of walks or polygons, call a pattern S *proper* if for every m there exists a walk (or polygon) for which S occurs at least m times.

Theorem 2.3 (Kesten's Pattern Theorem [65, 64])**.** *Let S be a proper pattern and let $c_n[m, S]$ and $g_n[m, S]$ denote the number of self-avoiding walks or polygons of n steps for which S occurs at no more than m different indices. Then there exists an $a > 0$ and a $b > 0$ so that*

$$\limsup_{n\to\infty} (c_n[an, S])^{1/n} < \mu \quad \textit{and} \quad \limsup_{n\to\infty} (g_n[bn, S])^{1/n} < \mu,$$

where μ is the connective constant of the lattice.

Sumners and Whittington's key observation then was that there exist proper patterns whose inclusion guarantees nontrivial knotting. While there are a large class of such patterns, the tight trefoil pattern T in Figure 2.9 is sufficient: Any polygon P who contains the pattern T is guaranteed to have the knot type 3_1 in the prime decomposition of its knot type $[P]$.

This method of proof by pattern theorem was a breakthrough in the study of random knotting. Shortly afterwards, the method of proof was extended and applied to other models including random equilateral polygons by Diao [36] and random Gaussian polygons by Jungreis [59]. As it is then so ubiquitous, one might first expect to show that any alternative model of random knotting satisfies the FWD conjecture.

2.4 Meanders

We will also find inspiration in another unsolved (*i.e.* uncounted) combinatorial model; meanders. Meanders can be defined simply, but have proven difficult to understand fully due to another "long-term memory" condition.

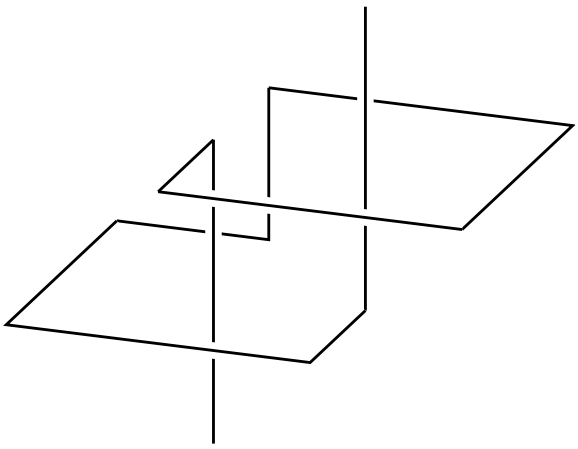

Figure 2.9: A tight trefoil proper pattern T.

Definition 2.4. Given an oriented line L in $\mathbb{R}^2$, a *meander* of size n is a homeomorphism class of curves in $\mathbb{R}^2$ which 1) have no self-intersections and 2) intersect the line L precisely $2n$ times.

An example of a meander is given in Figure 2.10. Although meanders do not exhibit knotting in the same sense as self-avoiding polygons, they are a useful model of polymers. Namely, meanders are a useful model for studying polymers which fold in on themselves [46] such as RNA [52, 5]. Meanders are hence an interesting model in their own right.

We have an alternate definition for a meander in terms of permutations of $2n$ called non-crossing perfect matchings: A meander is a pair (α_1, α_2) of permutations so that

1. α_i is a product of n disjoint cycle permutations of length 2 for each i (the α_i are *perfect matchings*),

2. no two cycles $(ab), (cd)$ in α_i interlace; *i.e.* if we assume without loss of generality that $a < b$, $a < c$, and $c < d$ then exactly one of $a < b < c < d$ or $a < c < d < b$ (so that $a < c < b < d$ is forbidden; each α_i is *non-crossing*), and

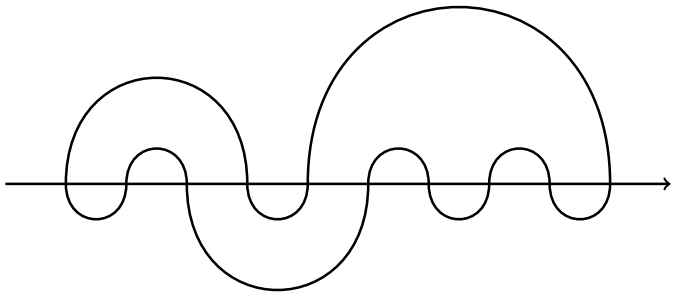

Figure 2.10: A meander of size 5 given by the pair of non-crossing perfect matchings $(\alpha_1, \alpha_2) = ((14)(23)(5\ 10)(67)(89), (12)(36)(45)(78)(9\ 10))$.

3. the product permutation $\alpha_2 \circ \alpha_1$ is a cyclic permutation of 2 disjoint cycles each of length n (the meander is *connected*).

It is simple to sample a pair of permutations satisfying properties (1) and (2); such permutations are in bijection with Dyck words [97] and counted by the Catalan numbers. Given those, however, it is still difficult to impose property (3). This mirrors the case of self-avoiding walks—it is easy to sample random walks but difficult to impose non-self-intersection. These properties are "global" in the sense that one cannot ascertain whether an object satisfies them using local information alone. They hence make understanding the models far more difficult.

As a result, there is not yet a closed formula for the counts m_n of meanders of size n. This parallels the case of self-avoiding walks and polygons above. In fact, the asymptotic growth of the counts m_n is strikingly similar [47];

$$m_n \underset{n\to\infty}{\sim} C(R^2)^n n^{-\alpha}.$$

Similarly, exact values of R^2 and α are unknown: Numerical experiments estimate that $R^2 \approx 12.262874$ and quantum field theory arguments predict that $\alpha = \sqrt{29}\frac{\sqrt{29}+\sqrt{5}}{12}$ [47] (this exact value of α has been numerically checked [35] to a significant degree), but there is not yet a concrete proof.

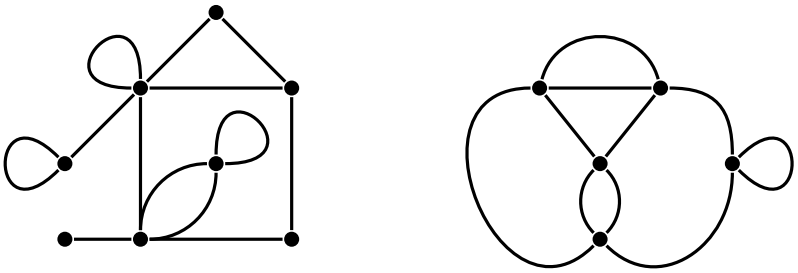

Figure 2.11: Two planar maps. The map on the right is 4-valent.

2.5 Topological maps

The goal of this manuscript is foremost to present the random diagram model as a model for random knotting. This requires first that we formalize key notions about knot and link diagrams previously defined loosely. The equivalence on diagrams that we imposed earlier is precisely *embedded graph isomorphism*. This precisely means that the viewpoint we should have is that of *topological maps* on surfaces [105, 16, 68].

2.5.1 Maps

Definition 2.5. A *map with n vertices* M is a (multi-)graph $\Gamma(M)$ with n vertices embedded on a surface Σ so that every connected component of $\Sigma \setminus M$ is a topological disk. The connected components of $\Sigma \setminus M$ are called the *faces* of M. If Σ is the oriented sphere, then the map M is *planar*. As each face must be a disk, maps' underlying graphs are necessarily connected.

A map M is *4-valent* (sometimes also called *4-regular* or *quartic*) if every vertex in the underlying graph $\Gamma(M)$ has degree 4. An example of a planar map and a 4-valent planar map can be seen in Figure 2.11

In the literature, maps are also known as cyclic graphs [13], fatgraphs [74], fat graphs [45], and ribbon graphs [14]. Maps find use as a critical tool for studying many topics, including;

quantum mechanics [16], quantum field theory [108], moduli spaces of Riemann surfaces [74], fiber bundles over Riemann surfaces [72], and random surfaces and metrics [40]. As a result, maps have a rich theory—although there is still much yet unknown.

A map with n vertices decomposes as a triple $M = (A, E, V)$ called a *combinatorial map* [28] or an *arc-decomposition* into arcs, edges, and vertices, where A consists of *arcs* (sometimes called *flags*[2]), E consists of unordered pairs of arcs (the edges), and V consists of n cyclic quadruples of arcs (the vertices), up to re-naming of arcs, so that each arc appears in exactly *one* edge and *one* vertex. Maps are the same if they differ only by changing the set A (re-indexing). These data define the embedding of a graph into a surface; the map is planar if this surface is the sphere. If a is an arc in M, define $e(a)$ to be the unique edge containing a and $v(a)$ to be the unique vertex which contains a. If the map is 4-valent, there are precisely $4n$ arcs and $2n$ edges.

The set of edges E and vertices V of a map M can both be viewed as permutations acting on the arcs A. E is a product of disjoint transpositions of arcs. V is a product of n disjoint cyclic permutations of arcs, each of whom permute their arcs counterclockwise. Under this view, the permutation $F = V \circ E$ consists of the faces of M; it is a product of disjoint cyclic permutations, where each cycle permutes the arcs around each given face clockwise. As a map is a CW-complex structure for its embedding surface Σ, we have the relationship between Euler characteristic $\chi(\Sigma)$ and the counts of vertices, edges, and faces;

$$\chi(\Sigma) = |V| - |E| + |F|.$$

Namely, a map which is 4-valent and planar will have precisely $n+2$ faces. Figure 2.12 depicts a 4-valent planar map with

$$E = (0\ 1)(2\ 3)(4\ 5)(6\ 7)(8\ 9)(10\ 11)(12\ 13)(14\ 15),$$

$$V = (0\ 10\ 15\ 9)(1\ 8\ 2\ 7)(3\ 14\ 4\ 13)(5\ 11\ 6\ 12),$$

[2]The notation of flag indicates that arcs belong to a unique vertex, edge, and face.

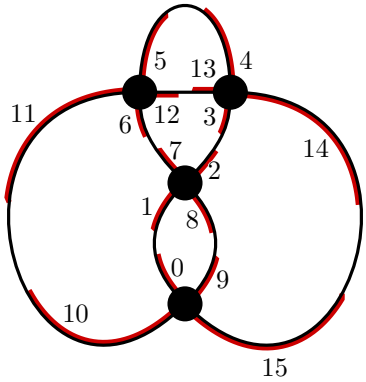

Figure 2.12: A planar map with its arcs labeled.

and

$$F = V \circ E = (0\ 8)(1\ 10\ 6)(2\ 14\ 9)(3\ 7\ 12)(4\ 11\ 15)(5\ 13).$$

We will primarily consider planar maps, although by considering maps on any oriented surface of arbitrary genus and applying the ideas of this work one arrives at the study of *virtual* diagrams [115, 63]. We discuss extensions to the virtual theory in Chapter 8.

Symmetry complicates the study of maps. A strategy to avoid this issue is to *root* the map by picking and directing a single edge:

Definition 2.6. A *rooted map* is a map together with a single edge marked with a direction, called a *root edge*. Equivalently, it is a map together with a marked arc, called a *root arc*.

Example rootings of each of the maps from Figure 2.11 are depicted in Figure 2.13.

An automorphism of a rooted map M would be required to fix the root edge, its direction, and the orientation of the surface near the root; hence $\mathrm{aut}(M)$ is the trivial group. In the $M = (A, E, V)$ arc-decomposition, a rooting of M is a pair (M, a) of M with an arc a. We will assume our maps are rooted.

Maps M have a well defined notion of *dual map* M^*, where there is an edge $(f_1, f_2) \in M^*$ if the face f_1 is adjacent to the face f_2 in M (faces are adjacent if they share an edge along their

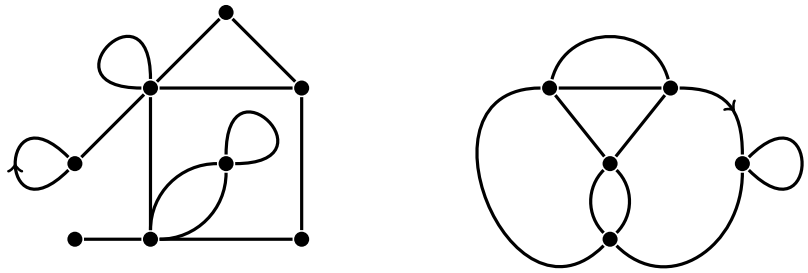

Figure 2.13: Two rooted planar maps. The map on the right is in the class of rooted knot shadows.

boundaries). This definition guarantees a bijection between the vertices of M and the faces of M^*. Given the arc-decomposition (A, E, V) of M, the dual map M^* has decomposition $(A, E, (V \circ E)^{-1})$ (the inverse is to account for face permutations in $V \circ E = F$ permuting arcs in clockwise order, while vertices should permute arcs in counterclockwise order). The dual map of a 4-regular map is a *quadrangulation*, *i.e.* a map for which the boundary of every face is a cycle of four edges. A quadrangulation is *simple* if it contains no parallel edges or loop edges (its underlying graph is simple). If a map is rooted with root arc a, so too is its dual with the same root arc a.

Much like self-avoiding walks and polygons, maps have a notion of substructure:

Definition 2.7. A map P with a marked face of k-edges is a *submap* of a map M if there exists a cycle of k edges (the cycle may repeat edges) in M so that one of the two halves of M separated by the cycle is identical to P.

An example of a submap is given in Figure 2.14. Submaps will be the crucial ingredient in our pattern theorem for diagrams.

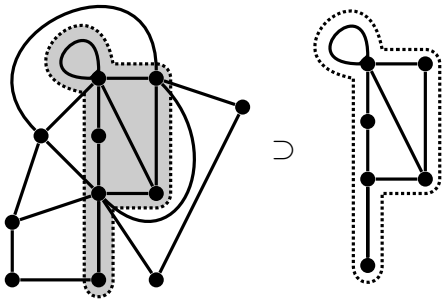

Figure 2.14: The map with marked boundary on the right is contained in the map on the left.

2.5.2 Schaeffer's bijection with trees

Surprisingly many classes of maps admit bijections to classes of trees [93, 12, 25, 3]. Much is known about classes of trees; in many cases they are exactly counted and easy to sample uniformly. An important type of tree which is used in the enumeration of degree-restricted maps (such as the 4-valent maps which we will consider in the following sections) is that of a blossom tree.

Definition 2.8. A k-valent *blossom tree* with n nodes is a rooted, embedded tree with three types of vertices:

1. *Leaves*, who have no children,
2. *Buds*, who have no children and are different from leaves, and
3. *Nodes*, who each have k children who may be either leaves or nodes, and precisely 1 additional bud child.

Buds are denoted pictorially by loose edges, and leaves by hollow arrowheads. In order to study 4-valent maps, we will take $k = 2$ (in general, to study $2m$-valent maps one takes $k = 2m - 2$). An example of a blossom tree is given in Figure 2.15. Such 2-valent, or *binary* blossom trees admit a simple *recursive specification*; if, for any number of nodes

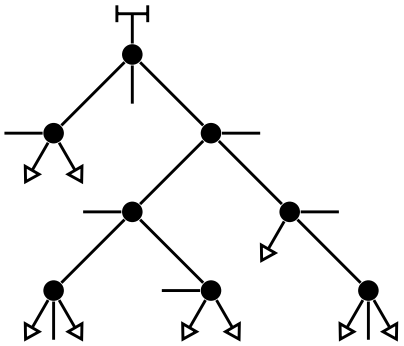

Figure 2.15: A blossom tree.

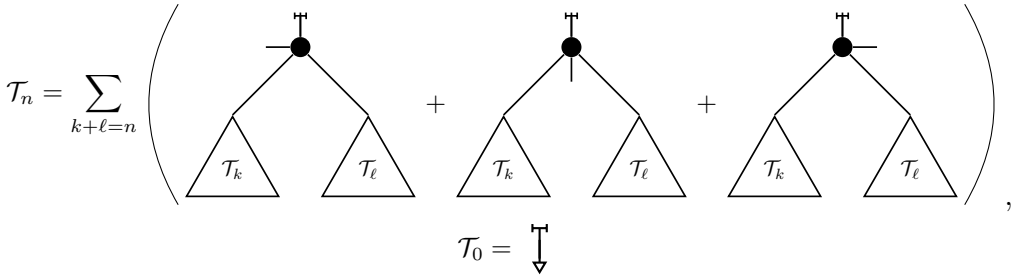

Figure 2.16: A recursive decomposition for binary blossom trees.

$\ell \geq 0$, T_ℓ denotes a binary blossom tree of ℓ nodes, T_ℓ either is the trivial tree or admits a decomposition as depicted in Figure 2.16. It is precisely this recursive specification which enables the enumeration and uniform sampling of these objects in such small time.

Schaeffer showed that these types of trees are bijective to classes of planar maps [93], and has implemented this bijection as a sampler in the software `PlanarMap` [94]. The algorithm goes as follows: The embedding of the tree provides a cyclic list of leaves and buds produced by traversing the exterior of the tree in a counterclockwise direction. Iterate through the list; when iterating over a bud followed immediately by a leaf, join the bud-leaf pair into an edge and remove them from the list of leaves and buds. Proceed until the list consists only of

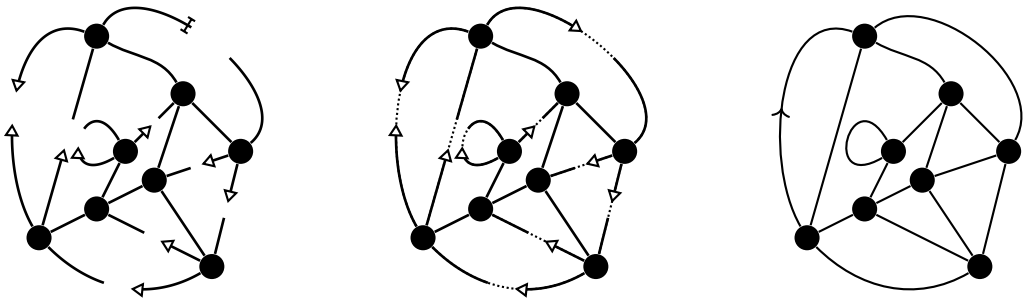

Figure 2.17: Closure of a blossom tree by Schaeffer's algorithm.

two leaves; join them into the root edge, picking either direction with equal probability. An example of this process is given in Figure 2.17.

Chapter 3

The Random Diagram Model

In this chapter we apply the combinatorics of maps to knot theory, in order to formally define the *random diagram model* of random knotting. The model was originally formulated in [20], and we use the notation of [24]. We begin by defining precisely what diagrams are.

3.1 Shadows and Diagrams

Definition 3.1. A *map decorated by a set* S, (M, s) is a map $M = (A, E, V)$ together with a mapping $s : V \to S$ which associates to each vertex of M an element of S.

We can now rephrase the definitions of diagrams using the vocabulary of maps.

3.1.1 Links

We start with the (simpler) case of links.

Definition 3.2. A *link shadow with* n *crossings* is a 4-regular planar map of n vertices. We call the vertices of a shadow *crossings* to line up with knot theory terminology. We will denote by $\mathscr{L}_n$ the set of all n-crossing link shadows and $\mathscr{L} = \bigcup_n \mathscr{L}_n$ the class of all link shadows.

A *link diagram with* n *crossings* is a link shadow with n crossings, which are decorated with a set S of *crossing signs*. We primarily consider $S = \{+, -\}$ which yields usual link diagrams. This is equivalent to making a choice of over-under strand information at each vertex given a deterministic method of doing so (see Proposition 3.1), as demonstrated in Figure 3.1. We will denote the set of n-crossing link diagrams by $\mathcal{L}_n$ and the class of all link diagrams by $\mathcal{L} = \bigcup_n \mathcal{L}_n$.

Similar to maps, we can view link diagrams through an arc-decomposition $D = (A, E, C)$, where A and E are the same, but C is the set of crossings.

As mentioned, we will primarily consider $S = \{+, -\}$, although structural theorems will hold for any sets S. Interesting examples include,

1. *Alternating link diagrams.* If $S = \{+\}$, then diagrams can always be viewed as *alternating*: Every piece of string represented by the diagram weaves over, then under, and so on. Any link type or knot type which can be represented by such a diagram is itself called *alternating*.

2. *Singular link diagrams.* If $S = \{+, -, 0\}$ where a marking of 0 represents a double point (singular point) for a singular link (that is, a link which only need be an *immersion* rather than an embedding), we produce the set of singular link diagrams.

3. *Virtual link diagrams.* If $S = \{+, -, v\}$ where a marking of v represents a virtual crossing, we produce the set of planar-embedded virtual diagrams. This is *different* than the virtual case alluded to in the prior chapter—we'll discuss both in Chapter 8.

Notation. When it is clear, we will use the term *diagram* to refer both to shadow and diagram objects (as shadows are diagrams with crossings decorated by a set of one element).

Like maps, shadows and diagrams may be *rooted* by taking additionally an edge together with a choice of direction (equivalently, by designating an arc), as in Figure 2.13. From here on, maps, shadows, and diagrams will be assumed rooted unless otherwise noted.

As defined, $\mathscr{L}$ is just another name for the class of 4-regular planar maps counted by vertices; itself dual to the class of rooted planar quadrangulations. Hence, the class $\mathscr{L}$ of link shadows has been counted exactly [16, 105]: If $\ell_n = |\mathscr{L}_n|$ is the number of link shadows of n crossings, then:

$$\ell_n = \frac{2(3^n)}{(n+2)(n+1)}\binom{2n}{n} \underset{n\to\infty}{\sim} \frac{2}{\sqrt{\pi}} 12^n n^{-5/2}.$$

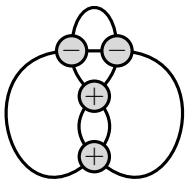

(a) A figure-eight diagram viewed as a decorated shadow.

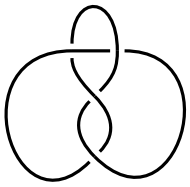

(b) A figure-eight diagram viewed as a knot drawing.

Figure 3.1: After choosing once and for all a way to view signs as "over-under" information (*i.e.* orientation around the knot), knot and link diagrams can be drawn as usual.

From this the exact counts of link diagrams can be determined as well. As rooting breaks symmetry, we have that there are exactly $|S|^n = 2^n$ link diagrams (with the usual $S = \{+, -\}$ signs) to each link shadow of n crossings. If $\lambda_n = |\mathcal{L}_n|$, then

$$\lambda_n = 2^n \ell_n = \frac{2^{n+1}(3^n)}{(n+2)(n+1)} \binom{2n}{n} \underset{n\to\infty}{\sim} \frac{2}{\sqrt{\pi}} 24^n n^{-5/2}.$$

Remark. These formulas only hold in the cases of rooted link shadows and diagrams. Symmetry complicates the counting of unrooted cases, and hence closed formulas are still unknown. However, as these objects are asymmetric in the limit (we prove this in Section 5.1), the exponential growth rates are equivalent.

3.1.2 Knots

Knot diagrams are the subset of link diagrams that have precisely one "link component:"

Definition 3.3. Define an equivalence relation on arcs of a link shadow or diagram so that two arcs are equivalent if a) they are contained in the same edge, or b) they meet at opposite sides of a vertex. *I.e.* if the arcs meeting at a vertex are indexed counterclockwise as *abcd*, then the arcs labeled a and c are equivalent, as are those labeled b and d. A *link component* of a link shadow or diagram D is an equivalence class of arcs under this equivalence relation. Figure 3.2 shows this equivalence as a coloring rule.

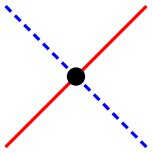

Figure 3.2: A coloring rule for arcs defining link components.

Remark. Link components can be defined entirely in the combinatorial map language as well. Recall that for a shadow or diagram $D = (A, E, C)$, E and C are permutations representing the edges and crossings. Similar to how the cycles of $C \circ E$ represent the faces of D, each cycle of $C^2 \circ E$ represents a traversal of a link component of D in one of two directions. There are hence twice as many cycles in $C^2 \circ E$ as there are link components in D. An *orientation* of a link component is a choice of cycle corresponding to the component in $C^2 \circ E$.

For instance, the shadow in Figure 2.12 has

$$C^2 \circ E = (0\ 2\ 4\ 6\ 8\ 10\ 12\ 14)(1\ 15\ 13\ 11\ 9\ 7\ 5\ 3),$$

and hence has only one link component.

Proposition 3.1. *There is a deterministic way to orient every link component of a rooted link diagram.*

Proof. Given a rooted link diagram, we prove existence by providing an example. After fixing this strategy (or any other deterministic strategy), we will always be able to view signs in $\{+, -\}$ as over-under information.

Start with an stack S containing the pair (c_0, a_0) of the root arc a_0 and the link component c_0 containing a_0, and an empty set X of "visited" components.

Pop a pair (c, a) from S and add c to the set X. Then a immediately determines an orientation for c—the cycle in $C^2 \circ E$ containing a. Initialize $b := a$. Consider the arc $d := C(b)$ contained in the component o. If o is not in X, push the pair (o, d) to the stack S. Step along

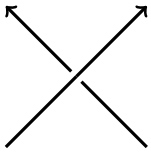

(a) A positive crossing +

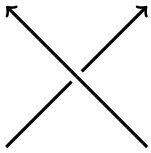

(b) A negative crossing −

Figure 3.3: The usual way to give crossings in oriented diagrams signs is based on the cross product between the over and under trajectories.

the component in the orientation direction, *i.e.* set $b := (C^2 \circ E)(b)$. When $b = a$, break and try popping from the stack S again. If S is empty, terminate.

This algorithm is deterministic (it depends only on the diagram and the root arc a_0), and terminates (there are only a finite number of components, and we run over each once at most). It furthermore orients every link component; as the underlying graph of the diagram is connected, we indeed orient and process *every* link component exactly once. □

Definition 3.4. A *knot shadow* is a link shadow which consists of precisely one link component. The set of knot shadows with n crossings is denoted by $\mathscr{K}_n$ and the class of all knot shadows is denoted $\mathscr{K} = \bigcup_n \mathscr{K}_n$.

A *knot diagram* is a link diagram which consists of precisely one link component. The set of knot diagrams with n crossings is denoted by $\mathcal{K}_n$ and the class of all knot diagrams is denoted $\mathcal{K} = \bigcup_n \mathcal{K}_n$.

Remark. Rooted knot diagrams have their unique link component oriented (there is a sense of direction around the circle), so there is a natural way to translate raw sign information into over-under crossing information by using the usual definition as the sign of the cross product from the over trajectory to the under trajectory as in Figure 3.3.

Knot shadows have also been studied as plane (or spherical) curves [6, 7, 107, 95], lacets [29], and knot universes [62]. Knot shadows $\mathscr{K}$ represent a curious, small subclass of

$\mathscr{L}$. Indeed, exact counts for $k_n = |\mathscr{K}_n|$ and $\kappa_n = |\mathcal{K}_n|$ are not known except by experiments and conjectures [56, 95]:

Conjecture 3.2 (Schaeffer-Zinn Justin 2004)**.** *There exist constants μ and c such that*

$$\frac{\kappa_n}{2^n} = k_n \underset{n\to\infty}{\sim} c\mu^n \cdot n^{\gamma-2}, \tag{3.1}$$

where

$$\gamma = -\frac{1+\sqrt{13}}{6},$$

and $\mu \approx 11.415 \pm 0.005$.

This conjecture is of similar flavor to conjectures of the counts of both self-avoiding lattice walks and self-avoiding lattice polygons [51] in Equations 2.1 and 2.2.

3.1.3 Gauss diagrams

As a result of the "global" nature with which link components are defined, it is very difficult to restrict classes of diagrams to a fixed number of link components. We describe an alternate viewpoint which fixes the number of link components at the cost of losing control over planarity and the genus of the embedding surface Σ.

Definition 3.5. A *Gauss diagram* [68] (also called a Gauss code [63]) is a rooted map of 1 vertex on an arbitrary, oriented surface. A *signed* Gauss diagram is a Gauss diagram together with a choice of sign in $\{+,-\}$ for each edge. We will denote by $\mathscr{G}$ the class of all signed Gauss diagrams sized by edge.

Gauss diagrams are typically viewed as chord diagrams, as in Figure 3.4, where the unique vertex is instead viewed as boundary of a disk containing chords. Additionally, we will re-interpret the data of the root as a *basepoint* on the boundary and an *orientation* around the boundary circle.

Definition 3.6. A *virtual link shadow* is a 4-valent map on an oriented surface Σ. A *virtual knot shadow* is a virtual link shadow with precisely one link component.

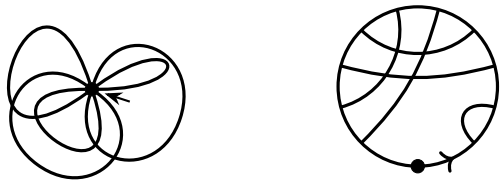

Figure 3.4: A Gauss diagram viewed as a map (left) and as a chord diagram (right). Besides the one central vertex, crossings between edges are a visual artifact due to the projection from a higher genus surface and are not part of the data of the Gauss diagram.

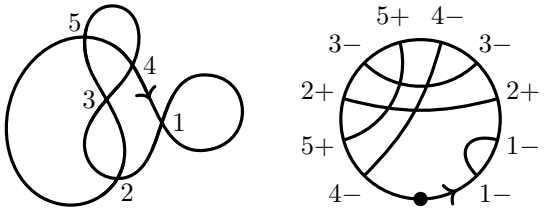

Figure 3.5: A rooted knot shadow and its equivalent signed Gauss diagram.

There is a one-to-one equivalence between the sets of signed Gauss diagrams with n edges and the sets of rooted virtual knot shadows with n crossings [63, 107, 69]. Restricting to the signed Gauss diagrams which embed in the sphere, we have that the sets of sphere-embedding signed Gauss diagrams with n edges and the sets of rooted knot shadows with n crossings are equivalent. This provides an alternate representation of knot shadows. An example of this equivalence is given in Figure 3.5.

Definition 3.7. A *directed* signed Gauss diagram is a signed Gauss diagram together with an additional decoration, viewed as a direction, chosen for each edge. We will denote by $\mathcal{G}$ the set of all directed signed Gauss diagrams sized by edge.

By interpreting the directional data in a directed signed Gauss diagram as pointing away from the over-strand and towards the under-strand, one obtains a one-to-one bijection

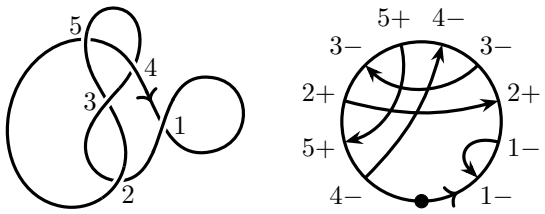

Figure 3.6: A rooted knot diagram and its equivalent signed directed Gauss diagram.

between the sets of sphere-embedding directed signed Gauss diagrams with n edges and the sets of rooted knot diagrams with n crossings. An example of this equivalence is given in Figure 3.6. Similar to the above case, relaxing the sphere-embedding condition describes the case of virtual knot diagrams; we will discuss this more in Chapter 8.

The number of signed Gauss diagrams is precisely [69],

$$|\mathscr{G}_n| = \frac{(2n)!}{n!}.$$

There are many results on necessary conditions and sufficient conditions for signed Gauss diagrams embedding in the sphere [91, 38, 19, 103]. However, the problem of counting sphere-embedding signed Gauss diagrams is yet unsolved—it is precisely the same problem as counting knot shadows! This provides a new perspective on the difficulty of counting knot shadows: It is easy to count planar link shadows, but difficult to restrict to a certain number of link components. Equivalently, it is easy to count virtual knot shadows, but difficult to restrict to a fixed surface (the sphere).

3.1.4 Tangles

Tangle diagrams are an important ingredient in our pattern theorem to come. They may also be viewed in the language of maps:

Definition 3.8. A *k-tangle shadow* is a map embedded on a sphere which is 4-valent except for one distinguished "external" vertex of degree $2k$. A *k-tangle diagram* is an k-tangle shadow decorated (at non-exterior vertices) with signs in S (usually, $S = \{+, -\}$).

A *component* of a tangle shadow or diagram is an equivalence class of edges under the equivalence in Definition 3.3 with *no* additional equivalence at the external vertex. Some components correspond to open strands and are *open*, while some components correspond to closed strand and are *closed*.

A tangle shadow (resp. diagram) T is *contained as a subtangle*, or simply *contained*, in a link shadow (diagram) D if the dual of T, T^* (with exterior face the dual of the exterior vertex), is a submap of D^*; for diagrams it is furthermore required that the signs of the crossings agree.

We will view the exterior vertex of tangle shadows and diagrams as being "at infinity" so that tangle shadows and diagrams appear to be 4-valent decorated maps with "loose" arcs in a common exterior face called *legs*, as shown in Figure 3.7. This view matches up with the previous definition of tangle diagrams in D^2.

Tangle diagrams admit an arc-decomposition (A, E, C); the exterior vertex is omitted from the crossings C (it is determined by the structure of the map). Under this view, the faces $F = C \circ E$ consist of all interior faces in addition to one (large) exterior face which contains all of the loose legs. The components $C^2 \circ E$ are slightly different than in the case of link diagrams: There are pairs of cycles for each *closed* component, and there is one cycle for each *open* component. An *orientation* for a closed component is a choice of cycle; an orientation of an open component is determined by a choice of leg arc.

Remark. It is possible to consider the case of tangle diagrams with exterior legs which *do not* end in the same face. We will discuss this in Chapter 7.

Remark. As in the case of rooted diagrams above, after picking a deterministic scheme to orient all components (open and closed) from a tangle diagram together with choice of leg arc, one can reconcile the view of crossing signs as over-under information.

Figure 3.7: A 3-tangle diagram with boundary vertex (left) and boundary vertex viewed as disk boundary (right).

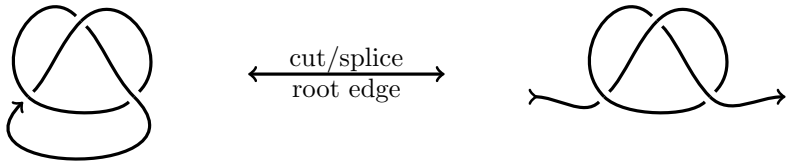

Figure 3.8: A rooted diagram of a trefoil, and its equivalent two-leg diagram

The proof of Proposition 3.1 extends to provide an example of such an algorithm for tangle diagrams: As we process an open component c with designated arc a after popping from the stack, we set as the component's orientation the *previous* leg arc before a (possibly a itself) in the cycle in $C^2 \circ E$.

Rooted diagrams may be viewed as directed *long curves* or *two-leg diagrams* by cutting the root edge into two directed half edges with one pointing towards its vertex (the *hind leg*) and one away (the *front leg*) as in Figure 3.8. Two-leg diagrams are rooted 1-tangle diagrams.

3.1.5 Primality

A key strength of the framework proposed in this manuscript is the simplicity with which the tools presented can be applied to other interesting classes of diagram objects. To demonstrate this, we will provide constructions for "prime" and "reduced" classes of diagrams as well;

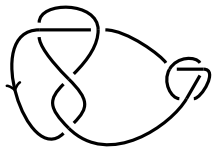

(a) A rooting which is two-leg-prime.

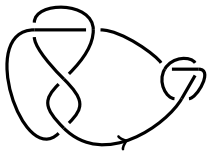

(b) A rooting which is not two-leg-prime.

Figure 3.9: Depending on the rooting, a composite shadow may be two-leg-prime.

Definition 3.9. A diagram D is *prime* if it has more than 1 vertex and is not 2-edge-connected, *i.e.* there is no way to disconnect the underlying graph of D, $\Gamma(D)$, by removing 2 edges. A diagram which is not prime is *composite*. A rooted diagram is *two-leg-prime* if it cannot be disconnected by removing two edges, *one being the root edge*. This property is dependent on the choice of root; Figure 3.9 gives a diagram for which one rooting is two-leg prime, but the other is not.

A shadow or diagram D is *reduced* if it has no disconnecting vertices called *isthmi*.

It is important to note that prime knot diagrams can represent knot types which are *composite*. The condition of being a prime knot diagram is purely graph-theoretic.

We will denote by $\mathscr{PL}$ the class of prime link shadows, $\mathscr{PK}$ the class of prime knot shadows, $\mathcal{PL}$ the class of prime link diagrams, $\mathcal{PK}$ the class of prime knot diagrams, and $p\ell_n$, pk_n, $p\lambda_n$, and $p\kappa_n$ their respective cardinalities for a fixed number n of crossings.

Again, the counts of prime link shadows and prime link diagrams are known precisely. Exact counts are known from their bijection with simple quadrangulations [2];

$$\frac{p\lambda_n}{2^n} = p\ell_n = \frac{4(3n)!}{n!(2n+2)!}.$$

The counts for prime knot diagrams are again unknown. Schaeffer and Zinn-Justin [95] conjecture that the asymptotic growth rates for diagrams and shadows are of the form

$$\frac{p\kappa_n}{2^n} = pk_n \underset{n\to\infty}{\sim} c\mu^n \cdot n^{\gamma'-2},$$

where μ is the same as that for knot shadows in Equation 3.1.

3.2 Composition of tangle diagrams

In order to prove a pattern theorem for diagrams, we will require the ability to compose two diagrams in order to produce new diagrams with certain properties. We will describe this by first discussing methods of composition for tangle diagrams and then providing equivalences between diagrams and tangle diagrams.

Given two tangle diagrams $T = (A_T, E_T, C_T), S = (A_S, E_S, C_S)$ with respective leg arcs $\{t_1, t_2, \ldots, t_{2k}\}$ and $\{s_1, s_2, \ldots, s_{2\ell}\}$ and a collection of unordered pairings

$$\mu = \{(t_{i_1}, s_{j_1}), (t_{i_2}, s_{j_2}), \ldots, (t_{i_r}, s_{i_r})\}$$

where each t_i and s_i appears at most once, define the $(k + \ell - r)$-tangle diagram $T\#_\mu S$ to be the tangle diagram

$$T\#_\mu S = (A_T \cup A_S, E_T \cup E_S \cup \mu, C_T \cup C_S).$$

Given an arbitrary choice of μ, it is possible that $T\#_\mu S$ is non-planar or that not all leg arcs of $T\#_\mu S$ lie on the same face. We will define and use some specific tangle diagram compositions which avoid these pitfalls.

3.2.1 Connect summation

Analogous to the connect sum operation on knots in space, there is a notion of *diagram connect sum* on diagrams.

Definition 3.10. Given 1-tangle diagrams T, S with leg arcs $\{t_1, t_2\}$, $\{s_1, s_2\}$ and a pair of arcs (t_i, s_j) with $i, j \in \{1, 2\}$, there is a complementary pair of arcs $(t_{i'}, s_{j'})$ with $i \neq i'$ and $j \neq j'$. So define the *connect sum* of the head t_i of T to the tail s_j of S;

$$T\#_{(t_i,s_j)}S = T\#_{\{(t_i,s_j),(t_{i'},s_{j'})\}}S.$$

An example of this process is given in Figure 3.10.

Given a diagram $D = (A, E, C)$ and an edge $e = (ab)$ in D, define the 1-tangle diagram $D \setminus e$ to be the 1-tangle diagram $(A, E \setminus \{e\}, C)$ with leg arcs a and b.

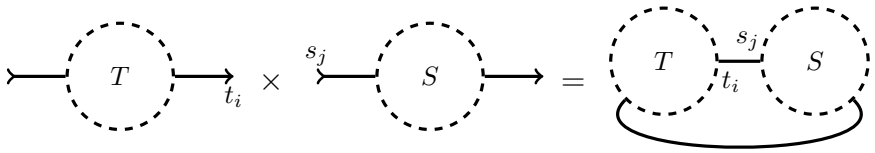

Figure 3.10: Connect sum of the head t_i of T to the tail s_j of S producing $T\#_{(t_i,s_j)}S$.

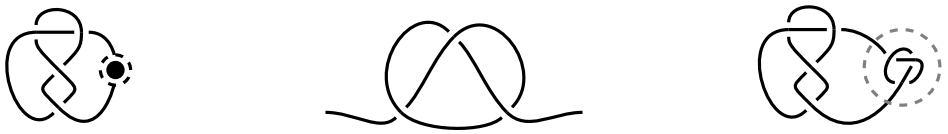

(a) Diagram with marked edge.

(b) A trefoil connect summand.

(c) After connect summation.

Figure 3.11: Connect sum of a trefoil into a figure-eight knot.

A diagram and a choice of arc (D, a) is equivalently a 1-tangle diagram $(D \setminus \{e(a)\}), a$. So given a 1-tangle diagram and a choice of "tail" leg arc (T, b), define the *connect sum* of T to D by a, b to be

$$D\#_{(a,b)}T = (D \setminus e(a))\#_{(a,b)}T.$$

An example of connect summation of a tangle diagram into a diagram is given in Figure 3.11.

Link components behave predictably under connect summation: If the tangle diagrams T, S have τ, σ closed components respectively, then $T\#S$ has exactly $\tau + \sigma + 1$ closed components (independent of choice of head and tail for the connect summation). It follows then that if D is a knot diagram and T is a tangle diagram with no closed components that $D\#T$ is always itself a knot diagram. This can be seen as the tangle diagram $D \setminus \{e\}$ itself has no closed components independent of choice of e as D was a knot diagram.

3.2.2 Cyclic composition

We can extend this definition to tangle diagrams with additional leg arcs, but we will then focus on tangle diagrams with precisely four.

Definition 3.11. Given k-tangle diagrams T, S with external arcs

$$\{t_1, \ldots, t_{2k}\}, \{s_1, \ldots, s_{2k}\},$$

choices t_{i_1} and s_{j_1} of arcs induce ordered tuples $t_{i_1}, \ldots, t_{i_{2k}}$ and $s_{j_1}, \ldots, s_{j_{2k}}$ by enumerating the external arcs of T counterclockwise and S clockwise, starting with the chosen arcs. Then with $\mu = \{(t_{i_1}, s_{j_1}), \ldots, (t_{i_{2k}}, s_{j_{2k}})\}$, define the composition to be the link diagram

$$T\#_{(t_{i_1}, s_{j_1})}S = T\#_{\mu}S.$$

By this choice of μ, as T and S are both planar, so too is the composition $T\#_{\mu}S$.

The number of components in the resulting diagram will depend (in addition to the count of closed loop components) on the ordering of the external arcs of T, S as well as the precise matching. If however we are dealing with tangle diagrams of four leg arcs, we can be assured the existence of a choice for μ which can guarantee some control over the number of link components of the resultant diagram.

Consider the case where T, S are 2-tangle diagrams with τ, σ closed components respectively. Let the leg arcs of T be indexed counterclockwise as $\{t_i\}_{i=1}^4$ and the leg arcs of S be indexed counterclockwise as $\{s_i\}_{i=1}^4$. For each tangle diagram, color one open strand blue and the other open strand red. Up to changing colors or switching T with S there are four possibilities for cyclic composition.

1. The leg arcs of both T and S are colored counterclockwise blue-red-blue-red. In this case, the two open components always close into two distinct link components, and the resulting number of components is $\tau + \sigma + 2$. This situation is shown in Figure 3.12a.

(a) Composition of two red-blue-red-blue tangle diagrams will always add an additional link component.

(b) This composition of a blue-blue-red-red and a blue-red-red-blue tangle diagram will add an additional link component.

Figure 3.12: Attachments for 2-tangle diagrams which introduce an additional link component.

2. The leg arcs of T are colored counterclockwise blue-blue-red-red and those of S are colored counterclockwise blue-red-red-blue. In this case, the two open components always close into two distinct link components, and the resulting number of components is $\tau + \sigma + 2$. This situation is shown in Figure 3.12b.

3. The leg arcs of T are colored counterclockwise blue-blue-red-red and those of S are colored counterclockwise blue-red-blue-red. In this case, the two open components always close into one link component, and so the resulting number of components is $\tau + \sigma + 1$. This situation is shown in Figure 3.13a.

4. Finally, if the leg arcs of T and S are both colored counterclockwise blue-blue-red-red, the two open components always close into one link component, and so the resulting number of components is $\tau + \sigma + 1$. This situation is shown in Figure 3.13b.

Notice then that given a knot diagram D, taking a crossing x, ignoring its sign, and designating it as the boundary vertex of a tangle diagram produces the 2-tangle diagram denoted $D \setminus x$ (there is some abuse of notation here; we are actually removing both the crossing x, the four arcs in x, and the edges in which those arcs resided from D). Furthermore, as D is a planar knot diagram, $D \setminus x$ must have its leg arcs colored blue-blue-red-red as in

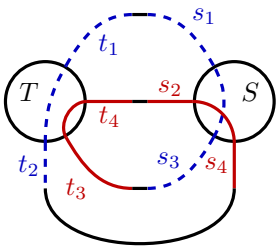

(a) Composition of a blue-blue-red-red tangle diagram with a red-blue-red-blue tangle diagram will never add an additional link component.

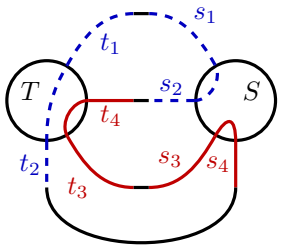

(b) Composition of a two blue-blue-red-red tangle diagrams will not add an additional link component.

Figure 3.13: Attachments for 2-tangle diagrams which introduce an additional link component.

the case of T in case (3) above (as the crossing x is necessarily colored blue-red-blue-red). Hence given any 2-tangle diagram S there exists at least one way to compose $(D \setminus x)\#S$ so that it is a planar knot diagram.

3.3 The random diagram model

With this in line, we are prepared to define the random diagram model. The idea is parallel to that for random self-avoiding polygons.

Definition 3.12. The *uniform* distribution on a class of diagrams $\mathscr{C}$ with n crossings has that the probability of drawing any one n-crossing diagram D is,

$$\mathbb{P}(D) = \frac{1}{c_n}.$$

Let $c_n([L])$ be the number of diagrams which represent the link or knot type $[L]$. The *(uniform) random diagram model* for $\mathscr{C}$ says that the probability of drawing the type $[L]$ is,

$$\mathbb{P}([L]) = \frac{c_n([L])}{c_n}.$$

One could devise other distributions on a fixed class of diagrams, but the important distinction about our formalization here from previous work on random diagrams [37, 39]

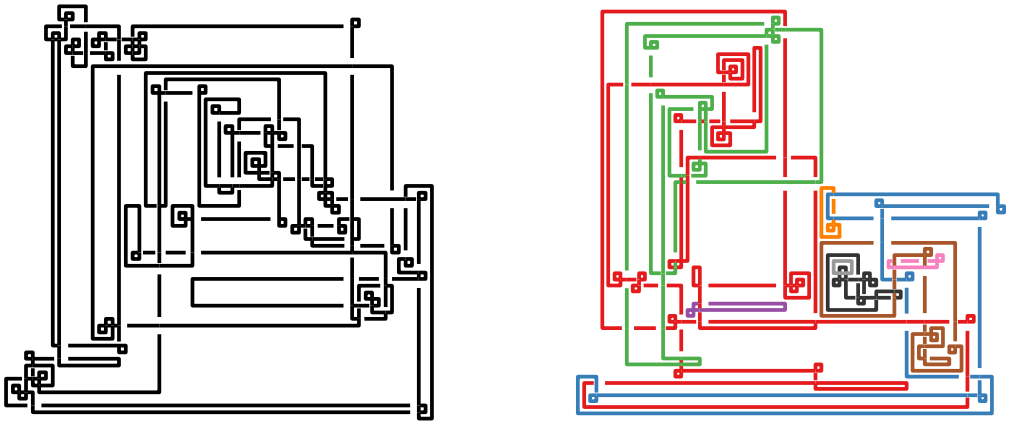

(a) Random knot diagram (b) Random link diagram

Figure 3.14: A random knot diagram and a random link diagram, each of 100 vertices.

is the requirement that we *know* which distribution we have chosen. When the class $\mathscr{C}$ is a class of link diagrams, it is possible to leverage the structure of the underlying maps to prove precise results, such as the number of alternating link types [114, 112] and the average hyperbolic volume of an alternating link [82]. When one considers knot diagrams as in this manuscript, much of this structure vanishes with the restriction on the number of link components, and similar results become more difficult to prove.

An important fact about the random diagram model is that *the underlying shadow* and *the crossing signs* which make up a random diagram are both independent random variables on the spaces of knot shadows of n crossings and the power set of crossing signs S^n (where S is the set of crossing signs). An example of a randomly sampled knot diagram and a randomly sampled link diagram is given in Figure 3.14. We discuss how these diagrams were sampled in Chapter 5.

As for random knotting in self-avoiding polygons, we can pose the FWD conjecture for knot diagrams:

Conjecture 3.3 (Frisch-Wasserman 1962, Delbrück 1961)**.** *As the number of crossings n of a random knot diagram grows large, the probability that it is knotted (that is, does not*

represent the knot type 0_1*) tends to 1. Conversely,*

$$\lim_{n\to\infty} \frac{\kappa_n(0_1)}{\kappa_n} = 0.$$

As expected for "reasonable" models of physical knotting, this conjecture holds true for the random diagram model! Chapter 4 is devoted to the proof of this theorem.

3.4 Exact tabulation of small knot diagrams

With Cantarella and Mastin, we tabulated small knot diagrams (*i.e.* diagrams with 10 or fewer crossings) and calculated precise knot type frequencies in [20]. We summarize the results below.

For the remainder of this section, we consider *unrooted* knot diagrams on the *unoriented* sphere. The asymptotic results of Chapter 4 still follow for these objects as most diagrams are entirely asymmetric (*c.f.* Section 5.1).

As mentioned before, the introduction of this symmetry makes computation more difficult; the small size of objects considered makes this feasible. From a different view though, symmetry was a saving grace for this tabulation: Accounting for symmetry made the number of objects which we had to store on disk significantly smaller.

For each $n \leq 10$, we tabulated the set of knot shadows—one representative per symmetry class—through two methods (for validity checking):

1. Using Brinkmann and McKay's `plantri` [17], we generated all connected planar embedded simple graphs with vertex degrees ≤ 4. We then a) used an expansion algorithm to produce all link shadows and b) separated out only those shadows with one link component.

2. Also with Brinkmann and McKay's `plantri`, we generated all planar simple quadrangulations. Planar simple quadrangulations are dual to prime link shadows; by rejecting all shadows with more than one link component, we obtained all prime knot shadows.

Then, for each partition $\lambda_1 + \lambda_2 + \ldots + \lambda_k = n$, we produced all composite diagrams formed from tuples of knot shadows with $(\lambda_1, \lambda_2, \ldots, \lambda_n)$ crossings.

Both methods are explained (and their completeness proved) in [20]. The result of either process is the database of *all* knot shadows with $3 \leq n \leq 10$ crossings.

Given this database of all knot shadows, we produced a database of all knot diagrams by:

1. For each n-crossing knot shadow representative, produce a knot diagram by picking n signs in $\{+, -\}$, then,

2. Add the resultant diagram to the knot diagram database *if it is not isomorphic to any other diagram in the database*.

The first step is trivial; the latter step is more complicated. The observation that knot diagrams are isomorphic only if their shadows are simplifies computations, but the large number of knot shadows and the computational complexity of isomorphism checking ensures this is a computationally difficult problem. Both of these issues (time and space) are significant obstructions to extending this exact enumeration beyond $n = 10$ crossings. For example, the database of all 10-crossing knot shadows is approximately .5GB large (a database of diagrams would require about 1.6TB), and we estimate that processing a set of 11-crossing knot diagrams should take at least a month without further optimizations and parallelization.

Using a cluster of machines organized using Amazon Web Services under the AWS Educate program, we were able to analyze these data. A full analysis is available in [20], but we reprint some data with which we will compare in later chapters. First, Table 3.1 presents the exact number of knot shadows and knot diagrams of a given size produced by our tabulation, in line with independent calculations of Coquereaux, *et al.* [28] and Valette [107]. Second, Figure 3.15 presents the *exact* probabilities of certain small knot types among all diagrams of given size.

The number $n = 10$ of crossings is astonishingly small, and the graph of knot probabilities does not exhibit the long term exponential decay as predicted in numerous other models

Table 3.1: Exact counts of unoriented knot objects on the unoriented sphere.

n	Knot shadows	Knot diagrams
3	6	36
4	19	276
5	76	2936
6	376	35872
7	2194	484088
8	14614	6967942
9	106421	105555336
10	823832	1664142836

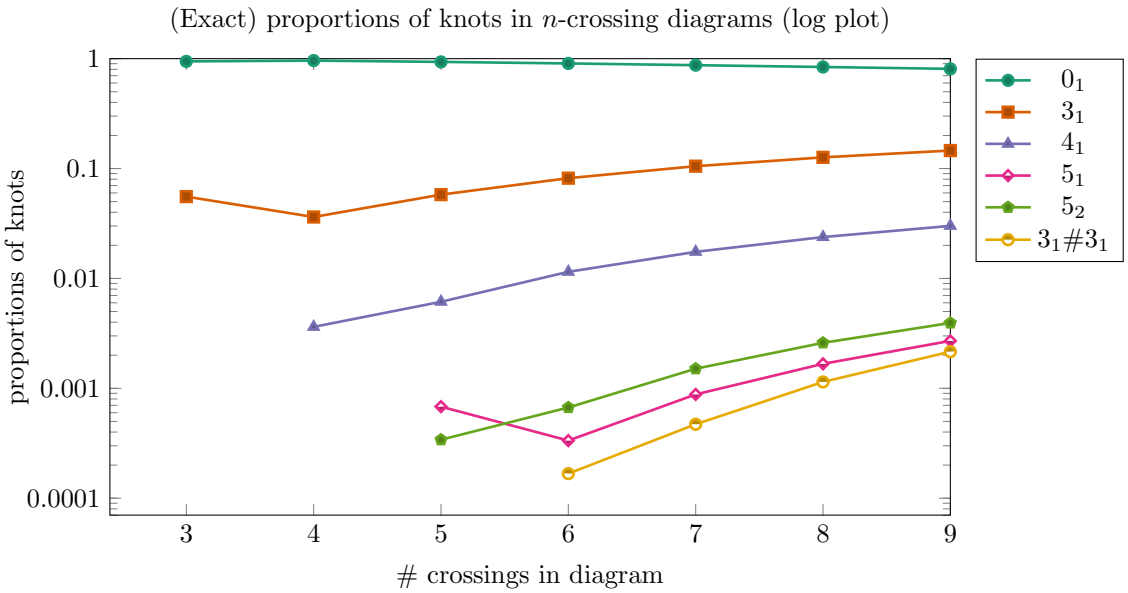

Figure 3.15: Exact probabilities of certain knot types among all diagrams of fixed size

of random knotting [102]. Also present in 10-crossing diagrams is an astonishing number of unknotted diagrams, despite the thesis of the FWD conjecture. In the following chapter, we turn to new techniques to prove these results and enable sampling of diagrams beyond this $n = 10$ barrier.

Chapter 4

The Pattern Theorem

Sumners and Whittington's proof of the FWD conjecture for self-avoiding lattice polygons makes use of Kesten's pattern theorem [64, 65, 71] which states that patterns—short walk configurations—appear linearly often in long self-avoiding walks. In this chapter, we prove a pattern theorem for random diagrams, which proves the FWD conjecture for diagram models.

4.1 The Pattern Theorem

We make use of a similar strategy: Theorem 2 of Bender *et al.* [11] provides a pattern theorem for maps, provided a strategy of attaching a desired pattern. However, we must be careful in the case of knot or link *diagrams*, our *decorated* maps with extra structure. We thus retrace the proof while keeping this in mind.

4.1.1 Attachment

Say that if D is a link diagram, then $e(D)$ is the number of edges in the diagram D. The proof depends on the existence of an "attachment" scheme:

Definition 4.1. Let Q be a tangle diagram, $\mathscr{M}$ some class of diagrams, and $\mathscr{H}$ a subclass of $\mathscr{M}$. A *viable attachment* of the tangle diagram Q into $\mathscr{H}$ is a method of taking a diagram $D \in \mathscr{H}$ and producing new diagrams D' that contain Q as a subtangle diagram satisfying:

1. For some fixed positive integer k, at least $\lfloor e(D)/k \rfloor$ possible non-conflicting places of attachment exist. This means that at least $\lfloor e(D)/k \rfloor$ attachment operations (of Q) to a single diagram can be "parallelized" and all performed at once to a diagram to produce a new diagram with at least $\lfloor e(D)/k \rfloor$ copies of Q contained as subtangle diagrams.

2. Only diagrams in $\mathscr{M}$ are produced.

3. For any diagram produced as such we can identify the copies of Q that have been added and they are all pairwise vertex disjoint. Identifying tangle diagrams in diagrams is simple since a diagram contains a tangle diagram if there is some dual cycle whose interior is the tangle diagram itself. We will consider only Q which are *always* pairwise disjoint, and hence any attachment would satisfy the latter half of this condition.

4. Given the copies of Q that have been added, the original diagram and associated places of attachment are uniquely determined. For our attachments, we will provide suitable "inverse" operations which are themselves parallelizable (since instances of Q are disjoint). This condition then follows.

Our tangle diagram compositions yield then the two attachment schemes which are relevant to the examples that follow.

Definition 4.2. Consider the 1-tangle diagram of one strand Q which is two-leg-prime and asymmetric with tail arc b. Let $\mathscr{M}$ be one of:

1. all (rooted) link diagrams,

2. all (rooted) knot diagrams, or

3. provided Q is reduced, all (rooted) reduced knot or link diagrams.

Then define the attachment *edge replacement* by, given a diagram D and any arc a in D, defining D' to be the new diagram $D' = D\#_{(b,a)}Q$.

Proposition 4.1. *Edge replacement is a viable attachment for choices of $\mathscr{M}$ enumerated above.*

Proof. We consider each required property.

1. There are at least $n - 1 \geq \lfloor n/2 \rfloor$ places of attachment to a rooted diagram D with n edges; non-conflicting ways to connect sum Q into D are precisely the number of non-root edges of D. Given a collection $\{a_i\}_{i=1}^{r}$ of different arcs, none of whom share an edge, in D, edge replacements performed in any order will produce the same diagram (since edge replacement does not alter any arcs or edges in D besides the arc chosen and its edge).

2. Depending on the choice of tangle diagram Q and class of diagrams $\mathscr{M}$, diagram connect sum can be shown to keep diagrams in $\mathscr{M}$. Namely, provided a tangle diagram Q of one strand, this attachment does not change the number of link components of diagrams. Furthermore, If Q is reduced, then the introduction of Q into a diagram by connect summation introduces no new disconnecting vertices.

3. We can identify the copies of Q inside the resultant diagram by our definition of what it means for a tangle diagram to be included in a diagram. Provided Q is two-leg-prime, occurrences of Q must be pairwise disjoint:

   Suppose to the contrary that Q_1 and Q_1 are instances of Q contained as subtangle diagrams in a diagram D which are *not* disjoint. The definition of being a subtangle diagram means there exists some dual cycle of edges (e_1, e_2) which isolates the tangle diagram Q_1 from the rest of D; the cycle is necessarily of length 2 as Q is a 1-tangle diagram.

   Now, the condition that Q_1 and Q_2 are not disjoint means that, without loss of generality, the edge e_2 appears in the interior of Q_2. However, $Q_2 \setminus e_2$ is necessarily disconnected, which contradicts that Q was two-leg prime. So instances of Q must be pairwise disjoint.

4. Edge replacement is an invertible operation. Given an instance of Q in D which is identified by the dual edge cycle (e_1, e_2), we can recover the diagram D': Without loss of generality, as Q is asymmetric, we can assume that $e_1 = (ab)$ is the edge which connects the tail arc b of Q to the arc a of D. Removing e_1 and e_2 from D yields the

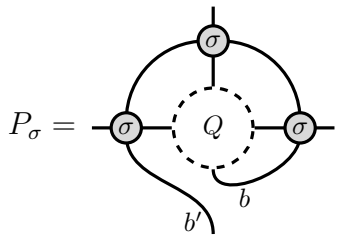

Figure 4.1: Definition of the tangle diagram P_σ in the definition of crossing replacement.

pair of 1-tangle diagrams D^o and Q. Denote by c the arc of D^o which is not a. Then D' is the tangle diagram D^o together with additional closing edge $e_3 = (ac)$ and we have that $D = D'\#_{(a,b)}Q$. We made no choices in this procedure beyond choice of instance of Q inside D and each step was entirely local.

Hence, edge replacement is a viable attachment. □

If instead we have a k-tangle diagram Q (for $k > 1$) we can still define an attachment into diagrams by first joining together pairs of all but two exterior edges to produce a 1-tangle diagram Q' (some choice is involved here—there are infinitely many ways to close any given tangle). This 1-tangle diagram Q' can then be attached by edge replacement.

For classes of prime diagrams which are not closed under connect summation, we have an alternate attachment;

Definition 4.3. Consider the nontrivial 2-tangle diagram Q that is asymmetric and at least 4-edge-connected with designated arc b. Let $\mathscr{M}$ be either the class of prime link diagrams or, if Q consists of precisely two open strands and no closed components, the class of prime knot diagrams. Then define the *crossing replacement* of a given diagram D and an arc a in D to be the diagram $D' = D\#_{(a,b')}P_\sigma$, where σ is the sign of the crossing $c(a)$ in D and P_σ is the tangle diagram containing Q as defined in Figure 4.1.

Proposition 4.2. *Crossing replacement is a viable attachment for choices of $\mathscr{M}$ enumerated above.*

Proof. We consider each required property.

1. For the class of all prime link diagrams, any choice of an arc in a diagram provides a crossing attachment of Q which is a link diagram. For the class of all prime knot diagrams on the other hand, each crossing has at least one choice of arc for which the insertion of P_σ produces a knot diagram. So for any diagram and for each crossing inside the diagram, there exists at least one viable location for crossing replacement, and provided crossing replacements happen at different crossings, they are independent. So there exist at least $n/2 \geq \lfloor n/2 \rfloor$ non-conflicting places of attachment of Q into a diagram with n edges.

2. Provided an appropriate Q, the attachment is closed in $\mathscr{M}$ as we only choose appropriate arcs.

3. We can identify the copies of P_σ inside the resultant diagram by our definition of what it means for a tangle diagram to be included in a diagram. Suppose that P_1 and P_2 are instances of P_σ which are not disjoint in D (σ does not matter and can be different for each P_i).

   That P_1 and P_2 are not disjoint means that the boundary cycle (e_1, e_2, e_3, e_4) of P_1 must in some part enter the interior of the instance P_2. Notice that as Q is nontrivial, there is no dual path of length 1 through P_2; this implies that the subpath which is inside P_2 cannot be length 1. Conversely, it cannot be length 3 (switch the roles of P_1 and P_2). So the subpath would have to be of length 2; as the dual map is a quadrangulation, a dual path of length two would have to be trivial (which cannot happen by the structure of P_i) to begin at one face and end at the face opposite. However, by the structure of P_i and by the fact that Q is nontrivial this is impossible.

4. Crossing replacement is an invertible operation. Given an instance of P_σ in D which is identified by the dual edge cycle (e_1, e_2, e_3, e_4), we can recover the diagram D': Without loss of generality, as P_σ is asymmetric, we can assume that $e_1 = (ab')$ is the edge which connects the tail arc b' of P_σ to the arc a of D. Removing e_1, e_2, e_3, and e_4 from D yields the pair of 2-tangle diagrams D^o and P_σ. Denote by x, y, z the arcs counterclockwise around D^o after a. Then D' is the tangle diagram D^o together with the four arcs brought together into a crossing x with sign σ identified from P_σ. We have that $D = D' \#_{(a,b')} P_\sigma$. We made no choices in this procedure beyond choice of instance of P_σ inside D and each step was entirely local.

Hence, crossing replacement is a viable attachment. □

4.1.2 Pattern theorems for diagrams

Given a generating function F, let $r(F)$ be its radius of convergence. Being able to attach desired subtangle diagrams as above yields;

Theorem 4.3. *Let $\mathscr{M}$ be some class of decorated map on any surface and let Q be a tangle diagram that can be contained in diagrams in $\mathscr{M}$. Let $M(x)$ be the generating function by the number of edges for $\mathscr{M}$. Let $H(x)$ be the generating function by the number of edges for those decorated maps D in $\mathscr{M}$ that contain less than $ce(D)$ pairwise disjoint copies of Q; call this class $\mathscr{H}$. Suppose there is a viable attachment for Q into $\mathscr{H}$. If $0 < c < 1$ is sufficiently small, then $r(M) < r(H)$. The diagrams may be rooted or not.*

The proof of the theorem makes use of a lemma of Bender *et al.*:

Lemma 4.4 ([11], Lemma 3)**.** *If*

1. *$F(z) \neq 0$ is a polynomial with non-negative coefficients and $F(0) = 0$,*

2. *$H(w)$ has a power series expansion with non-negative coefficients and $0 < r(H) < \infty$,*

3. *for some positive integer k the linear operator $\mathscr{L}$ is given by $\mathscr{L}(w^n) = z^n(F(z)/z)^{\lfloor n/k \rfloor}$, and*

4. *$G(z) = \mathscr{L}(H(w))$,*

then $r(H)^k = r(G)^{k-1}F(r(G))$.

The proof of the theorem then remains almost unchanged from the original theorem. The class $\mathscr{M}$ of diagrams and tangle diagrams P considered determine the attachment scheme.

Proof of Theorem 4.3.. Let $G(z)$ be the generating function which counts the ways by edges of attaching some number between 0 and $\lfloor n/k \rfloor$ copies of Q to diagrams in $\mathscr{M}$ counted by $H(x) = \sum h_n x^n$. The method of attachment leads to the relation $G(z) = \mathscr{L}(H(w))$, with $\mathscr{L}$ as defined in the lemma, where $F(z) = z + z^q$ and q, is the number of edges added when a copy of Q is attached, as

$$G(z) = \sum_{Y \in \mathscr{H}} z^{e(Y)} \left(1 + z^{q-1}\right)^{\lfloor e(Y)/k \rfloor} = \mathscr{L}(H(w)).$$

Let g_n be the coefficients of $G(z)$.

Suppose $D \in \mathscr{M}$ contains m copies of Q. By property (3) of our attachment, $m \leq n = e(D)$. If D had been produced from some diagram K in $\mathscr{H}$ by our attachment process, we can find all possible K by removing at least $m - cn$ copies of Q from D, as for any such K, $m - cn < m - ce(K)$. It is possible to bound from above the number of ways to do this by

$$\begin{aligned} \sum_{j \geq m - cn} \binom{m}{j} = \sum_{k < cn} \binom{m}{k} &< \sum_{k < cn} \binom{n}{k} \leq n \binom{n}{cn} \\ &\leq \frac{n(ne)^{cn}}{(cn)^{cn}} = n\left(\frac{e}{c}\right)^{cn} =: t_n. \end{aligned}$$

If $M(x) = \sum m_n x^n$, then this means that $t_n m_n \geq g_n$, so that $m_n \geq g_n/t_n$. Hence,

$$1/r(M) = \limsup_{n \to \infty} m_n^{1/n} \geq \limsup_{n \to \infty} (g_n/t_n)^{1/n} = \frac{\limsup_{n \to \infty} (g_n)^{1/n}}{\lim_{n \to \infty} (t_n)^{1/n}} \geq (c/e)^c / r(G).^1$$

[1]The power of $1/n$ on $\limsup_{n \to \infty} (g_n)$ is missing in the original proof of Bender *et al.*

By the prior lemma, $r(H)^k = r(G)^k(1 + r(G)^{q-1})$ so that

$$r(H)/r(M) \ \geq (1 + r(G)^{q-1})^{1/k}(c/e)^c.$$

As there are fewer than 12^n planar maps with n edges [10], a trivial bound on the coefficients h_n of $H(x)$ is $h_n \leq (12^n)(\kappa^{n/2})$ where $\kappa \geq 1$ is the size of the set of decorations on the vertices of the diagram (in the scope of this paper, $\kappa = 2$ or 1). This provides the bound $r(H)^k \geq 1/(12\sqrt{\kappa})^k$. Then, as $\lim_{c\to 0^+}(c/e)^c = 1$ and $r(G)^k(1 + r(G)^{q-1}) = r(H)^k \geq 1/(12\sqrt{\kappa})^k$ so that

$$r(G) \geq 1/(12\sqrt{\kappa}(1 + r(G)^{q-1})^{1/k}) \geq 1/(24\sqrt{\kappa}),$$

it follows that $r(H)/r(M) > 1$ for sufficiently small c, completing the proof of the theorem. □

The conclusion is about radii of convergence of two power series; application of the Cauchy-Hadamard theorem, together with one additional hypothesis, gives the stronger result:

Theorem 4.5 (Pattern Theorem; [11])**.** *Suppose that for the class $\mathscr{M}$ and the tangle Q all of the hypotheses of Theorem 4.3 apply. Additionally suppose that $\mathscr{M}$ grows smoothly, i.e. that, with $m_n = |\mathscr{M}_n|$, the limit $\lim_{n\to\infty} m_n^{1/n}$ exists.*

Then there exists constants $c > 0$ and $d < 1$ and $N > 0$ so that for all $n \geq N$, we have that the number of diagrams m_n and the number h_n of such diagrams which contain fewer than cn copies of the tangle Q obey;

$$\frac{h_n}{m_n} < d^n.$$

I.e., the tangle Q is ubiquitous.

Because of Euler's formula, the number of vertices, edges, or faces in a link shadow or planar quadrangulation is entirely determined by choosing any one cardinality. Hence, we can size shadows and diagrams by the number of vertices and still keep the above results.

4.2 Smooth growth

In order for the (stronger) corollary to hold, we require that the class of diagrams *grow smoothly*, *i.e.* that (for $m_n = |\mathscr{M}_n|$) the limit

$$\lim_{n\to\infty} m_n^{1/n}$$

exists.

The key in proving this behavior is the strengthening of Fekete's lemma [87, 110] reproduced below:

Theorem 4.6 (Wilker-Whittington 1979 [110])**.** *Let $f(m)$ be a function with $\lim_{m\to\infty} m^{-1}f(m) = 1$ and $\{a_n\}$ be a sequence. Suppose that $a_n a_m \leq a_{n+f(m)}$ for all n, m sufficiently large and that $a_n^{1/n}$ is bounded above (for all of our cases we have the trivial bound for all planar maps of 144). Then*

$$\lim_{n\to\infty} {a_n}^{1/n} = \limsup_{n\to\infty} {a_n}^{1/n} = 1/r < \infty$$

where r is the radius of convergence of the series $\sum_{n=1}^{\infty} a_n z^n$ and furthermore $a_n \leq (1/r)^{f(n)}$.

For $f(m) = m$ we recover the usual result. Observe as well that functions $f(m) = m + k$ satisfy the hypothesis for fixed k.

4.3 The Pattern Theorem for rooted link diagrams

As noted, the classes $\mathcal{L}$ of rooted link shadows and $\mathcal{PL}$ of rooted prime link shadows have been counted exactly; they both hence grow *smoothly*. Pattern theorems for these two classes hence follow given satisfactory tangle diagrams P and attachment operations.

4.3.1 Rooted link diagrams

For the class of all rooted link shadows and *any* two-leg-prime 1-tangle diagram P, the connect summation with P is a viable attachment, *c.f.* Proposition 4.1. Hence we conclude

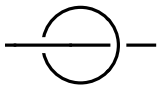

(a) A tangle diagram Φ which can be attached into diagrams in $\mathcal{L}$ by connect sum.

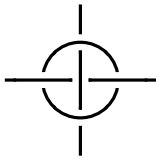

(b) A tangle diagram X which can be attached into diagrams in $\mathcal{PL}$ by crossing replacement.

Figure 4.2: Examples of tangle diagrams for attachment to link diagrams.

that asymptotically almost surely any two-leg-prime tangle diagram P is contained linearly often in an arbitrary link diagram D.

From this we see that:

Proposition 4.7. *Almost every rooted link diagram has more than one component. Additionally, almost every rooted link diagram is neither the unknot nor a split link of unknots. In other words there exists $d < 1$ and $N > 0$ so that for $n \geq N$,*

$$\mathbb{P}(\textit{a rooted link diagram } L \textit{ with } n \textit{ crossings has one component}) < d^n,$$

$$\mathbb{P}(\textit{a rooted link diagram } L \textit{ with } n \textit{ crossings represents the unknot}) < d^n,$$

and

$$\mathbb{P}\left(\begin{array}{c}\textit{a rooted link diagram } L \textit{ with } n \textit{ crossings} \\ \textit{represents a split link of unknots}\end{array}\right) < d^n.$$

Proof. Consider the attachment of tangle diagram Φ in Figure 4.2a. This attachment satisfies the hypotheses of Theorem 4.5 and the class of rooted link diagrams grows smoothly, so there exists $c > 0$, $d < 1$, and $N > 0$ so that for all $n \geq N$,

$$\mathbb{P}(\text{a rooted link diagram } L \text{ with } n \text{ crossings contains} \leq cn \text{ copies of } \Phi) < d^n.$$

Now, any of the conditions enumerated in the proposition would imply that the rooted link diagram with n crossings contains precisely no copies of the tangle diagram Φ; but this condition happens with probability less than d^n, providing the result. □

4.3.2 Rooted prime link diagrams

In the case of rooted *prime* link diagrams, however, connect summation with *any* nontrivial 1-tangle diagram P immediately removes the prime condition. Hence in this case we must use crossing replacement with 2-tangle diagrams that are prime, which is viable by Proposition 4.2. We can see then that:

Proposition 4.8. *Almost all rooted prime link diagrams consist of more than one component. Additionally, almost all rooted prime link diagrams are neither unknots nor split links of unknots.*

Proof. Consider the tangle diagram X in Figure 4.2b. For a rooted prime link diagram to satisfy any of the claims above, it would have to not contain a copy of X. However, X can be attached by crossing replacement into the class of rooted prime link diagrams in a way satisfying the hypotheses of Theorem 4.5. Furthermore, the class of rooted prime link diagrams grows smoothly, leaving the result. □

4.4 The Pattern Theorem for rooted knot diagrams

Unlike classes of rooted link diagrams, $\mathcal{K}$ and its subclasses often do not have exact counting formulas. Hence in these cases we not only must provide satisfactory attachment schemes for tangle diagrams, we must additionally prove smooth growth of the counting sequences.

4.4.1 Rooted knot diagrams

Provided that the tangle diagram P consists of precisely one component, Proposition 4.1 has that the class $\mathcal{K}$ of all rooted knot diagrams is closed under connect sum with P.

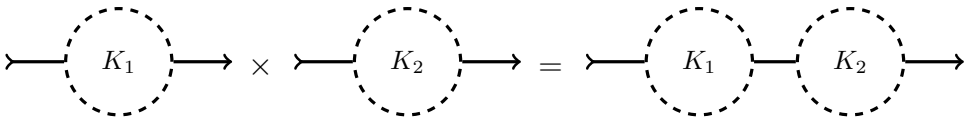

Figure 4.3: The injection from $\mathscr{K}_n \times \mathscr{K}_m$ into $\mathscr{K}_{n+m}$. The edge between K_1 and K_2 is the edge connecting the nth and $(n+1)$th crossings (by traversal order) and provides a well-defined inverse.

So it only remains to prove that the class of knot diagrams grows smoothly for pattern theorem results to follow. It suffices to prove that the class of rooted knot *shadows* grow smoothly as there exist precisely 2^n rooted knot diagrams for each rooted knot shadow of n crossings.

Theorem 4.9. *The class $\mathscr{K}$ of rooted knot shadows grows smoothly. That is, the limit $\lim_{n\to\infty} k_n^{1/n}$ exists and is equal to $1/r(K)$.*

Additionally, the class of reduced rooted knot shadows grows smoothly.

Proof. Observe that $k_n k_m \leq k_{n+m}$ for any pair n, m as given any two knot shadows of size n, m, say K_1 and K_2 respectively, we have the injection defined as in Figure 4.3 where the shadows are joined end-to-end. As n and m are known quantities, the separating edge between K_1 and K_2 in the product is determined, and the inverse is well defined on the image.

The result then follows by the above result on super-multiplicative sequences, with $f(m) = m$. This proof works for both the case of general knot diagrams, as well as the case of reduced rooted diagrams, as connect summation does not introduce any new isthmi. □

Proposition 4.10. *Almost every rooted (general or reduced) knot diagram is knotted. Furthermore, almost every rooted (general or reduced) knot diagram contains any 1-component, prime 1-tangle diagram P "linearly often:" For any such prime 1-tangle diagram P, there*

exists $N \geq 0$ and constants $d < 1$, $c > 0$ so that for $n \geq N$,

$$\mathbb{P}(\textit{a knot diagram } K \textit{ contains} \leq cn \textit{ copies of } P \textit{ as connect summands}) < d^n.$$

Proof. The first statement will follow immediately from the second, given a prime 1-tangle diagram corresponding to a prime knot diagram which is not an unknot such as the prime trefoil tangle diagram T in Figure 3.11b. The second is a corollary of Theorems 4.5 and 4.9: Let P be a prime 1-tangle diagram which can be found as a connect summand of a knot diagram (*i.e.*, it has one link component). If m_n is the number of knot diagrams, then there exists $c > 0$, $d < 1$, and $N > 0$ so that for all $n \geq N$, $\frac{h_n}{m_n} < d^n$, where h_n is the number of knot diagrams which contain at most cn copies of P as connect summands. This ratio is precisely the probability in the second statement.

The proof follows for reduced rooted knot diagrams precisely the same. □

4.4.2 Rooted prime knot diagrams

We can also show that, given a prime 2-tangle diagram P with reasonable assumptions, we can obtain a pattern theorem for P inside of the class $\mathcal{PK}$ of prime knot diagrams. The viable attachment here is crossing replacement discussed earlier.

It does however remain to be shown that the class $\mathscr{PK}$ grows appropriately smoothly. We only need apply a slight modification to the prior argument.

Theorem 4.11. *The class $\mathscr{PK}$ of prime knot shadows grows smoothly.*

Proof. For any $n > 3$ a prime shadow will have *no* monogons, and we can define a composition on prime shadows as in Figure 4.4.

This operation adds precisely two vertices and is invertible on its image. We will define the inverse of a diagram D to be the diagram obtained by performing a "flat Reidemeister II move" to delete the bigon containing the arc labeled g_1 and then by deleting the edge (bc) between vertices indexed m and $m + 1$ by traversal order starting at the tail d, *if such a*

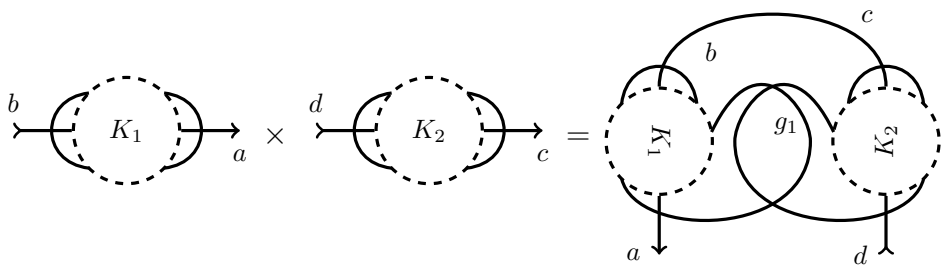

Figure 4.4: The composition × for prime shadows from $\mathscr{PK}_n \times \mathscr{PK}_m$ into $\mathscr{PK}_{n+m+2}$.

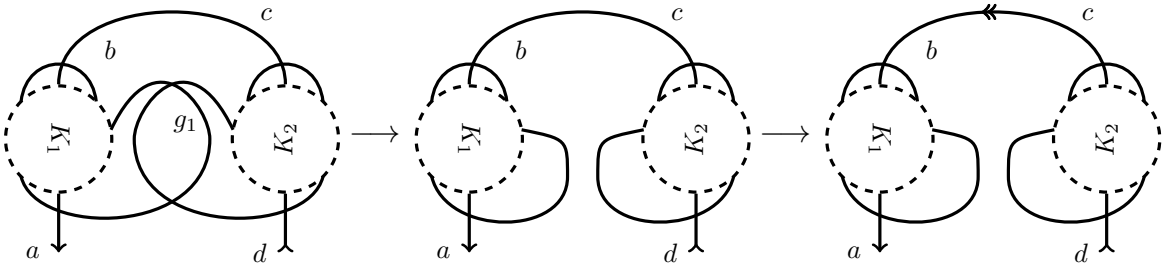

Figure 4.5: The inverse of the composition × for prime shadows. If the map is in the image of ×, the arc g_1 uniquely determines the bigon to remove, and the disconnecting edge (bc) is determined.

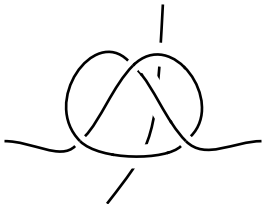

Figure 4.6: A prime 2-tangle diagram whose insertion into a diagram guarantees knottedness, as it adds a 3_1 connect sum component.

diagram exists and is valid. This process is depicted in Figure 4.5. This inverse proves that

$$p_n p_m \leq p_{n+f(m)},$$

where $f(m) = m + 2$. This, together with the above theorem on super-multiplicativity completes the proof. □

Hence,

Proposition 4.12. *Almost every rooted prime knot diagram is knotted. Furthermore, almost every rooted prime knot diagram contains any 2-component, prime 2-tangle diagram P "linearly often:" For any such prime 2-tangle diagram P, there exists $N \geq 0$ and constants $d < 1$, $c > 0$ so that for $n \geq N$,*

$$\mathbb{P}(\textit{a prime knot diagram } K \textit{ contains} \leq cn \textit{ copies of } P) < d^n.$$

Proof. The proof of the latter statement is nearly identical to that of Proposition 4.10, except with crossing replacement instead of connect summation. A 2-tangle diagram whose insertion guarantees that a diagram be knotted is depicted in Figure 4.6, from which the former statement follows. □

Chapter 5

Experimental Data

Using Schaeffer's bijection for maps and trees in Section 2.5.2 we can produce an algorithm for the uniform sampling of rooted knot diagrams. With this, we can explore knotting probabilities well beyond our tabulation data in Section 3.4. Of course, the tabulation data accounted for symmetry—how do the two models compare? Our pattern theorem answers this in the large crossing limit; most diagrams have no symmetry, and hence any results hold (probabilistically) for the unrooted case.

5.1 Asymmetry of diagrams

Richmond and Wormald [89] proved that "almost all maps are asymmetric", provided the class of maps has a pattern theorem. Indeed, this theorem applies to classes of shadows considered in this paper. Notice then that classes of diagrams then too are asymmetric as decoration imposes additional constraints on symmetry. In this section we provide explicit constructions proving this result.

Say a tangle shadow P is *free* in a class of rooted knot shadows $\mathscr{C}$ if any knot shadow obtained by removing a copy P_1 of P from a shadow K so that any cyclic composition $(K \setminus P_1)\#_\mu P$ is in $\mathscr{C}$.

We then restate Richmond and Wormald's result as it pertains to shadows:

Theorem 5.1 (Richmond-Wormald 1995)**.** *Let $\mathscr{C}$ be a class of rooted shadows. Suppose that there is a tangle shadow P such that for all shadows in $\mathscr{C}$, all copies of P are pairwise disjoint and such that P*

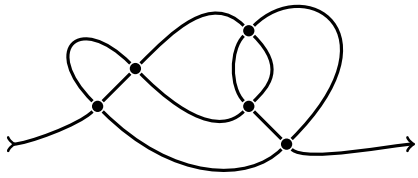

Figure 5.1: The (prime, reduced) 1-tangle shadow P which shows that knot shadows are asymmetric.

1. *has no reflective symmetry in the plane,*

2. *satisfies the hypotheses for the Pattern Theorem 4.5 for $\mathscr{C}$, and*

3. *is free in $\mathscr{C}$*

Then the proportion of n-crossing shadows in $\mathscr{C}$ with nontrivial automorphisms (that need not preserve neither root nor orientation of the underlying surface) is exponentially small.

It has been suggested without proof in [28, 95] that classes of knot shadows are almost surely asymmetric. We can now prove these results for $\mathscr{K}$ and $\mathscr{PK}$ by providing appropriate tangle shadows P.

Proposition 5.2. *The proportion of knot shadows in $\mathscr{K}$ with nontrivial automorphisms is exponentially small. Additionally, the proportion of knot diagrams in $\mathcal{K}$ with nontrivial automorphisms is exponentially small.*

This is true for reduced knot shadows as well.

Proof. Let P be the 1-tangle shadow in Figure 5.1. P is a viable candidate for the Pattern Theorem for knot shadows under connect sum attachment.

Furthermore P has no reflective symmetry by inspection, and any of the ways of attaching P keep the object in the class of knot shadows (as P is a 1-tangle shadow consisting of one component). This proves that knot shadows are asymmetric. The proof for reduced knot shadows is identical. □

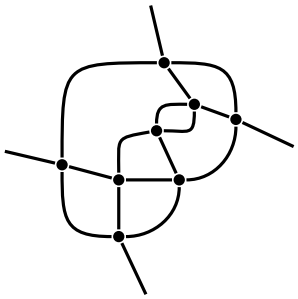

Figure 5.2: Choice of 2-tangle shadow P for proving that prime knot shadows are asymmetric.

Proposition 5.3. *The proportion of prime knot shadows in $\mathscr{PK}$ with nontrivial automorphisms is exponentially small. Additionally, the proportion of knot diagrams in $\mathcal{PK}$ with nontrivial automorphisms is exponentially small.*

Proof. Take P as in Figure 5.2. Then P consists of exactly two link components and is of blue-red-blue-red type; any way of replacing a vertex in a knot shadow with a 2-tangle shadow of blue-red-blue-red type keeps the number of link components constant and hence is free. Furthermore, P satisfies the hypotheses for Theorem 4.10 together with crossing replacement. Finally, asymmetry of P proves the claim. □

Application of the above theorems provides us with the following corollary which enables us to transfer any asymptotic numerical results or sampling results on rooted diagrams to unrooted diagrams.

Corollary 5.4. *Let L be a uniform random variable taking values in the space $\mathcal{K}_n$ or $\mathcal{L}_n$. Then there exist constants $C, \alpha > 0$ so that $\mathbb{P}(\operatorname{aut} L \neq 1) < Ce^{-\alpha n}$. Hence, rooted diagrams behave like unrooted diagrams and there are a.a.s. $4n$ rooted diagrams to each unrooted diagram.*

Indeed, link diagrams with n vertices are dual to quadrangulations with $n+2$ faces; there are $n+2$ ways of choosing the "exterior" root face and then 4 ways of rooting the edges

around this chosen face. Hence if $\tilde{\ell}_n$, $\tilde{k}_n$ are the counts of unrooted link or knot diagrams we have that in the limit,

$$\tilde{\ell}_n \underset{n\to\infty}{\sim} \frac{\ell_n}{4(n+2)} \text{ and } \tilde{k}_n \underset{n\to\infty}{\sim} \frac{k_n}{4(n+2)}.$$

5.2 Sampling random diagrams

We have added to the space curve and knot diagram toolkit `plCurve` [9] new routines for sampling and inspecting (random) knot diagrams. We describe in this section the functionality which was added—and how it was applied to generate data for the following section.

Gilles Schaeffer's `PlanarMap` software [94] is able to uniformly sample in $O(n)$ time many different classes of maps including both rooted 4-valent planar maps (rooted link shadows) and rooted 4-connected 4-valent planar maps (rooted prime link shadows) by using a bijection between maps and objects called *blossom trees* [95, 93] discussed prior in Section 2.5.2.

We have incorporated `PlanarMap` as a library into `plCurve`. This has enabled functionality in `plCurve` to uniformly sample rooted link diagrams (resp. rooted prime link diagrams) with n crossings by:

1. Sample a rooted link shadow (resp. rooted prime link shadow) with the aid of `PlanarMap` uniformly in $O(n)$ time. (Additional details on how `PlanarMap` does this, especially in the context of plane curves, can be found in [95].)

2. Sample a sign vector in $\{+,-\}^n$ uniformly. This information, together with the link shadow sampled in the step prior, uniquely yields a rooted link diagram or rooted prime link diagram sampled uniformly from the set of n-crossing rooted link diagrams or n-crossing rooted prime link diagrams, respectively.

As the condition of being a knot diagram or shadow is independent of choice of sign, we can furthermore introduce after step 1 a rejection of all shadows with more than 1 link component. Rejection does not affect the probabilities which with valid diagrams are sampled,

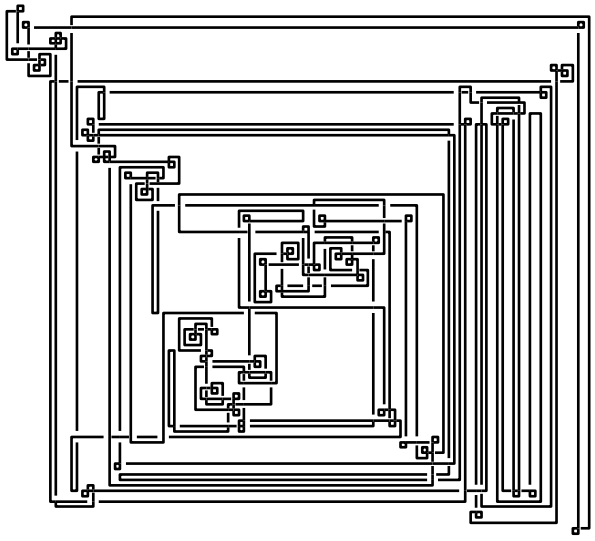

Figure 5.3: A randomly sampled knot diagram with 150 crossings, presented in a particular orthogonal projection. The drawing itself was produced using `PLink`.

and hence this augmented procedure uniformly samples rooted *knot* diagrams (resp. rooted prime *knot* diagrams).

Culler and Dunfield's `PLink` software [30] is able to produce images of knot and link diagrams using an orthogonal projection routine. This enables one to visualize individual diagram objects. There are two important caveats to this visualization:

1. Currently, `PLink` does not support rooting of edges.

2. `PLink` can produce a number of geometrically different embeddings for any given diagram object, all of which are combinatorially equivalent.

The `plCurve` software has an interface to `PLink` which enables viewing graphical representations of the diagrams sampled. An example of such a knot diagram with 150 crossings is presented in Figure 5.3.

The data below was gathered from the following experiments:

1. First, for each $10 \leq 5n \leq 60$, we attempted to gather 500,000 uniform n-crossing rooted knot diagram samples, with 49 tries to sample a knot diagram per sample. This means that for each of the 500,000 calls to sample a rooted knot diagram, we generated at most 49 rooted link shadows, rejecting shadows until either a) a rooted knot shadow was sampled, or b) 49 unsuccessful attempts were made. This data is exhibited in Figures 5.4a, 5.5, and 5.7a.

   We further sampled precisely 20,000 diagrams for all $65 \leq 5n \leq 100$ for the curve fitting data in Figure 5.8, Table 5.1, and Figure 5.9.

2. A similar experiment was run, for all $5 \leq 5n \leq 60$ with 49 attempts, except we sampled rooted prime knot diagrams by rejection sampling on rooted prime link diagrams as described above. This data is exhibited in Figures 5.4b, 5.6, and 5.7a.

3. To detect the ratios of knot diagrams to link diagrams, another experiment was run wherein for each $10 \leq n \leq 65$, we sampled uniformly 100,000 rooted link diagrams. The same was done for rooted prime link diagrams. This data is the basis for Figure 5.7b.

Knots were classified by their HOMFLY polynomial, which distinguishes knots of the types studied $(0_1, 3_1, 4_1, 5_1, 5_2, 3_1\#3_1)$ for diagrams of low crossing number. HOMFLY polynomials are computed for diagrams using the software `lmpoly` of Ewing and Millett [42] implemented within `plCurve`. For larger diagrams, the HOMFLY polynomial is not necessarily a complete invariant. However, these clashes are expected to be rare and hence immaterial for the analysis that follows. As discussed prior, it is believed at least that the HOMFLY polynomial distinguishes the unknot; a counterexample would disprove the Jones Conjecture, and would be a monumental discovery by itself[1].

We note additionally that our data ignores chirality of knot types: The knot types $3_1, 5_1, 5_2$ admit both left- and right-handed chiralities (which are distinguished by the HOMFLY polynomial), but the chirality is ignored as the probability of the two mirror-images are

[1] A recent paper of Tuzun and Sikora has verified the conjecture up to 22 crossings [106], so our data on the unknot is accurate at least up to and including $n = 22$.

identical in the diagram model. Finally, under the composite knot type $3_1\#3_1$ is data for both the granny knot, its mirror image, and the square knot, all of whom have equal probability as well. As a result, the granny knot (of either chirality) is immediately twice as likely as the square knot.

5.3 Knotting in large random diagrams

A typical concern with results on asymptotic behavior is whether it only applies to knot diagrams with an absurd number of crossings. This is common when discussing physical knotting—most polymers are not infinitely long and hence exhibit only finite complexity! However, exact and numerical results show that the asymptotic behavior we have discussed (namely the FWD conjecture) is actually attained very quickly.

5.3.1 Asymmetry in diagrams

A critical example of this is that almost all 10-crossing knot diagrams have no nontrivial automorphisms. This is exhibited in Figure 5.4, where knot diagrams with at least 8 crossings and prime knot diagrams with at least 13 crossings have nearly no symmetries. Hence while it is infeasible to sample unrooted knot diagrams by enumeration, by Corollary 5.4 sampling rooted knot diagrams is greatly effective.

5.3.2 Knotting in diagrams

We will now consider relative appearances of various knot types among knot diagrams. This expands beyond our results in Section 3.4. Although we no longer have *exact* numerics, we can break past the 10-crossing barrier with relative ease and good precision. Compare the chart in Figure 5.5 to Figure 3.15 in Section 3.4 and Table III in [20].

Of note is the exponential decay of the proportion of unknots 0_1 as the number of crossings grow large. In fact, data shows that the number of (both left- and right-) trefoils 3_1 exceeds that of the unknot 0_1 at around $n = 44$ crossings. Additionally, the trend for the square

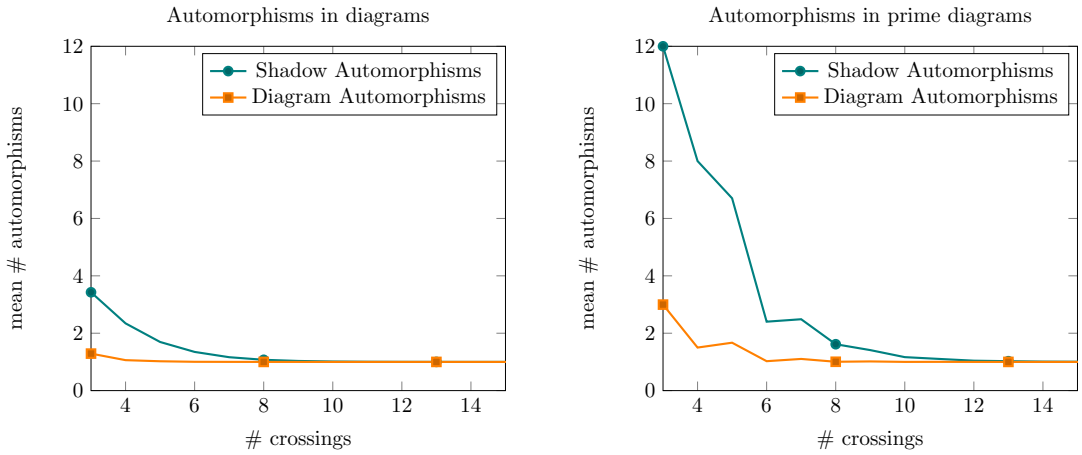

(a) Nearly all rooted knot diagrams of 8 or more crossings have no automorphisms.

(b) Nearly all rooted prime knot diagrams of 13 or more crossings have no automorphisms.

Figure 5.4: Automorphisms in knot diagrams decrease exponentially quickly.

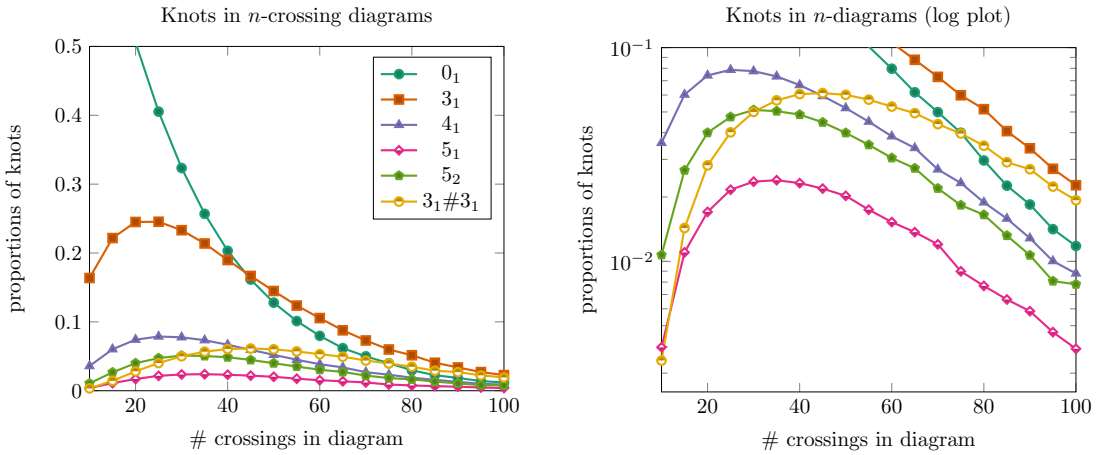

Figure 5.5: Probabilities of some typical knot types as the number of crossings varies from $n = 10$ to $n = 100$.

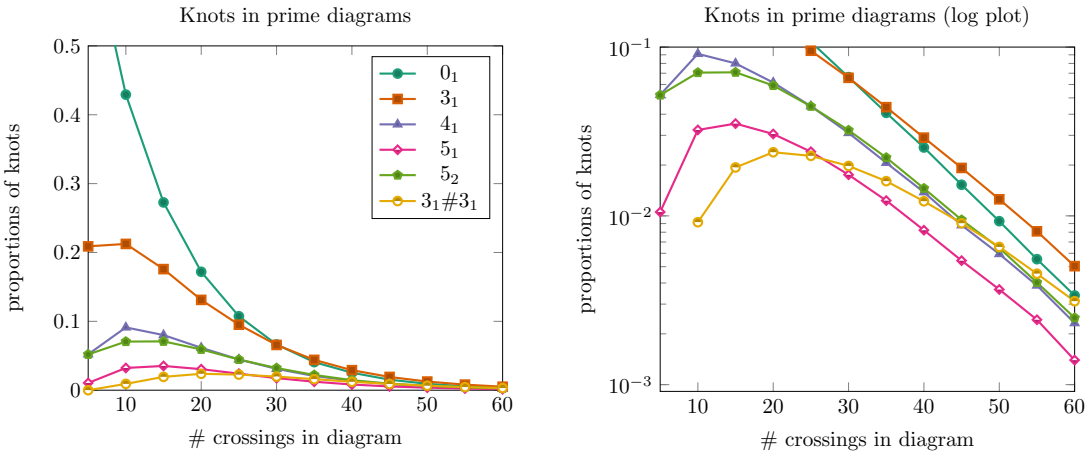

Figure 5.6: Probabilities of some typical knot types in prime diagrams as the number of crossings varies from $n = 5$ to $n = 60$.

and granny knots, labeled $3_1\#3_1$, has it decaying at a far slower rate than any of the prime knot types. This is in line with conjectures for models of random knots that the growth rates of knot types K should accrue an additional polynomial growth factor of n for each prime knot type in the decomposition of K [88]. Also of note is the so-called "$5_1, 5_2$ inversion," where the knot 5_2 is more likely than the torus knot 5_1. This was exhibited in the earlier exact data of [20] and persists through the entire scope of the data gathered. We present a more thorough examination of this data with comparisons to other models in the following Section 5.3.3.

Our rejection sampling methods additionally apply in the case of sampling knot diagrams with different graph-theoretic constraints. For instance, it extends to provide a sampler for prime knot diagrams, which have underlying map structure which is 4-edge connected. As dictated by Proposition 5.3, the number of asymmetries of prime knot diagrams tends to zero exponentially quickly as in Figure 5.4. We also present data for the proportions of knots in prime diagrams in Figure 5.6. While the precise numerics differ, notice that prime diagrams exhibit the same interesting behavior as generic diagrams discussed prior. Namely,

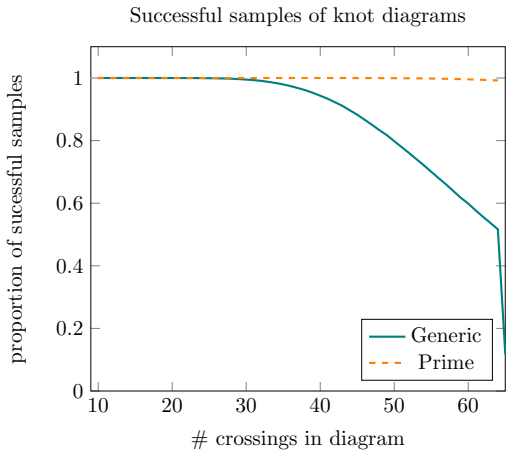

(a) Number of successful samples for diagrams in gathering the above data. For each of 500,000 samples, a maximum of 49 attempts is made to generate a knot diagram, and if unsuccessful, the sample is discarded.

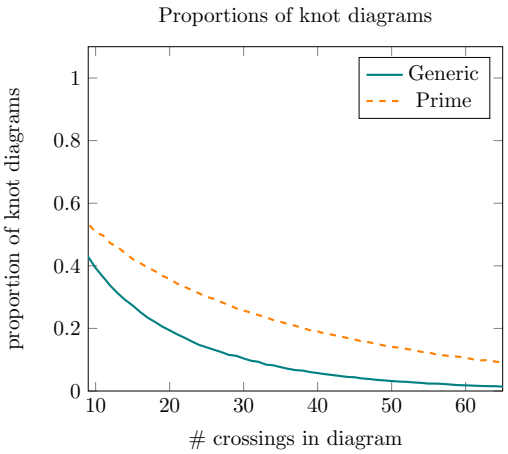

(b) Ratio of knot diagrams to link diagrams in the generic and prime cases. Data was gathered by sampling 100,000 link diagrams and counting the number of samples with precisely one link component.

Figure 5.7: The exponential decay of knot diagrams among link diagrams makes rejection sampling more difficult as the number of crossings increases.

(1) unknots are exponentially rare and become less prevalent than trefoils (albeit sooner in the case of prime diagrams, occurring at around $n = 30$ crossings), (2) the composite square and granny knots show slower decay than knots of prime type, and (3) the $5_1, 5_2$ inversion.

An observation from running the above experiments is that knot diagrams appear to be more prevalent in prime diagrams than generic knot diagrams! Indeed, nearly all rejection samples of prime knot diagrams are successful (see Figure 5.7a) as opposed to the 50% success rate of sampling generic diagrams of 64 crossings. A more precise computation of the proportion of knot diagrams to link diagrams is exhibited in Figure 5.7b, where we can see that there is indeed a far greater proportion of knot diagrams in the prime diagram case to the generic, at least up to 65 crossings. Fitting the curve $k_n/\ell_n = C\mu^n n^\alpha$ to each of these data sets yields $C = 1.26 \pm 0.01, \mu = 0.9503 \pm 0.0002, a = -0.287 \pm 0.005$ in the generic case and $C = 0.99 \pm 0.03, \mu = 0.9749 \pm 0.0006, a = -0.17 \pm 0.01$ in the prime case. In the

generic case, multiplying by the (known) number of link shadows yields that the exponential growth of knot shadows is approximately $12\mu = 11.404 \pm 0.0024$ close to that of prior work of Jacobsen and Zinn Justin [56] discussed in Section 3.1.2 and that the power law growth term is $a - 5/2 = -2.287 \pm 0.005$. This differs from the conjectured value of $-\frac{1+\sqrt{13}}{6} - 2 \approx -2.67$, and suggests that further data is required for an adequate fit. Applying the same analysis to the prime case yields that the exponential growth rate of prime knot shadows should be $24\mu = 23.40 \pm 0.0145$ and the power law growth term to be $a - 5/2 = -2.67 \pm 0.01$, which agrees rather well with Schaeffer and Zinn Justin's conjectured value of $-\frac{1+\sqrt{13}}{6} - 2 \approx -2.67$.

Hence it is worth summarizing these interesting properties of the prime knot diagram model. First, prime link diagrams admit exact enumeration like general link diagrams and are hence easy to sample. In addition, there is a higher success rate of sampling knot diagrams inside of prime diagrams as opposed to general diagrams. Second, the difficulty of inserting "boring" structure into prime knot diagrams suggests that there is far more variety in the knot types which arise than in the general case. So, prime diagrams are a natural class to find diagrams representing exotic knot types with large minimum crossing number. Some evidence to this is the fact that *alternating*, prime knot diagrams are minimal in that they have the fewest number of crossings over all diagram representations of their knot type. Finally, the smaller size of the class of prime diagrams (as opposed to the general case) suggests that fewer samples may be required to have a better statistical understanding of the space.

5.3.3 Expected behavior and comparisons to other models

As noted by many prior authors [102, 88], it is expected that, for a fixed knot type $[K]$ with a factorization into $N_{[K]}$ components, the probability $p_n([K])$ that a knot diagram of n crossings is of type $[K]$ obeys asymptotically

$$p_n([K]) = C_{[K]}\mu_0^n n^{\alpha-3+N_{[K]}}$$

for a constant $C_{[K]}$ depending on $[K]$, and constants μ_0, and α which are expected to be independent of $[K]$. For the various knot-type probability data gathered in Figure 5.5 above,

Table 5.1: Parameters for the curve fits in Figure 5.8. Compare, *e.g.*, to Table II in [102] which presents similar data for the model of Gaussian random polygons.

Knot type $[K]$	$C_{[K]}$	μ_0	α
0_1	1.026 ± 0.009	$(9.524 \pm 0.002) \times 10^{-1}$	3.090 ± 0.004
3_1	$(1.32 \pm 0.08) \times 10^{-2}$	$(9.434 \pm 0.008) \times 10^{-1}$	3.36 ± 0.03
4_1	$(1.1 \pm 0.1) \times 10^{-3}$	$(9.36 \pm 0.02) \times 10^{-1}$	3.85 ± 0.06
5_1	$(1.4 \pm 0.4) \times 10^{-5}$	$(9.23 \pm 0.03) \times 10^{-1}$	4.9 ± 0.1
5_1, $n \geq 30$	$(1.1 \pm 0.3) \times 10^{-4}$	$(9.38 \pm 0.02) \times 10^{-1}$	4.15 ± 0.09
5_2	$(6 \pm 1) \times 10^{-5}$	$(9.24 \pm 0.03) \times 10^{-1}$	4.7 ± 0.1
5_2, $n \geq 30$	$(4.7 \pm 0.9) \times 10^{-4}$	$(9.41 \pm 0.01) \times 10^{-1}$	3.92 ± 0.07
$3_1\#3_1$	$(4 \pm 1) \times 10^{-6}$	$(9.27 \pm 0.03) \times 10^{-1}$	4.4 ± 0.1
$3_1\#3_1$, $n \geq 30$	$(2.8 \pm 0.4) \times 10^{-5}$	$(9.406 \pm 0.009) \times 10^{-1}$	3.74 ± 0.05

we used `scipy`'s [58] least-squares fitting algorithm to fit a curve of the form above. For latter types, we provide two fits; one using all available data and one only using points with $n \geq 30$. These fits are presented graphically in Figure 5.8 and the parameter data is provided in Table 5.1. Universality suggests that the parameters μ_0 and α for each fit should all be close, which they appear to be.

A stronger concept of universality for random knot models discussed by Rechnitzer and Rensburg in [88] posits that among models of random knotting that although the exponential growth rate μ_0 may change, for any knot types $[K_1]$ and $[K_2]$ which decompose into the same number of prime components the ratios $p_n([K_1])/p_n([K_2])$ may be universal. While their results suggest that their conjecture holds for different lattice polygon models of knotting, our data is strong evidence that the conjecture does not extend to the knot diagram model. Fits depicted in Figure 5.9 suggest that the limiting ratios $p_n(3_1)/p_n(4_1) \approx 2.4632 \pm 0.0001$, $p_n(3_1)/p_n(5_1) \approx 4.651 \pm 0.002$, and $p_n(4_1)/p_n(5_1) \approx 1.8872 \pm 0.0004$, all of which are orders of magnitude different from the lattice model ratios of Rensburg and Rechnitzer [88].

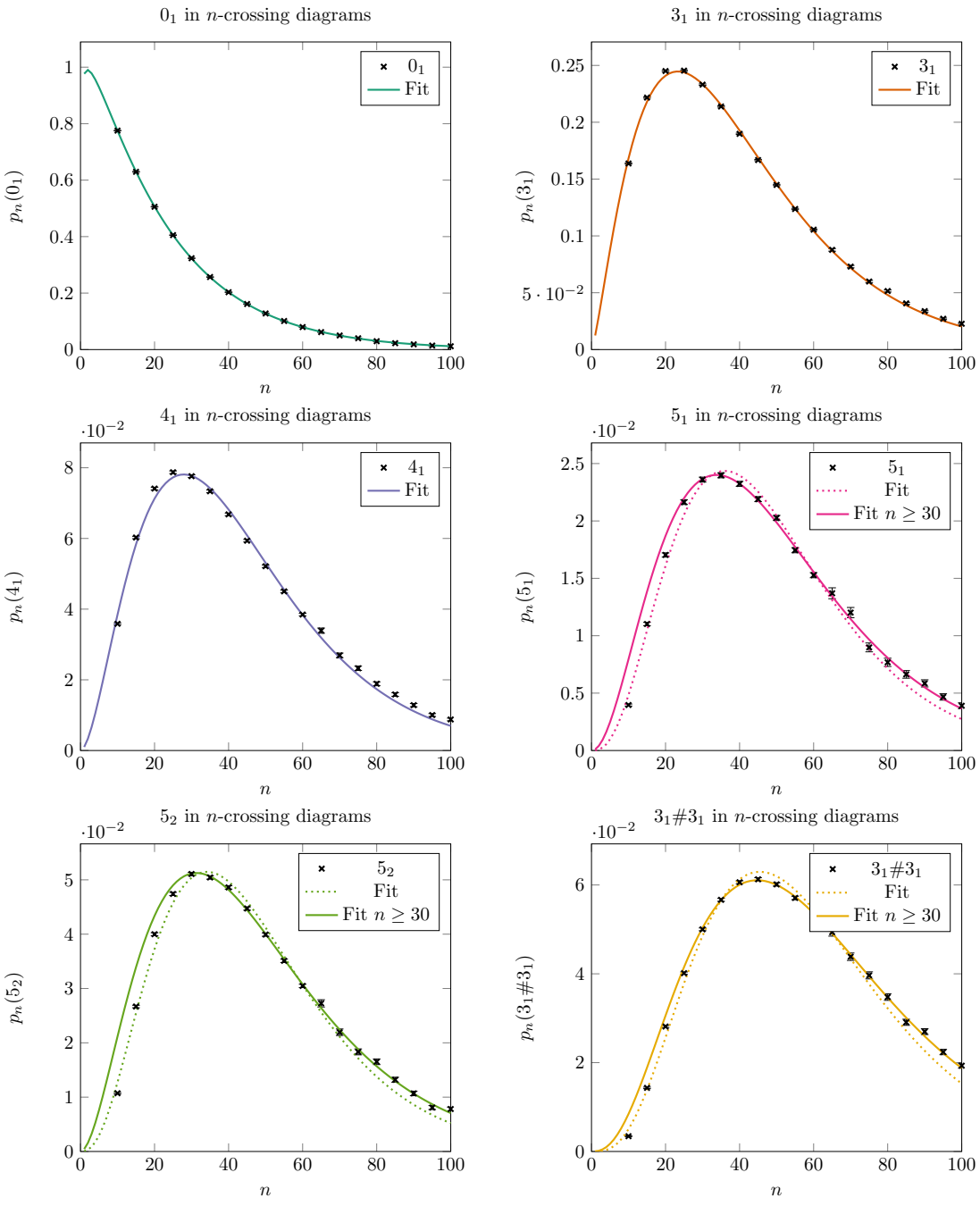

Figure 5.8: Curve fits of $p_n([K]) = C_{[K]}\mu_0^n n^{\alpha-3+N_{[K]}}$ for various knot types $[K]$. Compare, *e.g.*, to Figure 9 in [102] which presents similar data for the model of Gaussian random polygons.

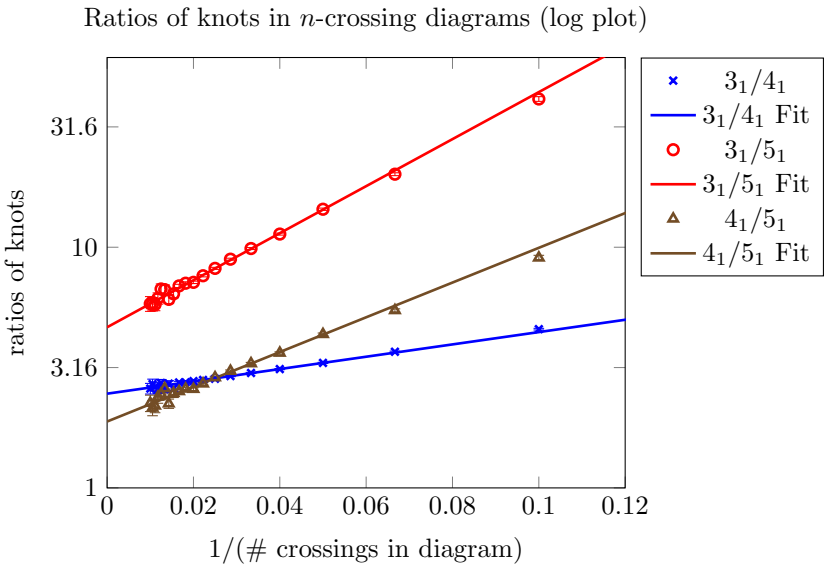

Figure 5.9: Fitting the curves $y = ae(b/n)$ to the ratios of knotting probabilities provides estimates for the asymptotic value.

Chapter 6

Knotted Spatial Graphs

It is very simple to extend and change the diagram model in order to consider different topics in knot theory. As a demonstration, in this chapter we extend the diagram model to study knotted objects with intrinsic topology different from the circle S^1. In the following chapter we will explore an interesting case where the intrinsic topology is that of an interval.

We present now results on the general case of diagrams representing objects of fixed, 1-dimensional topology into the 3-sphere, S^3. This corresponds to the theory of knotted spatial graphs.

6.1 Definitions

By a *graph*, we mean a pair $G = (V, E)$ of unlabeled *vertices* and *edges*, where an edge is one of:

1. An unordered pair (v_1, v_2) of vertices representing a path between v_1 and v_2; v_1 and v_2 need not be distinct (edges can be loops).

2. A single (v_1), corresponding to an edge which is connected to a vertex at only one end (and is loose at the other); this type of edge is a loose edge.

3. An interval I which is not connected to any vertices.

4. A closed circle O which is not connected to any vertices.

A graph can have duplicate edges (it is actually a *multi*-graph). Graphs need not be connected. An example of such a graph is given in Figure 6.1. Finally, we will assume that any such graph G has at least one edge and only vertices with at least one edge connection.

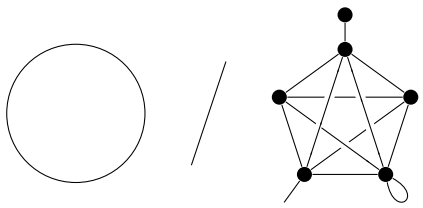

Figure 6.1: An example graph which is a union of three connected components.

Definition 6.1. A *spatial graph* is an embedding γ of a graph G into the 3-sphere S^3.

Knots and links are easily seen to be special cases of spatial graphs. As in these cases, we can consider embeddings of arbitrary spatial graphs up to *ambient isotopy*. We will call an equivalence class of embeddings $[\gamma]$ of a graph G under ambient isotopy a *knot type* for G.

Let $\sim$ be the coloring equivalence relation on arcs given in Section 3.1.2. Let $M = (A, E, V \cup C)$ be a map with two distinct types of vertices, *vertices* (which may be of any degree) and *crossings* (which are all 4-valent). Extend $\sim$ to the arcs of this map by only applying at crossings and edges (*not* vertices). Then the following is true about the set $R = A/\sim$ of *meta-edges* of M: There are four possibilities for a meta-edge $[a]$ in R, lining up with the types of edges in the definition of graph above:

1. Among the arcs in $[a]$, there are *exactly* two arcs which are attached to vertices v_1, v_2 in V (v_1 and v_2 may be the same vertex). Furthermore, all arcs in $[a]$ are contained in edges of E. In this case we say that the meta-edge $[a] = [v_1, v_2]$ connects v_1 and v_2.

2. There is exactly one arc in $[a]$ attached to a vertex v_1 in V, and exactly one arc in $[a]$ which contained in any edge in E. In this case, we say the meta-edge $[a] = [v_1]$ is connected to the vertex v_1 and corresponds to a loose edge.

3. There are no arcs in $[a]$ attached to a vertex in V, and there are two arcs which are not contained in any edge in E. This meta-edge corresponds to an interval-type edge.

4. There are no arcs in $[a]$ attached to a vertex in V, and all arcs of $[a]$ are contained in an edge in E. This meta-edge corresponds to a closed circle-type edge, and is precisely a link component as defined prior.

Definition 6.2. Let $G = (E_G, V_G)$ be a graph. A *spatial graph shadow* of n crossings for G is a planar map $M = (A, E, V \cup C)$ of arcs A, edges E, vertices V, and n crossings C so that there are one-to-one correspondences $\nu : V \to V_G$ and $\eta : R \to E_G$ with the property that:

1. For a meta-edge $[v_1, v_2] \in R$, $\eta([v_1, v_2]) = (\nu(v_1), \nu(v_2))$.
2. For a meta-edge $[v_1] \in R$, $\eta([v_1]) = (\nu(v_1))$.
3. ν bijectively maps interval-type meta-edges to interval-type edges in E_G.
4. ν bijectively maps closed circle-type meta-edges to closed circle-type edges in E_G.

Let $\mathscr{K}(G) = \bigcup \mathscr{K}_n(G)$ represent the class of spatial graph shadows for G.

A *spatial graph diagram* for G is a spatial graph shadow together with a mapping $C \to S$ of crossing signs. As usual, we will primarily consider $S = \{+, -\}$. Let $\mathcal{K}(G) = \bigcup \mathcal{K}_n(G)$ represent the class of spatial graph diagrams for G.

Spatial graph shadows and diagrams are *rooted* if additionally they have a marked *root* arc. As in previous cases, all diagrams will be rooted unless otherwise noted.

If in addition to the classical Reidemeister moves we consider the three additional moves in Figure 6.2, then there is a one-to-one correspondence between ambient isotopy classes of embeddings of a graph G and equivalence classes of spatial graph diagrams for G.

Just as our knot shadows are dual to a subclass of quadrangulations of the sphere, for a fixed graph G, the class $\mathscr{K}(G)$ is dual to a subclass of quadrangulations *with marked boundary* [12]. Similarly, there is a bijection for quadrangulations with marked boundary. Using this bijection, one could write software to sample quadrangulations with prescribed boundaries and, using rejection, uniformly sample spatial graph shadows for G. Another approach to sampling spatial graph shadows would be to use an extension of the Markov

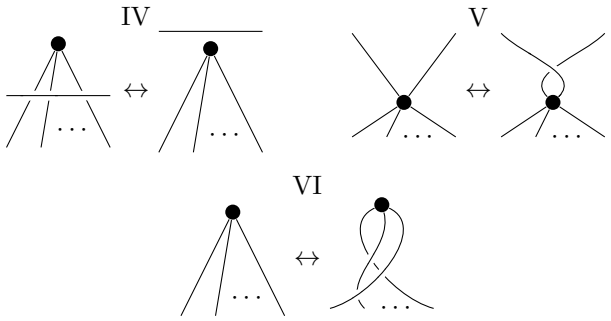

Figure 6.2: Additional Reidemeister moves for spatial graph diagrams.

chain Monte Carlo approach outlined in Chapter 9 which includes transitions (appropriately weighted) corresponding to flat versions of the spatial graph Reidemeister moves in Figure 6.2.

For a vertex v in a graph, we denote by $\deg(v)$ the *degree* of v; the number of edges which connect to v. Similarly, for a vertex or crossing x in a shadow or diagram, we denote by $\deg(x)$ the *degree* of x; the number of arcs connected to x. For a graph $G = (E_G, V_G)$ with total vertex degree $d = \sum_{v \in V_G} \deg(v)$, an spatial graph shadow or diagram with n crossings has precisely $d + 4n$ arcs and hence at most $(d + 4n)/2$ edges.

6.2 Pattern theorems for spatial graph diagrams

We can now leverage the machinery of Chapter 4 to gain insight on the asymptotic behavior of knotted spatial graphs. First, we have that:

Proposition 6.1. *Let G be a graph. For a prime tangle diagram Q of one open strand, edge replacement is a viable attachment into $\mathcal{K}(G)$.*

Proof. The proof is nearly identical to that for Proposition 4.1. In the proof of property (1), notice that there must be at least n edges in an n-crossing spatial graph diagram for G. In the proof of property (2), notice that edge replacement of Q fixes the meta-edges R of any diagram $D \in \mathcal{K}(G)$. □

With this in hand, we are able to prove a weak pattern theorem for spatial graph diagrams for a graph G:

Corollary 6.2. *Let G be a graph and let Q be a prime tangle diagram of one open strand. Let $M(x)$ be the generating function by the number of edges for $\mathcal{K}(G)$. Let $H(x)$ be the generating function by the number of edges for those diagrams D in $\mathcal{K}(G)$ that contain less than $ce(D)$ pairwise disjoint copies of Q; call this class $\mathscr{H}$. Suppose there is a viable attachment for Q into $\mathscr{H}$. If $0 < c < 1$ is sufficiently small, then $r(M) < r(H)$. The diagrams may be rooted or not.*

Proof. This follows immediately from Theorem 4.3 and Proposition 6.1. □

For generic graphs G, we are unable to prove any smooth growth results. It is simple to prove in all cases that their growth is bounded by below:

Proposition 6.3. *Let G be a graph and let $k_n(G)$ be the count of n-crossing shadows in $\mathscr{K}(G)$. Then*

$$\mu = \lim_{n\to\infty} k_n^{1/n} \leq \liminf_{n\to\infty} k_n(G)^{1/n}.$$

Proof. Let $D = (A, E, V \cup C) \in \mathscr{K}_M(G)$ be a fixed spatial graph shadow for G with M crossings. For every knot shadow $S \in \mathscr{K}$ of m crossings, edge replacement of S into the root edge of D produces a new, unique rooted spatial graph shadow D' for G with $n = m + M$ crossings and one marked edge. The number of edges in D' is bounded, loosely, by ℓn, where $\ell = \max_{v\in(V\cup C)} \deg(v) < \infty$. Hence,

$$\frac{1}{\ell n} k_{n-M} \leq k_n(G).$$

As ℓ remains constant while n dominates, passing to the n-th root and large n limit inferior yields the result. □

We do conjecture that smooth growth properties hold;

Conjecture 6.4 (Smooth growth for spatial graph shadows)**.** *Weak: Let G be a fixed graph, and let $k_n(G)$ be the count of n-crossing diagrams in $\mathscr{K}(G)$. Then the limit*

$$\lim_{n\to\infty} k_n(G)^{1/n}$$

exists.

Strong: Furthermore,

$$\lim_{n\to\infty} k_n(G)^{1/n} = \mu.$$

For any graph G for which the weak version of conjecture can be proven, the strong pattern theorem result follows immediately:

Corollary 6.5. *Let G be a fixed graph. Suppose that for the class $\mathcal{K}(G)$ and the tangle Q all of the hypotheses of Theorem 6.2 apply. Additionally suppose that $\mathcal{K}(G)$ grows smoothly, i.e. that, the above conjecture holds.*

Then there exist constants $c > 0$, $d < 1$ and $N > 0$ so that for all $n \geq N$, we have that the number of diagrams $\kappa_n(G)$ and the number h_n of such diagrams which contain fewer than cn copies of the tangle Q obey;

$$\frac{h_n}{\kappa_n(G)} < d^n.$$

Hence for any such graph, almost all spatial graph diagrams are *knotted*, just as in the case of knots and links proper.

6.3 Smooth growth for spatial graph diagrams

There are some graphs G whose classes of shadows grow smoothly (after which the results for diagrams immediately follow). The graph $G = S^1$ grows smoothly as

$$\lim_{n\to\infty} k_n(S^1)^{1/n} = \lim_{n\to\infty} k_n^{1/n} = \mu.$$

We can extend this result to a number of different graphs.

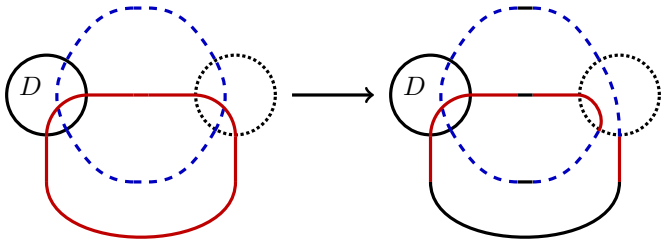

Figure 6.3: Smoothing a crossing at which two different components meet produces a new shadow with one fewer circle components.

Proposition 6.6. *Let $G = \bigcup^k S^1$ be a fixed disjoint union of $k \geq 1$ circles S^1, and let $k_n(G)$ be the count of n-crossing shadows in $\mathscr{K}(G)$. Then the limit*

$$\lim_{n\to\infty} k_n(G)^{1/n}$$

exists and is equal to $\mu = \lim_{n\to\infty} k_n^{1/n}$. That is, the class of link shadows with a fixed number k of link components grows smoothly at the same exponential rate as knot shadows.

Proof. We proceed by induction. Certainly if $k = 1$ the result is true as $k_n(G)$ is simply the number of n-crossing knot shadows.

Suppose now that for $G' = \bigcup^k S^1$ we know that $\lim_{n\to\infty} k_n(G')^{1/n} = \mu$ and let $G = \bigcup^{k+1} S^1$. As every shadow D in $\mathscr{K}_n(G)$ is connected and planar, there exists at least two crossings in D (at least one of which is not the root crossing) at which two different link components of D cross. At any one of those crossings, a smoothing as in Figure 6.3 produces a unique shadow in the class of shadows in $\mathscr{K}_{n-1}(G')$ with two marked arcs.

Hence,

$$k_n(G) \leq (4n)^2 k_{n-1}(G').$$

Passing to n-th roots and the large n limit together with Proposition 6.3 yields,

$$\mu \leq \lim_{n\to\infty} k_n(G)^{1/n} \leq \lim_{n\to\infty} k_n(G')^{1/n} = \mu,$$

proving the claim. □

With this result in hand, we can do even better;

Proposition 6.7. *Let $G = (V, E)$ be a graph such that*

1. *all edges in E are either circular link components or edges connecting two vertices in V, and*

2. *all vertices in V have even degree.*

Let $k_n(G)$ be the count of n-crossing shadows in $\mathscr{K}(G)$. Then the limit

$$\lim_{n\to\infty} k_n(G)^{1/n}$$

exists and is equal to $\mu = \lim_{n\to\infty} k_n^{1/n}$.

Proof. Once more we proceed by induction, this time on the number of vertices in G, $|V|$. The base case—a graph with no vertices and only circular link components—is covered by Proposition 6.6.

Suppose now that for graphs with $k - 1 \geq 0$ vertices all of even degree, the result holds. Consider a graph G with k vertices. Fix a vertex ν_k of degree d in G and let $D \in \mathscr{K}_n(G)$ be an spatial graph shadow for G with n crossings. Let v_k be the preimage non-crossing vertex of ν_k in D. Either smoothing the vertex (if $d = 2$), changing the vertex into a crossing (if $d = 4$), or opening up the vertex (if $d \geq 6$) v_k into $d/2$ marked crossings as in Figure 6.4 produces, for some G' with $k - 1$ vertices all of even degree (and no interval edges) a new shadow in $\mathscr{K}_{n+d/2}(G')$. Furthermore, there are at most $(d-1)!!$ choices of graph G' which can be produced from G by opening the vertex $\nu(v_k)$.

Hence,

$$k_n(G) \leq (d-1)!! \max_{G'} \{k_{n+d/2}(G')\},$$

and passing to n-th roots and the large n limit together with Proposition 6.3 yields,

$$\mu \leq \lim_{n\to\infty} k_n(G)^{1/n} \leq \max_{G'} \lim_{n\to\infty} k_n(G')^{1/n},$$

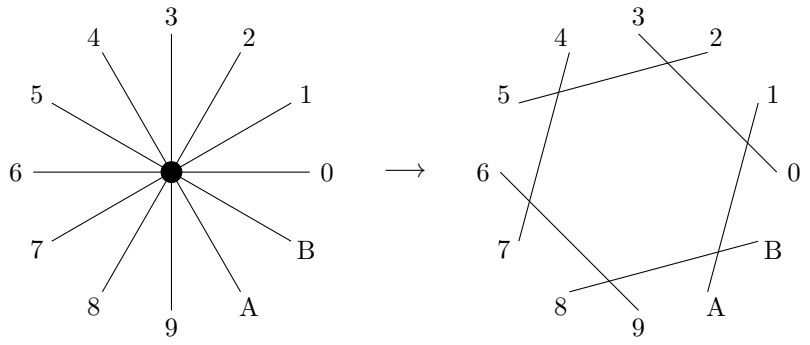

Figure 6.4: Opening up a vertex of degree $2d$ into a d-gon.

whence the inductive hypothesis yields that

$$\mu \leq \lim_{n\to\infty} k_n(G)^{1/n} \leq \mu,$$

proving the claim. □

If graphs G have either loose edges or vertices of odd degree, the issue becomes more complicated. This is a result of the unknown value of the growth rate of the graph G consisting of only an interval edge:

Proposition 6.8. *Let $G = I$ be the graph with no vertices and only an edge of interval type. Then*

$$\lim_{n\to\infty} k_n(G)$$

exists and is equal to $\mu_I \geq \mu$.

Proof. Notice that any diagram for G has *no* non-crossing vertices and *two* loose arcs which do not belong to any edge. If $D_1 = (A_1, E_1, C_1)$, $D_2 = (V_2, E_2, C_2)$ are two diagrams for G of n_1 and n_2 crossings respectively, then the following composition produces a new diagram for G with precisely $n_1 + n_2$ crossings and one additional marked arc:

Let a_1 and a_2 be loose arcs of D_1 and D_2 respectively chosen deterministically by using the root arcs r_1 and r_2. Then the diagram $D = (V_1 \cup V_2, E_1 \cup E_2 \cup \{(a_1 a_2), C_1 \cup C_2\})$ with root

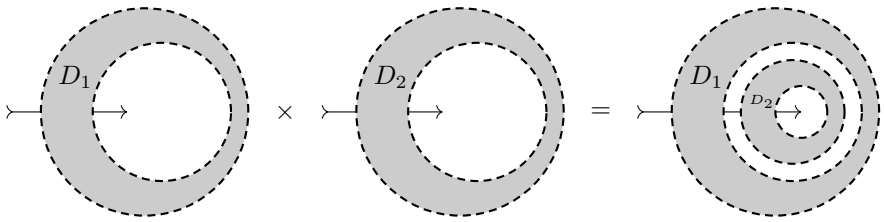

Figure 6.5: A reversible composition operation for interval diagrams.

arc r_1 and additional marked arc r_2 has $n_1 + n_2$ crossings and is a diagram for G. Furthermore, knowledge of n_1 and n_2 together with the additional marked arc provides an inverse mapping on diagrams produced this way. An example of this is given in Figure 6.5.

As there are $4n$ arcs in an n-crossing interval diagram,

$$k_{n_1}(G)k_{n_2}(G) \leq (4n)k_{n_1+n_2}(G).$$

Since k_N exhibits exponential growth by Proposition 6.3, we are guaranteed that there exists some fixed M for which

$$k_{n_1}(G)k_{n_2}(G) \leq (4n)k_{n_1+n_2}(G) \leq k_{n_1+n_2+M}(G).$$

Hence by Wilker-Whittington's theorem [110] (we still have the trivial bound on of $k_n(G)^{1/n}$ of 144), the limit

$$\lim_{n\to\infty} k_n(G)^{1/n}$$

exists, and we call its value μ_I. By Proposition 6.3, we know $\mu \leq \mu_I$. □

The value of μ_I is unknown, but based on similar models we conjecture,

Conjecture 6.9. *The exponential growth rates μ and μ_I are equivalent.*

Regardless, this growth rate μ_I is a lower bound for the growth rates of spatial graph diagrams of some graph types which do not satisfy the hypotheses for Proposition 6.7

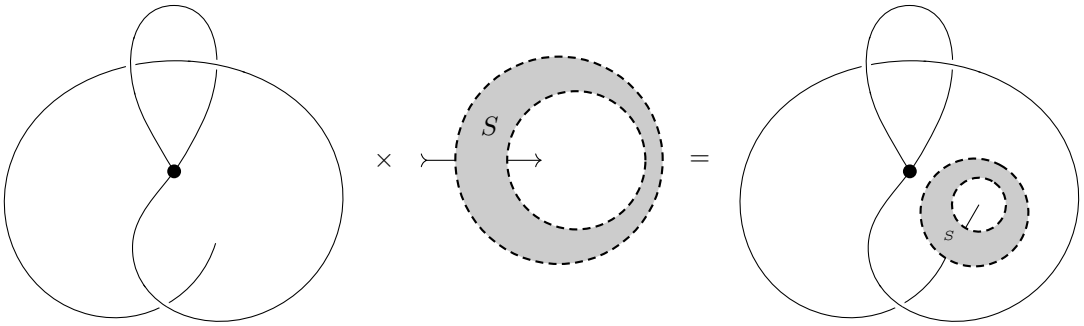

Figure 6.6: Attachment of an interval shadow into a diagram with a loose arc.

Proposition 6.10. *If G has either a vertex of degree 1, a loose edge, or an interval edge, then*

$$\mu_I \leq \liminf_{n\to\infty} k_n(G)^{1/n}.$$

Proof. Let $D = (A, E, V \cup C) \in \mathscr{K}_M(G)$ be a fixed spatial graph shadow for G with M crossings. Suppose first that G has at least one loose arc a. Let I be the graph consisting only of one interval edge. For every interval shadow $S = (A_I, E_I, C_I) \in \mathscr{K}(I)$ of m crossings with root arc r and determined loose arc b, the diagram $D' = (A \cup A_I, E \cup E_I \cup \{(ab)\}, V \cup C \cup C_I)$ with marked arc r and marked edge (ab) as depicted in Figure 6.6 is an element of $\mathscr{K}_{m+M}(G)$. Given the marked edge, this procedure is reversible, so this composition induces an injective map.

If instead G has a vertex v of degree 1, then we define a similar composition. Then D contains the non-crossing vertex (z), where the arc z is contained in an edge (az). For every interval shadow $S = (A_I, E_I, C_I) \in \mathscr{K}(I)$ of m crossings with root arc r, and a determined ordered pair of loose arcs (b, y), the diagram $D' = (A \cup A_I, E \cup E_I \cup \{(ab), (yz)\}, V \cup C \cup C_I)$ with marked arc r and marked edge (ab) is an element of $\mathscr{K}_{m+M}(G)$. Given the marked edge, this procedure is reversible, so this composition induces an injective map. Intuitively, this operation only differs from the above in that we keep track of the "cap" vertex.

Let $n = m + M$. Independent of above scenario, The numbers of arcs and edges in D' both bounded, loosely, by ℓn, where $\ell = \max_{v \in (V \cup C)} \deg(v) < \infty$. Hence,

$$\frac{1}{(\ell n)^2} k_{n-M} \leq k_n(G).$$

As ℓ remains constant while n dominates, passing to the n-th root and large n limit inferior yields the result. $\square$

Chapter 7

Open Knots, Knotoids, and Fixed Knot Types

Any open strand is topologically equivalent to the straight interval (the so-called "light-bulb" theorem). So, knotting in an open strand is a result of its *geometry*. Identifying knots in open strands is important in physics and biology: Long chain polymers, such as proteins and DNA are often modeled as open strands. Moreover "knotting" in polymers has been shown to affect their behavior and effectiveness: Enzymes, for example, may not function with their usual efficacy (or at all!) if they are not an appropriately knotted contortion of their protein [85, 98]. Knotting and slipknotting in space curves is summarized in [76].

7.1 Open diagrams

An *open diagram* $D = (A, E, C)$ is a spatial diagram for the graph G consisting of precisely one interval edge and any number of circular edges. For an open diagram, cycles of $C^2 \circ E$ enumerate all of the closed components of the diagram with either orientation, and there is *one* cycle corresponding to the open component traversed first forwards, then backwards. The condition that an open diagram is planar is now that $C \circ E$ has precisely $n + 1$ cycles; an open diagram is an *open knot diagram* if $C^2 \circ E$ has precisely one cycle. An example of an open knot diagram is given in Figure 7.1. Let $S\mathscr{K}$ be the class of open knot shadows sized by crossings with counts sk_n, and let $S\mathcal{K}$ be the class of open knot diagrams sized by crossings with counts $s\kappa_n$.

In parallel with Turaev's study of *knotoids* [104], we could call such diagrams *knotoid diagrams*. However, we plan to allow more generic definitions of *open knot types* than Turaev's knotoid type definition, and will instead use the term "open knot diagram" to distinguish

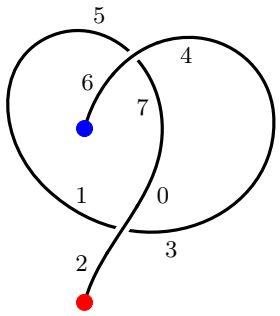

Figure 7.1: The open diagram defined by $C = (-0123)(-4567), E = (07)(15)(34)$. This diagram has knot type $\frac{1}{2}3_1 + \frac{1}{2}0_1$ under our definition. Arc labels are drawn inside of their face, *i.e.* their parent cycle in $C \circ E = (04)(167)(235)$.

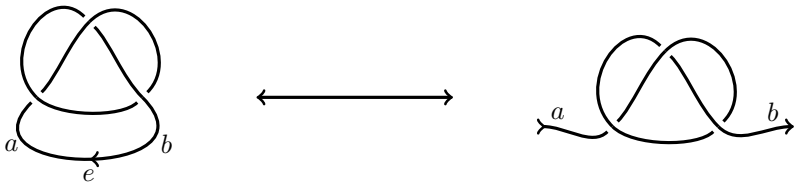

Figure 7.2: A diagram D and its open version cut at e, $D \setminus e$. Either diagram has 3_1 as its respective knot type.

this flexibility in choice of type. Let D be a diagram, and $e = (ab)$ an edge in D connecting arcs a and b. Then $D \setminus e$ is the 2-tangle diagram given by $(A, E \setminus \{e\}, C)$. Pictorially, $D \setminus e$ looks like D except with the edge e "cut" so that the arcs a and b are the loose arcs of the tangle, as in Figure 7.2.

Definition 7.1. Let S be an open diagram of at least one crossing and a, z its loose arcs. Say that a is connected to a crossing v joining arcs a, b_1, c_1, d_1, oriented counterclockwise (namely, arc c_1 meets the crossing opposite a). Say that the latter three arcs are part of edges $e_b = (b_1 b_2)$, $e_c = (c_1 c_2)$, and $e_d = (d_1 d_2)$.

Then the *contraction* $S - a$ *of* S *by arc* a is the new open diagram produced by deleting crossing v, edges e_b, e_c, e_d, and arcs a, b_1, c_1, d_1 and inserting the edge $e = (b_2 d_2)$ joining arcs

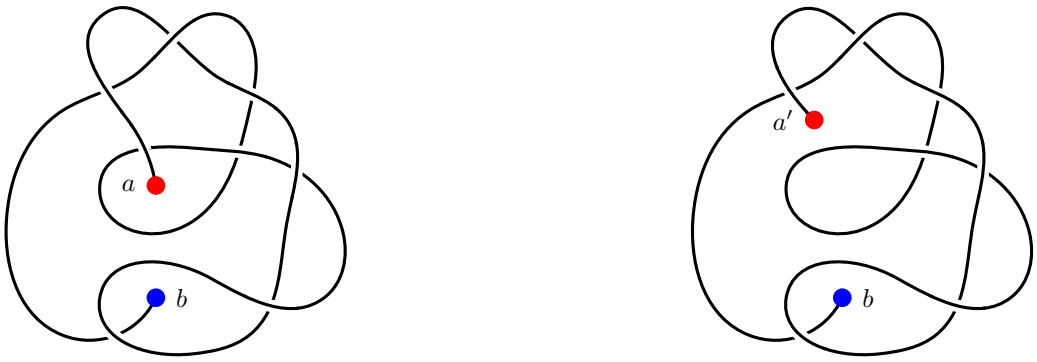

Figure 7.3: An open diagram D and its contraction along arc a, $D - a$. The diagram D has knot type $[D] = \frac{1}{2}4_1 + \frac{1}{2}0_1$, while the knot type of the contraction is $[D - a] = 0_1$.

b_2 and d_2. $S - a$ is a new open diagram with one fewer crossing, two fewer edges, and loose arcs c_2 and z. An example of the contraction operation can be seen in Figure 7.3.

If S has precisely one crossing, then its contraction (by either arc) is the "trivial" open diagram.

If T is an open diagram with no more crossings than S, then say S *contains* T *as a subdiagram*, $T \leq S$, if $S = T$ or there exists a series of contraction operations on S that produces the open diagram T. If D is a closed diagram with as many or more crossings than T, then say D *contains* T ($T \leq D$) as an open diagram if there exists an edge e in D so that $D \setminus e$ contains T. An example of a diagram and a subdiagram is given in Figure 7.4.

This is just one example of a contraction operation. Provided a different contraction operation behaves similarly enough, one can obtain the same results on subknotting presented here.

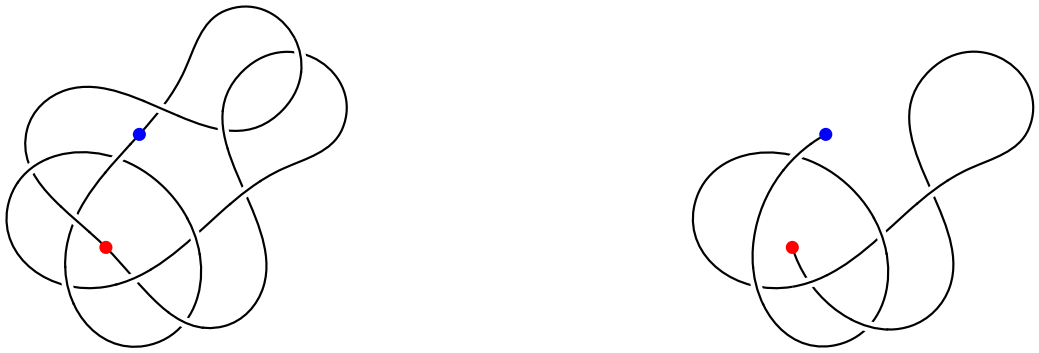

(a) The knot diagram D.

(b) A subdiagram S of D.

Figure 7.4: A minimal knot diagram D for 11a135 contains S as a subdiagram. As seen in Figure 7.5, the knot type of S is $[S] = \frac{1}{2}4_1 + \frac{1}{2}0_1$.

7.2 Subknots and slipknots

For open knots in space, knot type is defined as a probability distribution of knot types of actual knots obtained by closing the open knot in all ways dictated by some choice of closure scheme.

An advantage of working with open diagrams as opposed to open knots in space is that there exists a designated normal direction to the thickened plane in which the diagram resides. This suggests the following reasonable definition of the knot type of an open diagram:

Definition 7.2. Consider an open diagram S with loose arcs a, z. Then there exists a knot type $[S_o]$ represented by any of the diagrams produced by adding a generic non-self intersecting curve connecting a to z and passing *over* every edge of S; the knot type $[S_o]$ does not depend on the choice of closing curve by Reidemeister moves (indeed, if the open knot diagram represents an interval who lives entirely in a thickened sphere inside S^3, then these closing arcs can be made to exist entirely outside the sphere). Similarly, there is a knot type $[S_u]$ represented by diagrams similarly closed with a curve connecting a to z but passing

(a) An over closure of S, with knot type 4_1 (b) An under closure of S, with knot type 0_1

Figure 7.5: Closures of the open diagram S from Figure 7.4b: S_o and S_u.

under every edge in S^1. Examples of these closures are given in Figure 7.5. The *knot type of an open diagram* S is the normalized probability sum of knot types $\frac{1}{2}[S_o] + \frac{1}{2}[S_u]$ called the *knotting spectrum*. An open diagram whose knotting spectrum is 0_1 is unknotted, or *trivial*.

A diagram D *strongly contains a knot type* $[K]$ *as a subknot* if there exists an open diagram S contained in D whose knot type is precisely $[S] = [K]$. Say the diagram D *weakly contains* a knot type $[K]$ if there exists an open diagram S contained in D whose knot type is $[S] = \frac{1}{2}[K] + \frac{1}{2}[L]$, where $[L]$ is an arbitrary knot type.

If a diagram D strongly contains $[K]$ then it weakly contains it as well; the converse is not necessarily true. We will talk about diagrams containing knot types without specification of strength; the results in this paper do not depend on one or the other.

Importantly, this definition satisfies analogous characteristics to the MDS method [78, 76] of identifying subknots in open space polygons:

- *The knot type of an open diagram does not change under small perturbations.* Open knot diagrams are discrete objects and hence there are no perturbations; this property is hence satisfied vacuously.

[1] Turaev [104] calls these S_+ and S_- respectively.

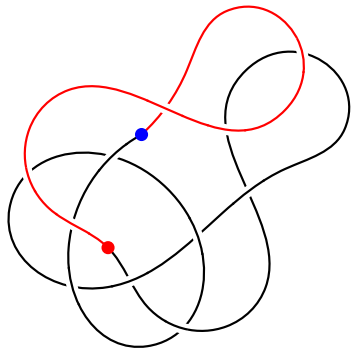

Figure 7.6: The ascending closure of the subdiagram S inside of D in Figure 7.4.

- *The knot type of an open diagram which is "almost closed" is the same as that of the "obvious closure".* As the knot type of $D \setminus e$ is precisely the same as the knot type of D, for any edge e in D, this property is satisfied.

Millett [75] has a definition of knot type for subdiagrams of knot diagrams which is equivalent to our definition of the knot type of the over closure. Indeed, this is as any *ascending* (possibly self-intersecting) over-closure path will produce a closed diagram with the same knot type, *c.f.* Figure 7.6.

This definition of knot type behaves well under contraction; if S is an open diagram of type $\frac{1}{2}[K_1] + \frac{1}{2}[K_2]$ and a is a loose arc of S, then there exists a knot type $[X]$ (it may be $[K_1], [K_2]$, or neither) so that $[S - a]$ is either $\frac{1}{2}[K_1] + \frac{1}{2}[X]$ or $\frac{1}{2}[X] + \frac{1}{2}[K_2]$.

Although it is not true that any two open knot diagrams with the same open knot type are necessarily related by Reidemeister moves, open knot type is at least invariant under them. That is:

Theorem 7.1. *Open knot type is invariant under the usual Reidemeister moves (i.e. those which do not interact with the loose ends).*

Proof. Let D and D' be two open diagrams which are related by a single Reidemeister move, ϕ. As the knot type $[D^o]$ is independent of choice of over-closure, we may choose D^o to be an

over-closure which does not intersect the region to which the Reidemeister move ϕ applies on D. Hence ϕ lifts to a Reidemeister move on D^o, producing $\phi(D^o) = D'^o$, a closure of D'. Hence $[D^o] = [D'^o]$ as (usual) knot type is Reidemeister invariant. This extends to both under-closures and arbitrary sequences of Reidemeister moves, proving the claim. □

Indeed, this was just one *choice* of definition of the knot type for open diagrams. Just as in the case of space polygons, one can construct other definitions that satisfy the same conditions as the MDS method. The results that follow *do not depend* on the definition chosen. For instance, they all follow if we take Turaev's choice $[S_-]$ of knotoid type (resp. $[S_+]$).

In a loose physical sense, a slipknot "appears" in a piece of string if, as the string is pulled taut, the slipknot unties itself. We can define this concept for diagrams.

Definition 7.3. Let $[K]$ be a knot type and D a diagram (open or closed). If D contains the knot type $[K]$ as a subknot but $[K]$ does not appear as a knot type in $[D]$, then D *contains* $[K]$ *as a slipknot*. The open diagram $S \leq D$ which represents the knot type $[K]$ is an *ephemeral knot*.

This definition is the analogue of that in [76] in the case of diagrams.

7.3 Pattern theorems for slipknots

With this machinery, we can prove a variety of theorems for slipknotting in different classes of diagrams.

7.3.1 Slipknots in knot diagrams

For the cases of link diagrams and knot diagrams, we have shown in Chapter 4 that there exist pattern theorems similar to those of Kesten for self avoiding lattice walks. We first show that we can construct tangles that insert slipknots into diagrams while preserving closure within these classes;

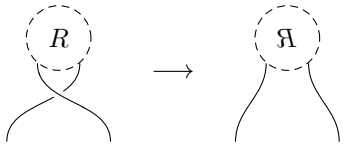

Figure 7.7: Isthmi can be removed while preserving knot type with this composite move.

Lemma 7.2. *Let $[K]$ be a knot type. Then there exists a reduced 2-tangle diagram T whose insertion into a knot diagram by edge replacement produces a new diagram which contains $[K]$ as a slipknot.*

Proof. By a Lemma of Millett [76], there exists an open self-avoiding walk γ whose inclusion in self-avoiding polygons guarantees that they include a slipknot of type $[K]$. Let T be an open diagram produced by projecting γ to a sphere, so that both of its external legs lie in the same face. The diagram T can then be reduced by a sequence of composite Reidemeister I type moves given in Figure 7.7.

By construction of T and parallels of our definition of slipknotting with Millett's, inclusion of T as a subtangle in a diagram requires that $[K]$ be contained as a slipknot. □

With this then we can see,

Theorem 7.3. *Let $[K]$ be any knot type, and $\mathscr{C}$ either the class of link diagrams or knot diagrams. Then there exists $c > 0$, $1 > d > 0$ and $N \geq 0$ so that for all $n \geq N$*

$$\mathbb{P}(D \text{ a diagram of } n \text{ crossings contains} \leq cn \text{ copies of } [K] \text{ as a subknot}) < d^n,$$

so that the probability that a random diagram in $\mathscr{C}$ contains the knot type $[K]$ as a subknot goes to one as the complexity of the diagram (i.e. the number of crossings) goes to infinity.

Proof. The result is a direct consequence of the pattern theorem, provided the construction for the appropriate tangle. We provide an example (Figure 7.8) for "edge replacement" (connect

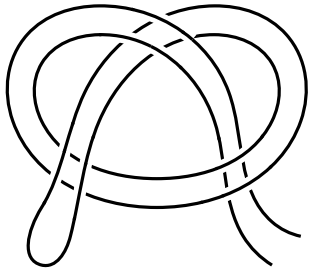

Figure 7.8: A tangle T which shows that trefoil slipknots are common in link diagrams and knot diagrams.

summation) which shows that trefoil slipknots are common in general and reduced diagrams. Others are guaranteed by Lemma 7.2.

□

7.3.2 Slipknots in unknot diagrams

As we are considering *slipknotting* rather than knotting proper, we are able instead to consider classes of diagrams with *fixed knot type* $[K]$! Consider the class of knot diagrams representing the unknot. Indeed, any tangle T whose inclusion in a diagram D would be sufficient to show that D would be knotted would be immediately excluded from a pattern theorem for unknot diagrams! Tangles which insert slipknots *but do not introduce any new knot type factors* however, namely those constructed in Theorem 7.3, may indeed be admissible. Hence, we can show,

Theorem 7.4. *Let $[K]$ be any knot type, and $\mathcal{K}(0_1)$ the class of unknot diagrams. Then there exists $c > 0$, $1 > d > 0$ and $N \geq 0$ so that for all $n \geq N$*

$$\mathbb{P}(D \text{ a diagram of } n \text{ crossings contains} \leq cn \text{ copies of } [K] \text{ as a subknot}) < d^n,$$

so that the probability that a random diagram in $\mathcal{K}(0_1)$ contains the knot type $[K]$ as a subknot goes to one as the complexity of the diagram (i.e. the number of crossings) goes to infinity.

Proof. Once we show the pattern theorem for the class of unknot diagrams, we would have the result by the proof of Theorem 7.3. □

Notice that this theorem answers Conjectures 2.12 and 2.19 from [76] in the affirmative for random unknot diagrams, and highlights an important property of the diagram model; attachments of patterns can be *strongly* local (e.g. connect summation of a 2-tangle to an edge doesn't affect any other edges in a diagram). The expected attachment operations mentioned in the proof of Theorem 7.3 above can be seen easily to be viable for unknots (provided tangles whose insertion does not change the knot type of a diagram). Hence all that is required to prove a pattern theorem for unknot diagrams is;

Proposition 7.5. *Let $\mathcal{K}(0_1)$ be the class of unknot diagrams, and let $\kappa_n(0_1)$ be the count of n-crossing diagrams in $\mathcal{K}(0_1)$. Then the limit*

$$\lim_{n\to\infty} \kappa_n(0_1)^{1/n}$$

exists and is equal to $\tau_0 < \infty$.

Proof. The proof is similar to those in prior chapters. The composition construction of shadows extends naturally to diagrams and only produces diagrams whose knot type *is the connect sum of its components' knot types*; hence unknot diagrams only compose into unknot diagrams. This provides the super-multiplicativity hypothesis that $\kappa_n(0_1)\kappa_m(0_1) \leq \kappa_{n+m}(0_1)$, and proves the claim. □

7.3.3 Slipknots in other fixed knot types

In fact, it is this observation which shows why the proof strategy *does not* immediately apply in general to classes $\mathcal{K}([K])$ of diagrams of some *other*, nontrivial knot type $[K]$. Indeed, to apply the theorems one would have to provide a composition that fixes knot type. This trouble mirrors other models of random knots, in particular self-avoiding polygons: The growth rates of all self avoiding polygons and those which represent the unknot are known to

exist. However the following is yet unknown; for any fixed knot type $[K]$, is the growth rate of polygons representing $[K]$ is equal to that of the unknot? Such results have been shown by restricting to very specific subclasses of self avoiding polygons, but are not known in the general case.

We do have a weak result for such classes:

Theorem 7.6. *Let $[L]$ and $[K]$ be any two knot types, and $\mathcal{K}([L])$ the class of diagrams of knot type $[L]$. Then there exists $c > 0$ so that the following holds: Let $\mathscr{H}_n$ be the subclass of diagrams in $\mathcal{K}_n([L])$ who contain fewer than cn copies of $[K]$ as a subknot. Then*

$$\limsup_{n\to\infty} |\mathscr{H}_n| < \limsup_{n\to\infty} \kappa_n([L]).$$

Proof. The argument here is the same as that for unknot diagrams above: Tangle diagrams which insert slipknots of type $[K]$ can be freely inserted without changing the knot type of a diagram. We are left with the weak result because we do not know enough about the growth rate of the class of diagrams $\mathcal{K}([L])$. □

We do conjecture that:

Conjecture 7.7. *Let $[L]$ be a fixed knot type and $\mathcal{K}([L])$ the class of diagrams of fixed knot type $[L]$, and let $\kappa_n([L])$ be the count of n-crossing diagrams in $\mathcal{K}([L])$. Then the limit*

$$\lim_{n\to\infty} \kappa_n([L])^{1/n}$$

exists.

If the above were true, then we would get the "strong" pattern theorem result:

Proposition 7.8. *Let $[L]$ and $[K]$ be any two knot types, and $\mathcal{K}([L])$ the class of either general, prime, or reduced diagrams of knot type $[L]$. Furthermore, suppose that Conjecture 7.7 is true. Then there exists $c > 0$, $1 > d > 0$, and $N \geq 0$ so that for all $n \geq N$,*

$$\mathbb{P}(D \text{ a diagram of } n \text{ crossings contains} \leq cn \text{ copies of } [K] \text{ as a subknot}) < d^n,$$

so that the probability that a random diagram in $\mathcal{K}([L])$ contains the knot type $[K]$ as a subknot goes to one as the complexity of the diagram (i.e. the number of crossings) goes to infinity.

Indeed, the belief is that not only do the limits

$$\lim_{n\to\infty} \kappa_n([L])^{1/n}$$

exist, but that for any two knot types $[K], [L]$, the limits are the same, *i.e.*,

$$\lim_{n\to\infty} \kappa_n([K])^{1/n} = \lim_{n\to\infty} \kappa_n([L])^{1/n}.$$

This is the belief for other models of random models of knotting, namely self avoiding polygons [88], where there is extensive numerical evidence.

7.3.4 Slipknots in classes with fixed unknotting number

Rather than partitioning diagrams along "knot invariant" lines (such as knot type) as we did in the prior sections, we can partition along "diagram invariant" lines. One such example is the *unknotting number* of a diagram D, which is the minimum number $\mathrm{Unk}(D)$ of crossings of a fixed diagram that need to be toggled in order to change a given diagram to the unknot. This is related to the usual definition of the unknotting number of a knot type $[K]$ by,

$$\mathrm{Unk}([K]) = \min_{D} \mathrm{Unk}(D),$$

where the minimum is over all diagrams D which represent the knot type $[K]$.

The unknotting number is biologically relevant; Topoisomerase enzymes are tasked with untangling DNA in cells [18]. Topoisomerase works locally on DNA molecules by passing an "upper" strand of DNA through another; diagrammatically this process is identical to a crossing toggle. Hence in this context, crossing toggles are called *strand passages*, and the unknotting number of a knot type is its distance from 0_1 under the *strand passage metric* [32, 96].

Theorem 7.9. *Let $c_n(\ell)$ be the count of n-crossing knot diagrams with unknotting number ℓ. Then $\lim_{n\to\infty}(c_n(\ell))^{1/n} = \tau_0$, the growth constant of counts of unknot diagrams.*

Proof. Let $\mathscr{C}_n(\ell)$ denote the set of rooted knot diagrams with unknotting number precisely ℓ. Define subsets $\mathscr{C}_n^+(\ell)$ and $\mathscr{C}_n^-(\ell)$ to be those diagrams with the property that toggling the root vertex (i.e. the vertex which the root points to) increases or decreases the unknotting number of the diagram, respectively. Observe from the bijection where one toggles the root vertex that $\mathscr{C}_n^+(\ell) \cong \mathscr{C}_n^-(\ell-1)$.

Let $c_n(\ell), c_n^+(\ell)$, and $c_n^-(\ell)$ be the sizes of the sets $\mathscr{C}_n(\ell), \mathscr{C}_n^+(\ell)$, and $\mathscr{C}_n^-(\ell)$ respectively.

Consider $\ell > 0$. A toggle of any crossing in a diagram in $\mathscr{C}_n(\ell)$ will either increase, decrease, or fix the unknotting number. As $\ell > 0$, there *must* be at least one crossing whose toggling decreases the unknotting number (this is the definition). Hence $|c_n(\ell)| \leq n|c_n^-(\ell)|$. Then,

$$\frac{1}{n}|c_n(\ell)| \leq |c_n^-(\ell)| \leq |c_n(\ell)|,$$

where the latter inequality comes from that one is the subset of the other. This implies then that

$$\lim_{n\to\infty}(c_n^-)^{1/n} = \lim_{n\to\infty}(c_n)^{1/n}.$$

Let D be a rooted standard diagram representation of the $(2, 2\ell+1)$ torus knot. It is known that D has unknotting number ℓ. So there is an injection from $\mathscr{C}_n(0) \hookrightarrow \mathscr{C}_{n+(2\ell+1)}(\ell)$ given by connect-summing D to each rooted unknot in $\mathscr{C}_n(0)$. This implies then that

$$\tau_0 = \lim_{n\to\infty}(c_n(0))^{1/n} \leq \lim_{n\to\infty}(c_{n+(2\ell+1)}(\ell))^{1/n} = \lim_{n\to\infty}(c_n(\ell))^{1/n}$$

The theorem then follows by an induction argument. For $\ell = 0$ we have that $|\mathscr{C}_n(0)|$ is simply the set of rooted unknot diagrams with n crossings and the growth rate of this class is τ_0 by definition.

On the other hand, suppose that for some $\ell \geq 0$, $\lim_{n\to\infty}(c_n(\ell))^{1/n} = \tau_0$. So,

$$\tau_0 = \lim_{n\to\infty}(c_n(\ell))^{1/n} \geq \lim_{n\to\infty}(c_n^+(\ell))^{1/n} = \lim_{n\to\infty}(c_n^-(\ell+1))^{1/n} = \lim_{n\to\infty}(c_n(\ell+1))^{1/n} \geq \tau_0,$$

where the final inequality was explained above. Hence $\tau_0 = \lim_{n\to\infty} (c_n(\ell+1))^{1/n}$ as desired, completing the proof of the theorem. □

Unknotting number of diagrams satisfies the following relation under connect summation of two diagrams A, B:

$$\mathrm{Unk}(A\#B) = \mathrm{Unk}(A) + \mathrm{Unk}(B).$$

This implies that connect summation of an unknotted 2-tangle to a diagram with unknotting number ℓ produces a resultant diagram which is also unknotting number ℓ. This means that if P is an unknotted tangle which is admissible for attachment into diagrams in $\mathscr{C}$, it is *also* admissible for attachment into diagrams $\mathscr{C}(\ell)$. This then implies;

Theorem 7.10. *Let $[K]$ be any knot type, and $\mathscr{C}(\ell)$ the class of knot diagrams with unknotting number ℓ. Then there exists $c > 0$, $1 > d > 0$, and $N \geq 0$ so that for all $n \geq N$*

$$\mathbb{P}(D \text{ a diagram of } n \text{ crossings contains} \leq cn \text{ copies of } [K] \text{ as a subknot}) < d^n,$$

so that the probability that a random diagram in $\mathscr{C}(\ell)$ contains the knot type $[K]$ as a subknot goes to one as the complexity of the diagram (i.e. the number of crossings) goes to infinity.

Proof. The argument is the same as in the proof of Theorem 7.4. Connect sum is a viable attachment scheme as connect summation of an unknot diagram cannot reduce the unknotting number. □

7.4 Asymptotics of open knot diagrams

In Chapter 3, we discuss that the asymptotic counts of knot diagrams are directly related to the asymptotic counts of plane curves, and hence are conjectured by Schaeffer and Zinn-Justin [95] to be

$$\frac{\kappa_n}{2^n} = k_n \underset{n\to\infty}{\sim} c\mu^n \cdot n^{\gamma-2}.$$

We have defined open knot diagrams as decorated open plane curves whose endpoints need not lie in the same face (*i.e.* open knot shadows). We conjecture:

Conjecture 7.11. *The asymptotic growth of open knot diagrams is in fact*

$$\frac{sk_n}{2^n} = sk_n \underset{n\to\infty}{\sim} c'\mu^n \cdot n^{\gamma'-2},$$

for some constant γ'.

It is in fact still unknown whether $\lim_{n\to\infty} sk_n^{1/n} = \mu$; this is Conjecture 6.9. This is different from the case of self-avoiding walks and self-avoiding polygons, whose growth rates are equal as a fundamental result of Hammersley [51]. Below we present evidence for the conjecture.

7.4.1 Conformal Field Theory

We will reason out the conjecture using a conformal field theory argument similar to that for meanders of [47]. Zinn-Justin and Zuber have proposed the following matrix integral [113] for the study of knot diagrams:

$$Z(N,\tau;x) = \int \prod_{a=1}^{\tau} dM_a \exp\left(-\frac{N}{2}\operatorname{Tr}\left(\sum_{a=1}^{\tau} M_a^2 - \frac{x}{2}\sum_{a,b=1}^{\tau}(M_aM_b)^2\right)\right),$$

where the integral is over all $N \times N$ Hermitian matrices, τ is the number of colors with which loops are marked, and x is a formal variable. What is important is that the formal series

$$F(x) = \lim_{\tau\to 0}\lim_{N\to\infty}\frac{\log Z(N,\tau;x)}{N^2}$$

is the generating function which counts all knot shadows, $\sum_n x^n k_n$. Applying the ideas of Di Francesco, *et al.*, one defines the operator

$$\varphi_1 = \lim_{N\to\infty}\frac{1}{N}\operatorname{Tr}\sum_{a=1}^{\tau} M_a,$$

which adds a single vertex of degree 1. Hence the limit of the expectation $\lim_{\tau\to 0}\frac{1}{\tau}\langle\varphi_1\varphi_1\rangle$ should be a generating series for the open knot shadows. One should then, after calculating the conformal dimension of φ_1 and using the KPZ [66, 40] formula which relates flat and random geometry, be able to conjecture precisely the the critical exponent of γ'.

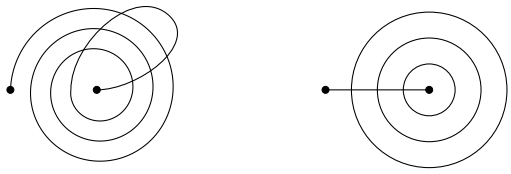

Figure 7.9: A minimal open knot shadow with geodesic distance 3 (left) has 6 crossings. A minimal open link shadow with geodesic distance 3 (right) only has 3.

This argument is non-rigorous, and any results would depend on the validity of the mathematical physical interpretation. We thus consider different reasoning, which only uses combinatorics.

7.4.2 Mean geodesic distance

There is another argument that the growth rates are equivalent which involves the geodesic distance of an open knot diagram:

Definition 7.4. The *geodesic distance* $d(L)$ of an open knot diagram L is the minimum number of edges that any path in the surface of the diagram connecting the two legs crosses.

This is a concept discussed for more general maps in [15]. One of their conclusions is that the average geodesic distance between the two open legs in the case of all open link shadows is the same as the average distance between any two faces in a closed link shadow, asymptotically proportional to $n^{1/4}$. It is believed that the average geodesic distance for knot shadows is the same or smaller, as it is "more difficult" for open knot shadows to have large geodesic distance. For instance, Figure 7.9 compares the smallest open knot shadow with geodesic distance 3 to the smallest open link shadow with the same geodesic distance.

Preliminary data suggests this conjecture. An alternate closure method for blossom trees of Bouttier, *et al* [15] is in bijection with open link shadows. Introducing this algorithm into

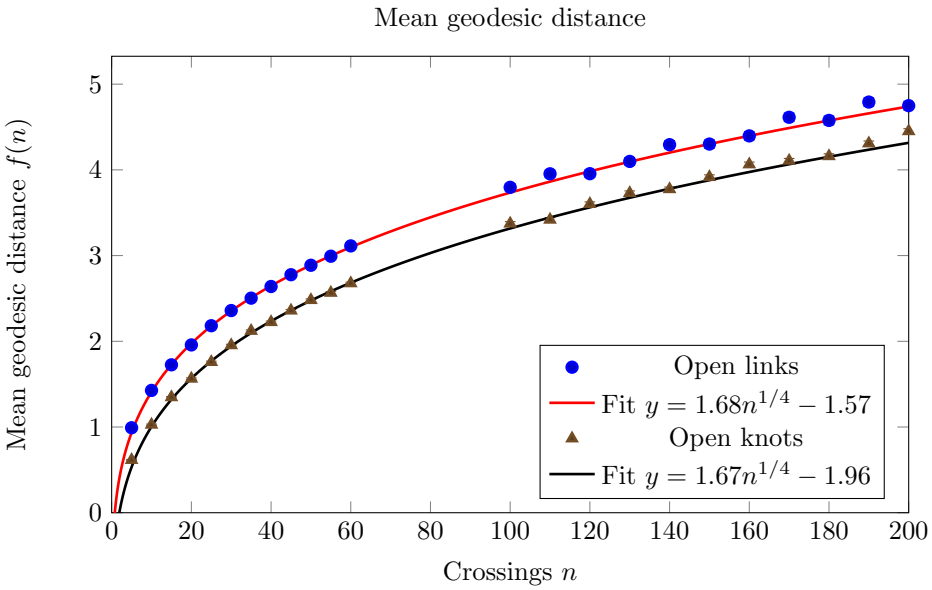

Figure 7.10: The mean geodesic distance of knot shadows appears to grow at the same rate as for link diagrams.

Gilles Schaeffer's `PlanarMap` [94] software we were able to gather data to test this conjecture. Figure 7.10 shows curves for the mean geodesic distance of open link diagrams and open knot diagrams.

If we assume this, notice that a result on the growth rates follows:

Theorem 7.12. *Let $f(n)$ denote the average geodesic distance of open knot shadows in $S\mathcal{K}_n$. Suppose that $\lim_{n\to\infty} f(n)/n = 0$. Then the growth rate of open knot shadows is,*

$$\lim_{n\to\infty} sk_n^{1/n} = \lim_{n\to\infty} k_n^{1/n} = \mu$$

Proof. Partition the numbers sk_n of open knot shadows with n crossings by geodesic distance: Let $sk_n[\ell]$ be the number of n-crossing open knot shadows of geodesic distance ℓ, so that $sk_n = \sum_{\ell=0}^{n} sk_n[\ell]$ (n is an upper bound on geodesic distance; $2n$ is even more trivial [it is the number of edges], and would equally suffice).

First notice that $k_n \leq sk_n$ and hence $\mu \leq \mu_I$ by splitting the root edge of knot shadows counted by k_n. Notice furthermore that $sk_n[\ell] \leq k_{n+\ell}$ as we can deterministically close any

distance ℓ open knot shadow by introducing ℓ new crossings (and this map is inverted on its image by contracting ℓ crossings back from the root).

Define $sk_n[> \ell] = \sum_{j=\lfloor \ell \rfloor + 1}^{n} sk_n[j]$ and $sk_n[\leq \ell] = \sum_{j=0}^{\lfloor \ell \rfloor} sk_n[j]$. For a nonnegative function $g(n)$ obeying $\lim_{n\to\infty} g(n)/n = 0$, let

$$m = \text{argmax}_{\ell \leq \lceil g(n) \rceil} \{sk_n[\ell]\}$$

so that $\lceil g(n) \rceil sk_n[m] \geq sk_n[\leq g(n)]$ (observe that trivially $\lceil g(n) \rceil \geq m$).

First, suppose we have some constant α for which, independently of n, we can partition $sk_n = sk_n[\leq g(n)] + sk_n[> g(n)]$ with $\alpha sk_n \leq sk_n[\leq g(n)]$. Say $g(n)$ is a *pivot* for α. Then $sk_n \leq \alpha^{-1} sk_n[\leq g(n)]$ and furthermore,

$$k_n \leq sk_n \leq \alpha^{-1} sk_n[\leq g(n)] \leq \alpha^{-1} \lceil g(n) \rceil sk_n[m] \leq \alpha^{-1} \lceil g(n) \rceil k_{n+m} \leq \alpha^{-1}(g(n)+1) k_{n+\lceil g(n) \rceil}$$

So,

$$\begin{aligned}
\ln(\mu) \leq \ln(\mu_I) &\leq \limsup_{n\to\infty} \frac{-\ln(\alpha) + \ln(g(n)+1) + \ln(k_{n+\lceil g(n) \rceil})}{n} \\
&= \limsup_{n\to\infty} \frac{\ln(k_{n+\lceil g(n) \rceil})}{n} \\
&= \left(\limsup_{n\to\infty} \frac{\ln(k_{n+\lceil g(n) \rceil})}{n + \lceil g(n) \rceil} \right) \left(\limsup_{n\to\infty} \frac{n + \lceil g(n) \rceil}{n} \right) \\
&\leq \ln(\mu),
\end{aligned}$$

provided the condition on $g(n)$ established prior.

Let $g(n) \geq 2f(n)$; then $g(n)$ obeys $\lim_{n\to\infty} g(n)/n = 0$, by the assumption on $f(n)$. By Markov's inequality [44], we have that $sk_n[\leq g(n)] \geq (f(n)/g(n)) sk_n = sk_n/2$. Hence $g(n)$ is a pivot for $\alpha = 1/2$. This then shows that the growth rate result follows. □

Of course, this is dependent on proving such a bound on the mean geodesic distance of knot shadows!

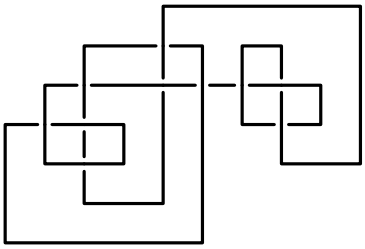

(a) A knot diagram of knot type $4_1\#3_1$.

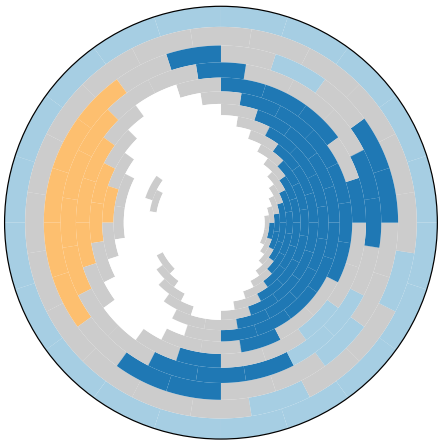

(b) Disk matrix of subknots in the diagram in 7.11a. Light blue is $4_1\#3_1$, orange is 4_1, and dark blue is 3_1. Mixed knot types are gray and unknots are white.

Figure 7.11: Visualization of subknots inside of a diagram for $4_1\#3_1$.

7.5 Visualization

We can produce graphics (Figures 7.11b and 7.12b) describing the appearances of subknots and slipknots inside of knot diagrams similar to those of [85, 98]. In these *disk matrices*, the (normalized) radius represents the fraction of the diagram used as the subdiagram; the outer circle hence describes the knot type of the whole diagram. The angle corresponds to the edge index, ordered around the knot diagram with an orientation, from which the diagram is split and contracted.

These graphics are produced in the same manner as Rawdon's [85] figures for space polygons. It is encouraging how similar these figures are. Namely, observe how slipknots represent as tendrils starting near the outer rim and slowly winding towards the center before disappearing.

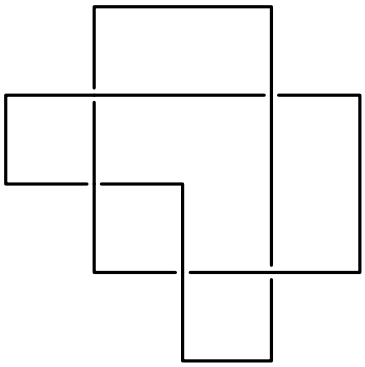

(a) The standard knot diagram for the torus knot 5_1.

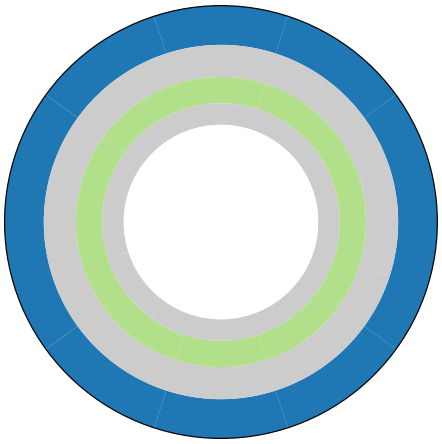

(b) Disk matrix of subknots in the diagram in 7.12a. Blue is 5_1, orange is 4_1, and light green is 3_1. Mixed knot types are gray and unknots are white. Cf. figure 2b in [85].

Figure 7.12: Visualization of subknots inside of a diagram for 5_1.

Chapter 8

Virtual Knots

By relaxing the condition of *planarity* which we have thus far required, we arrive in the realm of *virtual knot theory*. In this chapter, we will explore how the diagram model extends to this regime.

8.1 Virtual knot theory

If, rather than define knots as embeddings of circles into S^3, we had defined knots as embeddings of circles into the thickened sphere $S^2 \times [0,1]$, we would have developed an equivalent theory. Virtual knot theory [63, 60] is defined by picking a different thickened orientable surface:

Definition 8.1. A *virtual knot* is an embedding $K : S^1 \hookrightarrow \Sigma \times [0,1]$, for some orientable surface Σ. The *stabilization* of a virtual knot K embedded in the thickened surface Σ is an equivalent embedding into the thickened surface Σ' produced by connect summing an empty thickened handle onto Σ. The reverse operation (removal of an empty thickened handle) is *destabilization*.

A *virtual knot type* is an equivalence class of virtual knots up to 1) ambient isotopy and 2) (de)stabilization. For a virtual knot type $[K]$, the *underlying genus* [73] is the minimal genus over all thickened surfaces Σ in which $[K]$ has a representative.

Virtual knot theory is a natural extension of knot theory as two knot types are the same if and only if they are equivalent as virtual knot types. One wishes to work with diagrams for virtual knots as well, but this introduces a difficulty: Unlike the case of knot diagrams who

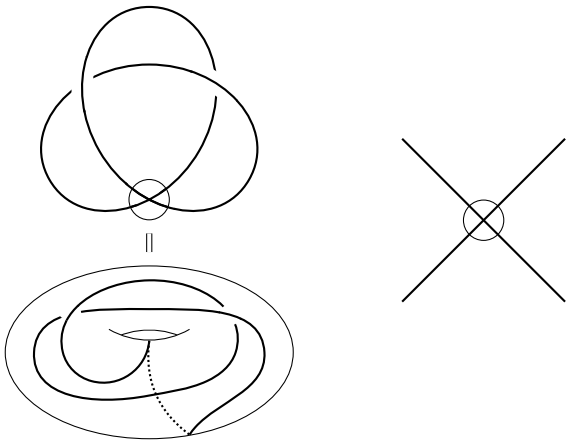

Figure 8.1: The virtual trefoil diagram on the left contains a virtual crossing (right). The crossing is an artifact of the projection from the torus-embedded diagram to the plane.

can be drawn on a plane, virtual knots must be drawn on surfaces which may have genus. One way to solve this problem is by introducing a new crossing type called a virtual crossing:

Definition 8.2. A *virtual knot diagram* is a knot diagram for which each crossing is either a usual crossing *or* a *virtual crossing*, depicted in Figure 8.1.

Virtual crossings "do not exist", in the sense that they are an artifact of a projection to the plane from a surface of genus. This means that the *virtual knot type* of a virtual knot diagram is the equivalence class of the diagram under both the classical Reidemeister moves as well as the *virtual Reidemeister moves* given in Figure 8.2.

8.2 The virtual knot diagram model

There are two ways by which we can extend the knot diagram model to the virtual theory. We will first discuss the strategy mentioned in Chapter 3 which is motivated by the definition of virtual knot diagram above.

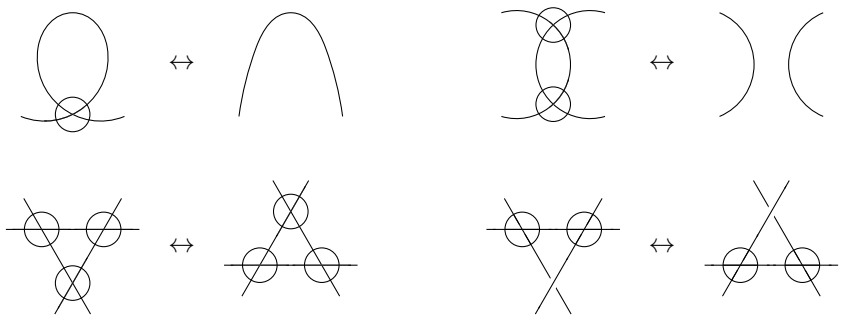

Figure 8.2: The four virtual Reidemeister moves.

8.2.1 Virtual knot diagrams with virtual crossings

We extend our definition of knot diagrams as decorated maps in order to describe virtual diagrams.

Definition 8.3. A *virtual knot diagram with virtual crossings* is a decorated knot shadow D with signs in the set $S = \{+, -, v\}$, where v denotes a *virtual crossing*. The class of all virtual knot diagrams with virtual crossings will be denoted by $\mathcal{VK} = \bigcup_n \mathcal{VK}_n$.

A *virtual tangle with virtual crossings* is a decorated tangle shadow D with signs in the set $S = \{+, -, v\}$.

Notice that as defined, this model counts virtual crossings just the same as real crossings. This definition could be tweaked to track actual crossings and virtual crossings separately, although we will not here. Under this model, the definition of a virtual knot type is clear: A *virtual knot type* is an equivalence class of virtual knot diagrams under both the classical Reidemeister moves and the virtual Reidemeister moves.

With this definition, we immediately have the main result of Chapter 4, which we reinterpret for the virtual case:

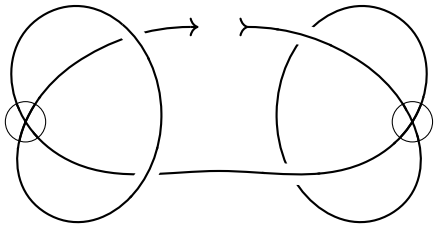

Figure 8.3: A virtual tangle whose closure has underlying genus 2, which is an opening of Kishino's knot.

Proposition 8.1. *Almost every rooted (general or reduced) virtual knot diagram is knotted. Furthermore, almost every rooted (general or reduced) virtual knot diagram contains any 1-component, prime 1-tangle virtual diagram P "linearly often:" For any such prime 1-tangle diagram P, there exists $N \geq 0$ and constants $d < 1$, $c > 0$ so that for $n \geq N$,*

$$\mathbb{P}(\textit{a virtual knot diagram } K \textit{ contains} \leq cn \textit{ copies of } P \textit{ as connect summands}) < d^n.$$

This proposition provides an important observation into the structure of large random virtual knot diagrams. P could be a virtual tangle which adds significant genus such as that in Figure 8.3. Then, because for two virtual knots K_1 and K_2 one has that $g(K_1 \# K_2) \geq g(K_1) + g(K_2) - 1$ [73], inclusion of linearly many $\geq cn$ copies of P guarantees that the underlying genus of the resultant random diagram's virtual knot type grows at least linearly in its number of (actual and virtual) crossings n.

8.2.2 Diagrams on a surface of fixed genus

The definition of a virtual diagram presented in the prior section has a few quirks. For one, it treats virtual crossings as equal citizens to real, signed crossings. As defined, virtual crossings are merely an artifact of a projection of a virtual knot to the sphere. Fortunately, the flexible map framework already exists to define a model of virtual diagrams in this light.

Definition 8.4. A *virtual link shadow* $M = (A, E, C)$ of genus g is a 4-valent map on the orientable surface Σ of genus g. The definition of link component for classical link shadows extends immediately to virtual link shadows. A *virtual knot shadow* is a virtual link shadow which has precisely one link component. We will use $\mathscr{K}^{\Sigma}$ to denote the class of knot shadows on a fixed surface Σ. Furthermore, we will denote by $\mathscr{G}$ the class of knot shadows on any orientable surface.

A *virtual knot diagram* D of genus g is a virtual knot shadow on an orientable surface Σ of genus g with each crossing decorated with signs from a set S (usually, $S = \{+, -\}$). We will use $\mathcal{K}^{\Sigma}$ to denote the class of knot diagrams on a fixed surface Σ. Furthermore, we will denote by $\mathcal{G}$ the class of knot diagrams on any orientable surface.

As discussed in Section 3.1.3, $\mathscr{G}$ and $\mathcal{G}$ are respectively the classes of signed Gauss diagrams and directed signed Gauss diagrams.

By Euler characteristic, we can compare counts of crossings, arcs, edges, and faces of a virtual link shadow as they relate to the genus g of the embedding surface. Namely, if there are n crossings, there must be $4n$ arcs, and $2n$ edges. The count on faces in $C \circ E$ then is $n + 2 - 2g$.

Under this definition for virtual knot diagrams, the notion of virtual knot type is a bit more obfuscated. We would like to impose a definition like, "a virtual knot type is an equivalence class of virtual knot diagrams modulo the classical Reidemeister moves," but we must be careful to incorporate (de)stabilization:

It is possible that a Reidemeister II type move can change the genus of a virtual knot diagram. We may say that two virtual knot diagrams D_1 and D_2 on surfaces of the same genus g have equivalent virtual knot type if they differ by a classical Reidemeister move (which does not change the genus of the diagram). Furthermore we require the following additional equivalence: Let D_1 be a virtual diagram on a surface of genus g and D_2 on a surface of genus $g + 1$. If a Reidemeister II type move which reduces the number of crossings

of D_2 reduces the genus by 1, consider its result D_2' to be embedded in that surface of genus g. If $D_2' = D_1$ in this surface, then say D_1 and D_2 have equivalent virtual knot type.

Definition 8.5. The *virtual knot type* of a virtual knot diagram is an equivalence class under the above equivalence.

For many different classes of maps $\mathscr{C}^S$ on a fixed surface S, it has been shown [25, 10] that

$$c_n^S \sim \kappa(\mathscr{C}, S)\tau(\mathscr{C})^n n^{\gamma(\mathscr{C},\chi(S))},$$

where $\kappa(\mathscr{C}, S)$ is a constant depending on the class and the surface, $\tau(\mathscr{C})$ is a constant depending on the class, and $\gamma(\mathscr{C}, \chi(S))$ is a constant depending on the class and the Euler characteristic of the surface. This naturally leads to the conjecture,

Conjecture 8.2. *The asymptotic growth of knot diagrams on an arbitrary fixed surface Σ is conjectured to be*

$$\frac{\kappa_n^\Sigma}{2^n} = k_n^\Sigma \underset{n\to\infty}{\sim} c''\mu^n \cdot n^{\gamma''(\mathscr{K},\chi(\Sigma))},$$

where μ is the same exponential growth rate conjectured for the class of knot shadows, c'' is an arbitrary constant, and $\gamma''(\mathscr{K}, \chi(\Sigma))$ is a constant depending only on the Euler characteristic of the surface Σ (it is believed that $\gamma''(\mathscr{K}, \chi(\Sigma)) = \chi(\Sigma)+$constant).

There is even difficulty in proving the existence of the exponential growth rate

$$\lim_{n\to\infty} (k_n^\Sigma)^{1/n};$$

composition by—for instance—connect summation is additive on the genus of the surface Σ, and hence produces diagrams on surfaces of higher genus for $\Sigma \neq S^2$. The methods of Bender and Canfield [10] require some understanding of the growth rates of maps with marked vertices of arbitrary degree which, are not yet well-enough understood: These growth rates are still only conjectured; see Chapter 6. As usual, a smooth growth result would prove a pattern theorem for virtual knot diagrams of fixed underlying genus, provided tangles whose insertion now must also *preserve the surface genus* of the resultant diagram.

In the case of virtual knot shadows of *arbitrary* genus $\mathscr{G}$, we know precise counts, as given in Section 3.1.3. These objects are differently complicated, as the limit

$$\lim_{n\to\infty} g_n^{1/n} = \lim_{n\to\infty} \left(\frac{(2n)!}{n!} \right)^{1/n} = \infty$$

is infinite. Hence a pattern theorem would need to be proved through different means, and may take on a different form. From this viewpoint, Linial and Nowik [69] have shown that the average underlying genus of a virtual knot shadow is $\frac{n}{2} + \Theta(\ln n)$. One could hope to further prove a result on the variance of the underlying genus [26] or even a Harer-Zagier formula [111] for the bivariate generating function of virtual knot shadows of fixed genus and size.

8.3 More reasoning on the growth rate of open knot diagrams

As mentioned in the section prior, the problem of fixing surface genus is closely related to the problem of fixing marked vertices of arbitrary degree. Hence there is yet another argument for the exponential growth term

$$\lim_{n\to\infty} sk_n^{1/n} = \mu$$

in Conjecture 6.9. Consider a subknot shadow. Its two loose ends either lie in the same face, or in two different faces. This leads to the decomposition of the class of subknot shadows into

$$S\mathscr{K} = S\mathscr{K}[0] \cup S\mathscr{K}[\geq 1],$$

where $S\mathscr{K}[0]$ consists of all subknot shadows whose loose ends lie in the same face and $S\mathscr{K}[\geq 1]$ consists of all subknot shadows whose loose ends lie in different faces. Observe that $S\mathscr{K}[0]$ is equivalent to $\mathscr{K}$ by joining the loose ends to form the root edge (whose direction is determined by the order of the loose ends which were joined).

On the other hand, consider a subknot shadow D in $S\mathscr{K}[\geq 1]$; by adding a handle connecting both of the faces in D with loose ends, one is able to produce a new rooted knot shadow D' on the *torus* by now joining the two loose ends in D by way of the added handle;

observe that all faces in D' are still disks as critical for the definition of a map. This produces an injection from $S\mathscr{K}[\geq 1]$ into $\mathscr{K}^T$, the class of knot shadows on the torus.

If in fact Conjecture 8.2 is true, that $S\mathscr{K}$ decomposes into rooted knot shadows and a subset of rooted knot shadows on the torus would imply that the exponential growth terms for subknot shadows is the same as knot shadows.

Chapter 9

A Markov Chain Monte Carlo Sampler for Knot Shadows

As we discussed in Chapter 5, knot shadows become exponentially rare in link shadows making rejection sampling progressively more difficult. In this chapter, we present an alternative approach by using a Markov chain whose transitions explore the space of knot diagrams. The work in this chapter is done together with Andrew Rechnitzer.

9.1 Flat Reidemeister moves

The Reidemeister moves in Figure 2.4 are fundamental in the study of knot diagrams. As knot shadows are knot diagrams without crossing information, define the flat Reidemeister moves to be the same as the normal moves, except ignoring crossing information [53]. Any two knot shadows are related by a sequence of flat Reidemeister moves:

Proposition 9.1. *Any knot shadow M can be brought to the trivial shadow by a sequence of flat Reidemeister moves.*

Proof. There is a crossing assignment for M which produces an unknotted diagram D: Continue around the link component from the root arc, picking a sign at each crossing so that the first time a crossing is visited, the strand we are traversing passes over the other. Reidemeister's theorem asserts the existence of a sequence $(\phi_1, \phi_2, \ldots, \phi_k)$ of Reidemeister moves which take D to the trivial diagram. The sequence $(\phi'_1, \phi'_2, \ldots, \phi'_k)$ of *flat* Reidemeister moves takes M to the trivial shadow. □

Notably, this method of proof does not guarantee that the sequence is minimal in any sense. Interesting questions remain open about the flat Reidemeister moves. For instance,

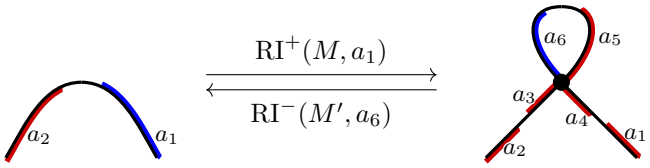

Figure 9.1: The flat Reidemeister I moves

neither the diameter of the spaces $\mathscr{K}_{\leq n}$ connected by flat Reidemeister transitions nor the expected distance between two arbitrary knot shadows are known [81].

The flat Reidemeister moves are then a natural set of basic transitions for a Markov chain on $\mathscr{K}$. A key property is that they are all reversible. Let D be a rooted knot shadow with root arc a.

Shadow Reidemeister I loop addition, RI^+. Given the root arc $a = a_1$, the loop addition RI^+ is always possible.

Loop addition is performed as follows. Let $(a_1 a_2) = e(a_1)$, and let a_3, a_4, a_5, a_6 be four new arcs. Then $\mathrm{RI}^+(D, a_1)$ is the rooted map produced by deleting edge $e(a_1)$ from D, then adding the vertex $(a_3 a_4 a_5 a_6)$ and edges $(a_1 a_4)$, $(a_5 a_6)$, and $(a_3 a_2)$. The new root is the arc a_6. One can verify that this process is invertible, in particular that:

$$D = \mathrm{RI}^-(\mathrm{RI}^+(D, a_1), a_6).$$

Shadow Reidemeister I loop deletion, RI^-. Loop deletion RI^- is possible whenever, given the arc $a = a_6$, the face $f(a_6)$ is a singleton.

If this is true, then $\mathrm{RI}^-(D, a_6)$ is the rooted map produced from deleting the vertex $v(a_6) = (a_3 a_4 a_5 a_6)$ and the edges $e(a_6) = (a_6 a_5)$, $e(a_3) = (a_3 a_2)$, $e(a_4) = (a_4 a_1)$ from D, and adding the edge $(a_1 a_2)$. The arcs a_3, a_4, a_5, a_6 are discarded. The new root is the arc a_1. This process is invertible:

$$D = \mathrm{RI}^+(\mathrm{RI}^-(D, a_6), a_1).$$

The moves RI^+ and RI^- are demonstrated in Figure 9.1.

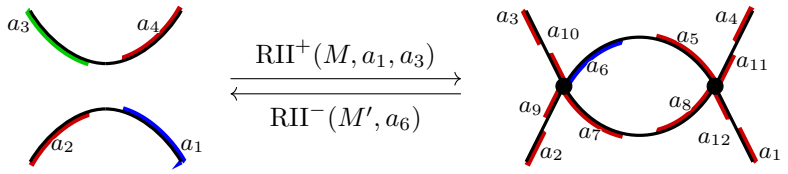

Figure 9.2: The flat Reidemeister II moves

Shadow Reidemeister II bigon addition, RII^+. Bigon addition RII^+ additionally requires a different arc b which is different from the root arc a in $f(a)$. Let $a = a_1$ and $b = a_3$.

The rooted map $\mathrm{RII}^+(D, a_1, a_3)$ is constructed from D as follows. Delete the edges $e(a_1) = (a_1 a_2)$ and $e(a_3) = (a_3 a_4)$ from D. Add eight new arcs $a_5, a_6, a_7, a_8, a_9, a_{10}, a_{11}, a_{12}$. Add the vertices $(a_6 a_{10} a_9 a_7)$ and $(a_5 a_8 a_{12} a_{11})$. Insert the edges $(a_2 a_9)$, $(a_3 a_{10})$, $(a_7 a_8)$, $(a_5 a_6)$, $(a_1 a_{12})$, and $(a_4 a_{11})$. The new root is the arc a_6. This process is invertible:

$$D = \mathrm{RII}^-(\mathrm{RII}^+(D, a_1, a_3), a_6).$$

Shadow Reidemeister II bigon deletion, RII^-. Bigon deletion RII^- is possible provided the root arc $a = a_6$ is on a face $f(a_6)$ which consists of precisely two arcs (*i.e.* a bigon).

Additionally, it is required that the two exterior faces which are merged by the transition be *distinct*; this is required to preserve connectedness and genus. Indeed, suppose that D is a shadow embedded on an orientable surface of genus g, so that $v(D) - e(D) + f(D) = 2(g-1)$, but that the faces to be merged are not distinct. The number of vertices and edges decrease by 2 and 4 respectively by a RII^- operation, as usual, but the number of faces now *remains fixed*. This implies that the produced shadow lives in either a surface of one fewer genus, or if the original map was embedded on the sphere, *two disjoint spheres*.

The rooted map $\mathrm{RII}^-(D, a_6)$ is constructed from D as follows. Delete the vertex $v(a_6) = (a_6 a_{10} a_9 a_7)$ and the edges $e(a_9) = (a_2 a_9)$, $e(a_{10}) = (a_3 a_{10})$, $e(a_7) = (a_7 a_8)$ and $e(a_6) = (a_6 a_5)$. Delete the vertex $v(a_5) = (a_5 a_8 a_{12} a_{11})$ and the edges $e(a_{12}) = (a_1 a_{12})$ and $e(a_{11}) = (a_4 a_{11})$. Add the edges $(a_1 a_2)$ and $(a_3 a_4)$. The arcs $a_5, a_6, a_7, a_8, a_9, a_{10}, a_{11}, a_{12}$ are discarded. The

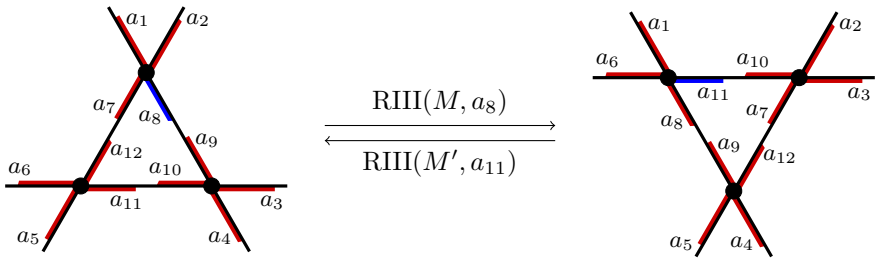

Figure 9.3: The flat Reidemeister III move

new root is the arc a_1. This process is invertible:

$$D = \text{RII}^+(\text{RII}^-(D, a_6), a_1, a_3).$$

The moves RII^+ and RII^- are demonstrated in Figure 9.2.

Shadow Reidemeister III triangle flip, RIII. Triangle flipping RIII is possible provided the root arc $a = a_8$ lies on a face $f(a_8)$ with precisely three arcs, all of whom are contained in *different* vertices (*i.e.* a nondegenerate triangle).

The rooted map $\text{RIII}(D, a_8)$ is constructed from D as follows. Say that $v(a_8) = (a_1 a_2 a_7 a_8)$, $e(a_8) = (a_8 a_9)$, $e(a_7) = (a_6 a_7)$, $v(a_6) = (a_5 a_{11} a_{12} a_6)$, and $v(a_9) = (a_3 a_9 a_{10} a_4)$. Delete vertices $v(a_7)$, $v(a_6)$, $v(a_9)$ and edges $e(a_7)$, $e(a_8)$, and $e(a_{10})$. Insert vertices $(a_6 a_8 a_{11} a_1)$, $(a_2 a_{10} a_7 a_3)$, $(a_4 a_{12} a_9 a_5)$ and edges $(a_6 a_9)$, $(a_7 a_{12})$, and $(a_{10} a_{11})$. The new root is the arc a_{11}. This process is invertible:

$$D = \text{RIII}(\text{RIII}(D, a_8), a_{11}).$$

The move RIII is demonstrated in Figure 9.3.

9.2 Markov Chain

Using the operations above, we describe a Markov chain on $\mathscr{K}$. We will subsequently show that it is ergodic. Let $0 < z < 1$ be an arbitrary parameter called a *Boltzmann weight*. Our Markov chain on knot shadows will limit on a *Boltzmann distribution*, where the probability

of sampling an object of size n is proportional to z^n. The Boltzmann weight z hence gives us control over the sizes of our samples, and prevents the chain from tending to produce infinitely large objects.

Let D_i be the input rooted knot shadow with n vertices and root arc a and perform one of the following six subprocedures with equal probability (*failure* means to set $D_{i+1} := D_i$):

1. Loop addition. Sample $0 \leq \alpha < 1$ and fail immediately if $\alpha > z$. Return $D_{i+1} := \mathrm{RI}^+(D_i, a)$.

   The probability that this transition succeeds on an n-vertex knot shadow D is $z/6$.

2. Loop deletion. Provided $f(a)$ is a loop, return $D_{i+1} := \mathrm{RI}^-(D_i, a)$.

   The probability that this transition succeeds if root arc a has $f(a)$ a loop in D is $1/6$.

3. Bigon addition. Sample $0 \leq \alpha < 1$ and fail immediately if $\alpha > z^2$. The arc a lies along a face of d edges; provided $d \neq 1$ (otherwise fail), uniformly sample the integer k between 1 and $d-1$. The arc $a' = (C \circ E)^k(a)$ is a distinct arc along the same face as a. Then return $D_{i+1} := \mathrm{RII}^+(D_i, a, a')$.

   The probability that this transition succeeds on any given additional arc a' along the root d-face is

   $$\frac{z^2}{6(d-1)}.$$

4. Bigon deletion. Fail if the arc a does not lie along a bigon. The size d of the face which would be produced by bigon deletion is the sum $|f(E \circ C(a))| + |f(C^3 \circ E(a))| - 2 = d$. Sample $0 \leq \beta < 1$ uniformly and fail if $\beta > (d-1)^{-1}$. Otherwise, return $D_{i+1} := \mathrm{RII}^-(D_i, a)$.

   The probability that this transition succeeds on a root a along a bigon is

   $$\frac{1}{6(d-1)}.$$

5. Triangle flipping. Fail if the arc a does not lie along a nondegenerate triangle. Otherwise, return $D_{i+1} := \mathrm{RIII}(D_i, a)$.

   The probability that this transition succeeds assuming the root lies along a nondegenerate triangle is $1/6$.

6. Re-rooting. Given the rooted diagram D_i, forget the root and select a new root b for D_{i+1} from the $(\operatorname{aut} D_i)/(4|D|)$ choices. The probability that this transition succeeds is $1/6$.

The we claim that the limiting distribution of this Markov chain has that the probability that any given n-crossing rooted knot shadow D is chosen is $\mathbb{P}(D) = z^n/K(z)$, and if $K(z)$ converges to a number, $\mathbb{P}(D) \propto z^n$. It follows that, if we ignore the roots of the sampled diagrams in order to sample *unrooted* diagrams, the probability of an unrooted diagram $\overline{D}$ being sampled is

$$\mathbb{P}(\overline{D}) \propto \frac{4n}{\operatorname{aut} \overline{D}} z^n.$$

We note that as the probability that the automorphism group of a knot shadow is trivial tends exponentially quickly to 1 [24], the actual probability of an unrooted diagram $\overline{D}$ will typically look like $\mathbb{P}(\overline{D}) \propto 4nz^n$.

The detailed balance condition is sufficient to show that a Markov chain has a stationary distribution. It amounts to showing, that for a probability distribution $\mathbb{P}$, the transition probabilities from states A to B, $\pi(A \to B)$, satisfy,

$$\pi(A \to B)\mathbb{P}(A) = \pi(B \to A)\mathbb{P}(B).$$

We prove:

Theorem 9.2. *This Markov chain satisfies detailed balance, and is ergodic. Hence, it has the unique limiting stationary distribution where the probability of sampling any n-crossing rooted knot shadow D is precisely,*

$$\mathbb{P}(D) = z^n/K(z).$$

Proof. Let D be a rooted knot shadow of n vertices and a be the root arc in D. Observe first that the three pairs of reversing transitions $(\mathrm{RI}^+, \mathrm{RI}^-)$, $(\mathrm{RII}^+, \mathrm{RII}^-)$, and $(\mathrm{RIII}, \mathrm{RIII})$ all change the number of vertices by distinct complementary amounts; hence any two diagrams can be related by at most one pair of transitions, or, if their vertex counts agree, a re-rooting.

Let $\mathbb{P}$ be the probability distribution on rooted knot shadows given by, $\mathbb{P}(D) = z^n/K(z)$. Then we show that our Markov chain, together with $\mathbb{P}$, satisfies detailed balance:

1. Suppose that $N = \mathrm{RI}^+(D, a)$ with root arc b. This means that N is unique in that $D = \mathrm{RI}^-(N, b)$. Then

$$\pi(D \to N)\mathbb{P}(D) = \pi(N \to D)\mathbb{P}(N)$$
$$\frac{z}{6}z^n = \frac{1}{6}z^{n+1}.$$

2. Suppose that $N = \mathrm{RII}^+(D, a, a')$ with root arc b. This means that N is unique in that $D = \mathrm{RII}^-(N, b)$. The arcs a, a' lie along a face in D of degree d. Then

$$\pi(D \to N)\mathbb{P}(D) = \pi(N \to D)\mathbb{P}(N)$$
$$\frac{z^2}{6(d-1)}z^n = \frac{1}{6(d-1)}z^{n+2}.$$

3. Suppose that $N \neq \mathrm{RIII}(D, a)$ and that N is a re-rooting of D. Then,

$$\pi(D \to N)\mathbb{P}(D) = \pi(N \to D)\mathbb{P}(N)$$
$$\frac{1}{6}\frac{\operatorname{aut} D}{4n}z^n = \frac{1}{6}\frac{\operatorname{aut} N}{4n}z^n.$$

   Note that $\operatorname{aut} D = \operatorname{aut} N$ as they have the same underlying map structure (and so may only differ by choice of root).

4. Suppose that $N = \mathrm{RIII}(D, a)$ has root b and that N is *not* a re-rooting of D. Then N is unique in that $D = \mathrm{RIII}(N, b)$, so

$$\pi(D \to N)\mathbb{P}(D) = \pi(N \to D)\mathbb{P}(N)$$
$$\frac{1}{6}z^n = \frac{1}{6}z^n.$$

5. If $N = \mathrm{RIII}(D, a)$ has root b *and* N is a re-rooting of D, then the transition probabilities of the previous two cases are summed, so that

$$\pi(D \to N)\mathbb{P}(D) = \pi(N \to D)\mathbb{P}(N)$$
$$\left(\frac{1}{6} + \frac{1}{6}\frac{\mathrm{aut}\, D}{4n}\right) z^n = \left(\frac{1}{6} + \frac{1}{6}\frac{\mathrm{aut}\, N}{4n}\right) z^n.$$

In all other cases, the transition probabilities are symmetrically zero. This proves detailed balance, and hence that $\mathbb{P}$ is a limiting stationary distribution for our Markov chain. Proposition 9.1 says that our Markov chain is *connected*—it is possible to get from any one state to any other. Furthermore, our Markov chain is *aperiodic*—any rooted shadow state may remain fixed during a transition step if it is re-rooted with the same root. These latter two conditions, together with detailed balance, say that the Markov chain is *ergodic*.

A Markov chain which satisfies detailed balance and is ergodic has a *unique* limiting stationary distribution, which necessarily is $\mathbb{P}$. □

Any knot shadow exhibits a sequence of flat Reidemeister moves which *never* increases the number of vertices and ultimately produces the trivial knot shadow [81]. This is in opposition to the case of all *knot diagrams*, where there exist diagrams of knots which can be reduced in crossing number, but only through sequences which increase the crossing number at some point. This property of knot shadows yields the result that truncating the Markov chain at some highest number of vertices n will still be ergodic on the truncated class of knot shadows.

Proposition 9.3. *Imposing the further restriction on the* loop addition *and* bigon addition *transitions that we fail if the input knot shadow D would transition to have more than L vertices (*i.e. *if D has L or $L-1$ vertices, respectively) yields a Markov chain which explores all of $\mathscr{K}_{i \le L}$ and is ergodic. Furthermore, the probability of sampling any knot shadow D with $m \le L$ crossings is,*

$$\mathbb{P}(D) = \frac{z^m}{\sum_{\ell=1}^{L} k_\ell z^\ell} \propto z^m.$$

Proof. If D, N are two knot shadows with at most L vertices, then there exists sequences of flat Reidemeister moves which reduce D and N to the trivial knot shadow without ever adding vertices [81]. Following the sequence for D followed by the inverse of the sequence for N yields a path through knot shadows from D to N which never involves an shadow with greater than L vertices (as both D and N have at most that many).

The detailed balance requirement and result about probabilities follows from the above proof; we have only symmetrically zeroed out the transition probabilities between knot shadows with at most L vertices and those with more. □

9.3 Simulations and Data

We implemented the Markov Chain Monte Carlo sampler in `C`. Planar knot shadows are stored as combinatorial maps; a collection of vertices, edges, and arcs with bidirectional references between arcs and their vertices, as well as arcs and their edges. At each step, an arc is selected from the diagram at random; this takes near $O(1)$ time, and the parameter α is sampled at random. Both of the RI moves, as well as the RIII move take constant time. The RII^+ move requires an extra random number γ which determines the second arc for the transition and is otherwise performed in constant time. The RII^- move requires both the sampling of the additional number β as well as a count of the face sizes diagonal to the bigon. A planar knot shadow has average face degree strictly increasing and limiting on 4, so counting the face sizes requires a constant number of operations on average.

9.3.1 Comparison with uniform rejection sampling

Recall the following summary of Chapter 5: For low numbers n of crossings, it is possible to sample knot shadows uniformly, by sampling uniformly 4-valent maps and then rejecting if they do not obey the knot shadow property. The sampling of maps can be done, *e.g.* with Gilles Schaeffer's bijection with blossom trees [94, 93] as in his `PlanarMap` software. The

rejection step is simple, but 4-valent maps which are knot shadows become rare exponentially quickly [95].

With this in mind, we can check how well our implementation converges to the uniform distribution by comparing statistics. The following charts are based on the following data:

1. *Uniform.* Using a rejection sampler for knot shadows over the course of 72 hours, we gathered more than 1.3×10^6 samples of knot shadows with n vertices, for each n from 3 to 60.

2. *All 4v.* Using a uniform sampler for all 4-valent maps, we gathered precisely 10^5 samples of 4-valent maps with n vertices, for each n from 3 to 60. This took approximately 24 minutes.

3. $z = 0.098$. Using our Markov Chain Monte Carlo algorithm on shadows of at most 100 vertices and a parameter of $z = 0.098$, we gathered a total of 10^5 samples of knot shadows.

4. *Wang-Landau.* Using our Markov Chain Monte Carlo together with an implementation of Wang-Landau tuning (see Section 9.3.2) we sampled a total of 10^7 knot shadows. Under this, every n had at least 9×10^4 samples.

First, we check the counts of faces of fixed degree which appear (this takes $O(n)$ time to compute as all knot shadows have $n+2$ faces). This data is presented in Figure 9.4. Similarly, we also compare the average sizes of the largest face in the knot shadow, in Figure 9.5.

We also check curve invariants in the nature of Arnol'd [7]; by following the crossings in order around the knot shadow and counting those which are "interlaced", we are able to compute $-\frac{1}{2}(2St + J^+)$, again in linear time. This invariant is related to the finite type invariant v_2 of knots; $-\frac{1}{8}(2St + J^+)$ is the average v_2 invariant over all possible over-under sign assignments to the knot shadow. This is presented in Figure 9.6.

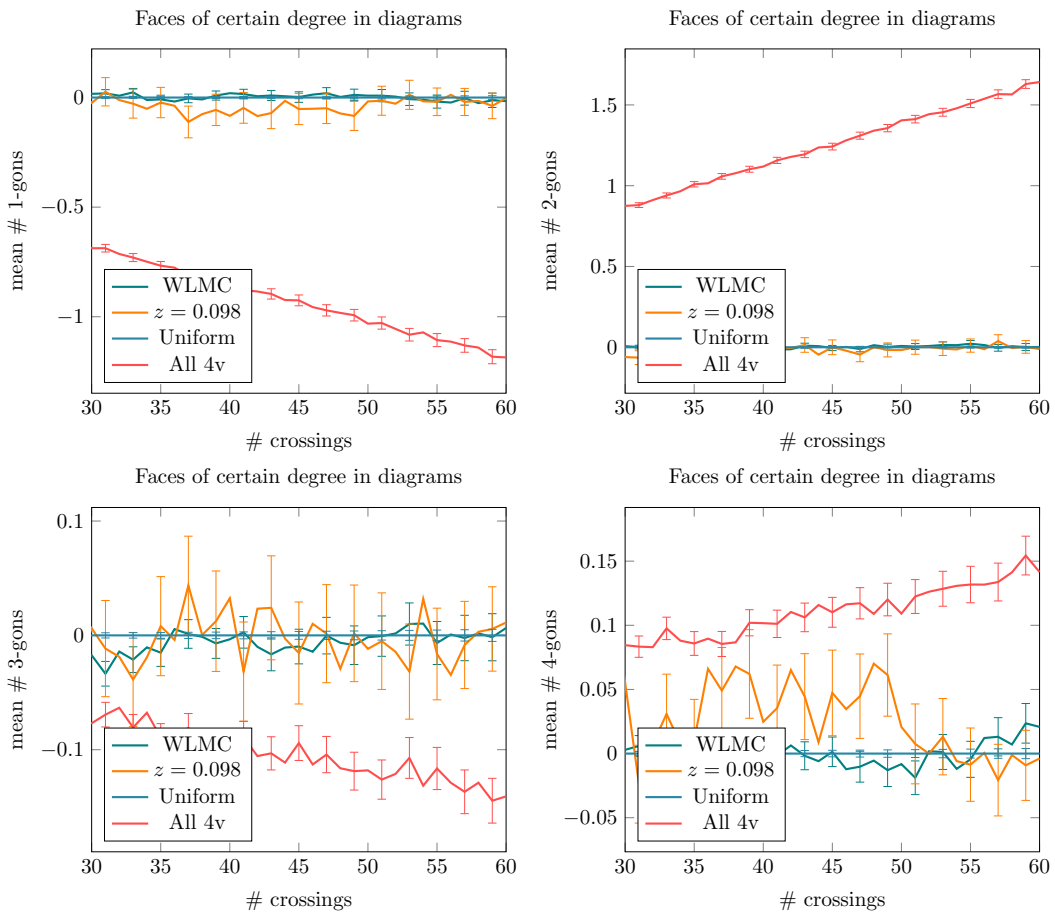

Figure 9.4: Difference from uniform data: Average counts of faces of degrees 1, 2, 3, 4.

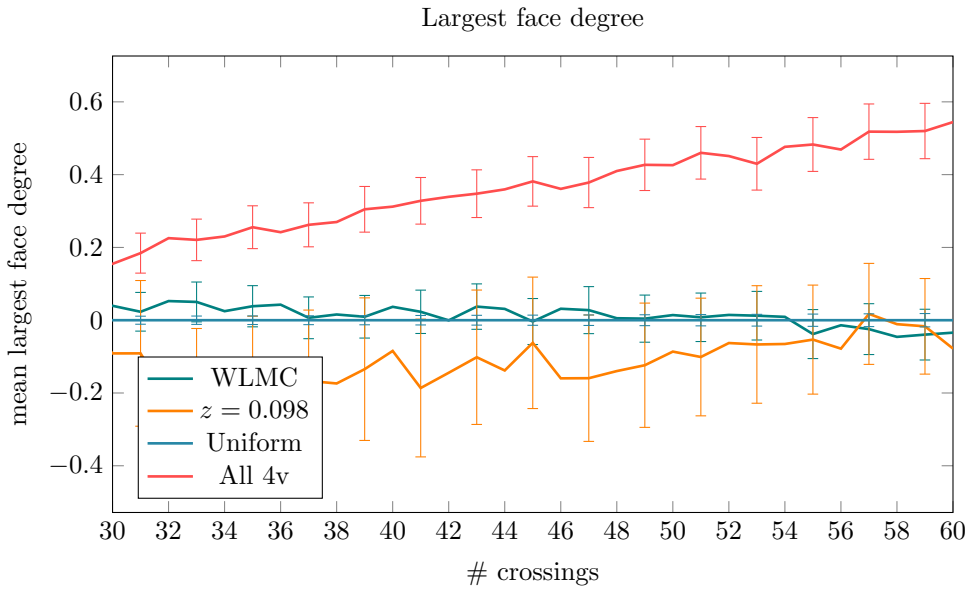

Figure 9.5: Difference from uniform data: Average size of largest face.

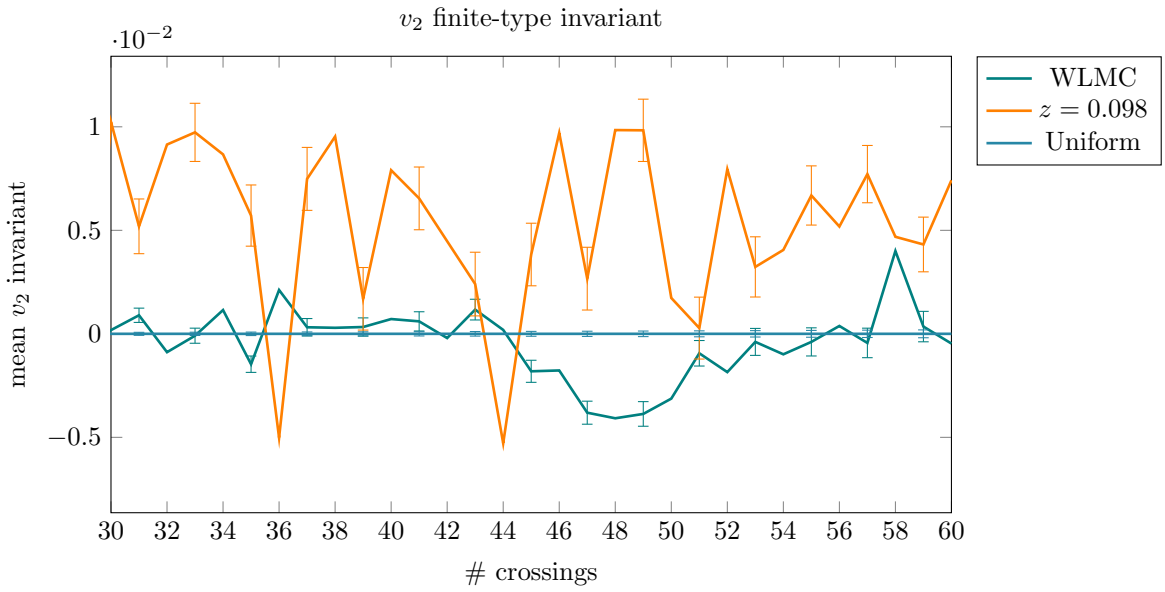

Figure 9.6: Difference from uniform data: Average $-\frac{1}{2}(2St + J^+)$. As this statistic is not well-defined for an arbitrary 4-valent map, that data is not present.

9.3.2 Wang-Landau implementation

It is possible to implement instead the Markov chain while making use of Wang and Landau's algorithm [109], which after a tuning phase, flattens the histogram of shadow sizes so as to lessen mixing time. As a consequence, the tuning phase provides approximate counts for the number of knot shadows by their sizes.

Rather than provide a parameter z, sampling via a Wang-Landau implementation requires a data structure (ℓ, L, g), where:

1. ℓ is the minimum size to permit shadows to be. To ensure ergodicity, we always have $\ell = 1$.

2. L is the maximum size to permit shadows to be.

3. $g = (g_i)_{i=\ell}^{L}$ is a vector of relative counting data in the following sense: If $G_n = e^{g_n}$, then $G_n/G_{n-1} \approx k_n/k_{n-1}$. As knot shadows k_n have no exact enumeration, this data is gathered via a tuning phase, described below.

Given the tuning data, define $tp(n, m) = g_n - g_m$, unless $m < \ell$ or $m > L$ in which case $tp(n, m) = 0$. Wang-Landau flattened MCMC sampling then works as follows. Let D_i be the input rooted knot shadow with n vertices and root arc a and perform one of the following six subprocedures with equal probability (*failure* means to set $D_{i+1} := D_i$):

1. Loop addition. Sample $0 \leq \alpha < 1$ and fail immediately if $\ln \alpha > tp(|D|, |D|+1)$. Return $D_{i+1} := \mathrm{RI}^{+}(D_i, a)$.

2. Loop deletion. Provided $f(a)$ is a loop, return $D_{i+1} := \mathrm{RI}^{-}(D_i, a)$.

3. Bigon addition. Sample $0 \leq \alpha < 1$ and fail immediately if $\ln \alpha > tp(|D|, |D| + 2)$. The arc a lies along a face of d edges; provided $d \neq 1$ (otherwise fail), uniformly sample the integer k between 1 and $d - 1$. The arc $a' = (C \circ E)^k(a)$ is a distinct arc along the same face as a. Then return $D_{i+1} := \mathrm{RII}^{+}(D_i, a, a')$.

4. Bigon deletion. Fail if the arc a does not lie along a bigon. The size d of the face which would be produced by bigon deletion is the sum $|f(E \circ C(a))| + |f(C^3 \circ E(a))| - 2 = d$. Sample $0 \leq \beta < 1$ uniformly and fail if $\beta > (d-1)^{-1}$. Otherwise, return $D_{i+1} := \mathrm{RII}^{-}(D_i, a)$.

5. Triangle flipping. Fail if the arc a does not lie along a nondegenerate triangle. Otherwise, return $D_{i+1} := \mathrm{RIII}(D_i, a)$.

6. Re-rooting. Given the rooted diagram D_i, forget the root and select a new root b for D_{i+1} from the $(\mathrm{aut}\, D_i)/(4|D|)$ choices.

Before sampling, we have to gather data for g via a tuning algorithm with parameters ℓ, the smallest size diagram to allow in the sample space (always in this article $\ell = 1$, as

otherwise it is not necessarily clear if the Markov chain is ergodic), L, the largest size diagram in the sample space, and ϵ, which describes the desired flatness of the sampling histogram, and Δ, a threshold for flatness of a histogram of occurrences (we set $\Delta = 0.05$).

A starting point D_0 in the sample space of diagrams is chosen; our algorithm starts with the figure-eight diagram. The vector g is initialized to 0. Finally, a scaling factor f is initialized; we start it at $f = 1$.

The algorithm then proceeds as follows.

1. If $f < \epsilon$, terminate.

2. A histogram $H = (H_n)_{n=\ell}^{L}$ of bins ℓ to L inclusive is initialized empty. This histogram will track the occurrences of diagrams of size n at each step of the Markov chain.

3. Step, via the Wang-Landau weighted algorithm described above, producing D_{i+1} from the current D_i. Increment $H_{|D_{i+1}|}$ by 1, and increment $g_{|D_{i+1}|}$ by f.

4. Check if the histogram is Δ-flat, *i.e.*, check if

$$\frac{\min H}{1-\Delta} > \frac{\sum_{i=\ell}^{L} H_i}{L-\ell} > \frac{\max H}{1+\Delta}.$$

   If so, let $f := f/2$ and proceed with step (1), otherwise repeat step (3).

After tuning to $\epsilon = 10^{-6}$, we obtained approximate counts for $n = 1$ to $n = 27$ and can compare the approximations to the precise counts from [113] in Table 9.1. Furthermore, we can compare concurrent ratios $e^{g_n - g_{n-1}} \approx k_n/k_{n-1}$ to experimental data of [95]. Namely, we compare our data to Schaeffer and Zinn-Justin's experimental estimation of $\mu \approx 11.4$ and conjectural value of $\gamma = -\frac{1+\sqrt{13}}{6}$ in Figure 9.7 by plotting the theoretical horizontal asymptote μ, as well as the curve $k_n/k_{n-1} \sim \mu(\frac{n}{n-1})^{\gamma-2}$.

Evidence suggests that data gathered using the Wang-Landau MCMC algorithm matches the proper uniform distribution. However, we have only presented data on the means of various statistics. We can compare and examine the distributions of our various statistics,

Table 9.1: Comparison of counts of rooted knot shadows from the Wang-Landau tuning step with $\varepsilon = 10^{-6}$, versus those gathered using a precise enumeration method [113].

n	Markov chain estimated k_n	Exact k_n
1	2.	2
2	8.01	8
3	42.55	42
4	261.8	260
5	1792.96	1796
6	13466.59	13396
7	106655.49	105706
8	875216.17	870772
9	7549328.53	7420836
10	66285927.69	65004584
11	587791105.84	582521748
12	5401476508.05	5320936416
13	50398345321.46	49402687392
14	470512414110.44	465189744448
15	4537054734491.55	4434492302426
16	43403803027731.8	42731740126228
17	425460054497142	415736458808868
18	4149163657635640	4079436831493480
19	41050203187910000	40338413922226212
20	402714061643008000	401652846850965808
21	4114866974623030000	4024556509468827432
22	40941798387842000000	40558226664529024000
23	415161875934869000000	410887438338905738908
24	4239414744208560000000	4182776248940752113344
25	42944527627509700000000	427701527115245695326l6
26	447510601388730000000000	439143340987014152920384
27	4594711410395330000000000	452617984210370896903929 6

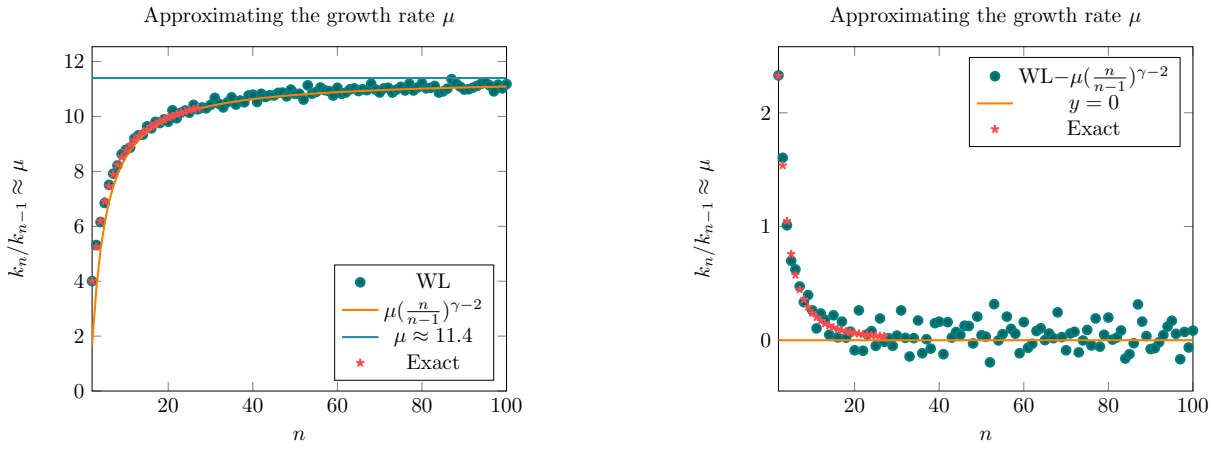

Figure 9.7: Plot of approximate size of $k_n/k_{n-1} \sim \mu(\frac{n}{n-1})^{\gamma-2} \to \mu$, obtained from Wang-Landau tuning data.

for different fixed diagram sizes. In Figures 9.8, 9.9, and 9.10, we compare distributions for $n = 30$ and $n = 60$ crossings.

9.4 Reidemeister Markov Chain and Similar Objects

Similar to how the Markov chain generated by BFCAF transitions can be used on other self-avoiding objects, we can consider running our algorithm on other objects similar to knot shadows.

For example, we can consider shadows of *pairs* of circles; the smallest such object is the unique 2-crossing 4-valent planar map of 2 link components. In this case, the Markov chain is still ergodic (the proof of Theorem 9.2 is not affected by the shadow having a different number of link components).

In fact, the proof of Theorem 9.2 follows no matter the (fixed) number of link diagrams of the space that the chain acts on. Hence this technique could be used to sample large shadows of any fixed number of link components.

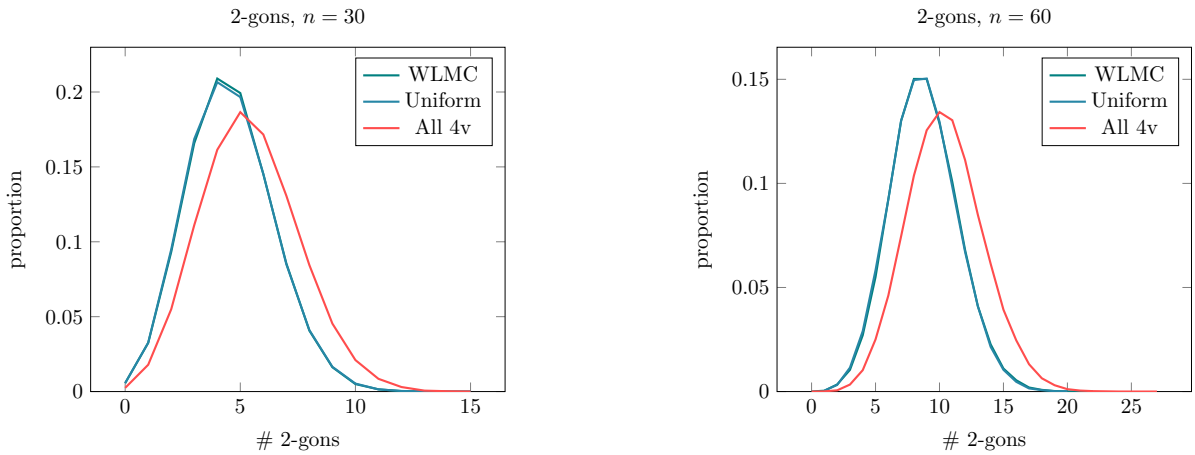

Figure 9.8: Distribution of 2-gon counts for $n = 30$ and $n = 60$ crossings.

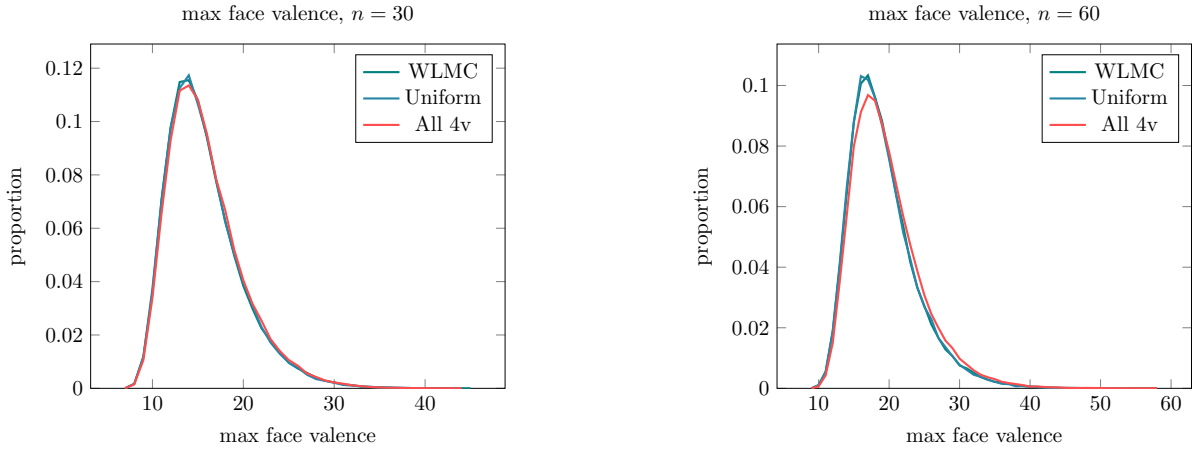

Figure 9.9: Distribution of max face valence for $n = 30$ and $n = 60$ crossings.

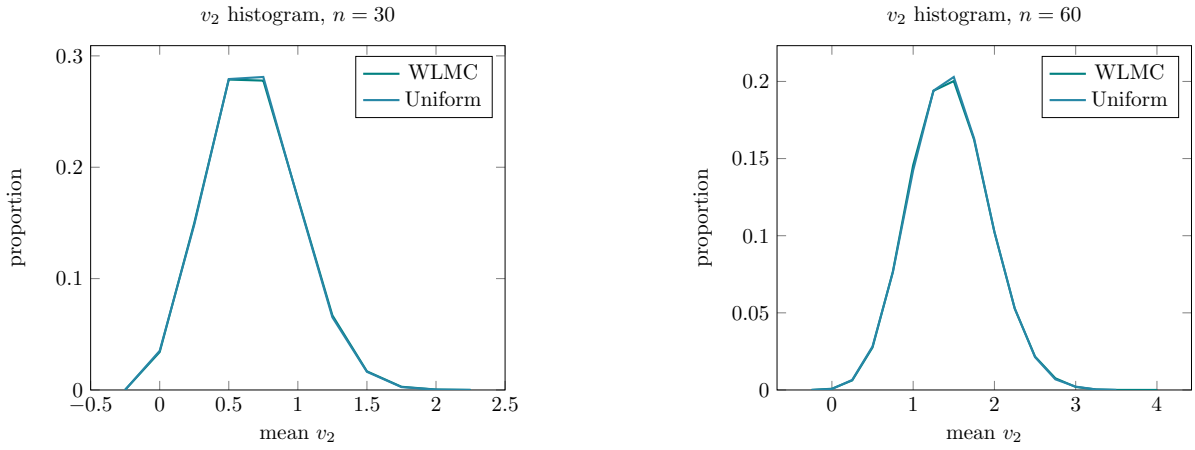

Figure 9.10: Distribution of mean v_2 invariant for $n = 30$ and $n = 60$ crossings.

The Markov transitions presented here are based on the Reidemeister moves on *knot diagrams*. It is thus natural to consider a Markov chain on knot diagrams generated by similar transitions corresponding to the proper Reidemeister moves, taking into account over-under signing of the diagram.

Indeed, we expect this Markov chain to be ergodic, and we expect transitions to be of similar computational complexity. However, we note that Proposition 9.3 fails in this case: It is known that there are diagrams who represent the same knot type, but whose transition paths all involve an increase in the number of crossings [60]. To make matters worse, unlike the spaces of knot shadows where the diameter has quadratic growth, the upper bound on the diameters of the spaces of knot diagrams is *exponential* [81].

Hence in the case of knot diagrams, care must be taken to ensure that there are satisfactory parameters for the Markov chain to converge to the uniform distribution in a reasonable amount of time. It should be noted however that it is even more difficult to sample knot diagrams of fixed knot type via uniform rejection sampling, as diagrams of any fixed knot type are asymptotically exponentially rare. Furthermore, the widespread success in the use of BFACF in sampling knotted polygons of fixed type yields hope for these methods.

Introduction of flat spatial graph Reidemeister moves described in Section 6.1—with appropriate transition probabilities—would lead to a Markov chain Monte Carlo sampler for spatial graph shadows for arbitrary fixed graphs G. Similarly, one could conceive of a sampler for spatial graph diagrams of fixed knot type.

Virtual knot shadows of arbitrary genus can be sampled directly, without the need for a Monte Carlo sampler, although one could examine if it is possible to develop such a Markov chain. One obstruction is that most virtual knot shadows are *nontrivial*—they cannot be reduced to the trivial diagram by a sequence of flat virtual Reidemeister moves [53, 55, 43]. It becomes even more complicated if we wished to create a sampler of shadows of fixed underlying genus. As not much is known about invariants of virtual knot shadows, these are interesting problems to consider.

Bibliography

[1] Colin C. Adams. *The Knot Book: An elementary introduction to the mathematical theory of knots*. American Mathematical Soc., 2004. ISBN: 978-0-8218-3678-1. URL: http://www.worldcat.org/oclc/265587824?referer=xid.

[2] Marie Albenque, Éric Fusy, and Dominique Poulalhon. "On Symmetric Quadrangulations and Triangulations". In: *Eur. J. Comb.* 35 (Jan. 2014), pp. 13–31. ISSN: 0195-6698. DOI: 10.1016/j.ejc.2013.06.031. URL: http://dx.doi.org/10.1016/j.ejc.2013.06.031.

[3] Marie Albenque and Dominique Poulalhon. "A Generic Method for Bijections between Blossoming Trees and Planar Maps". In: *The Electronic Journal of Combinatorics* 22.2 (2015), P2–38.

[4] J. W. Alexander. "Topological invariants of knots and links". In: *Transactions of the American Mathematical Society* 30.2 (Feb. 1928), pp. 275–275. ISSN: 0002-9947. DOI: 10.1090/s0002-9947-1928-1501429-1. URL: http://dx.doi.org/10.1090/s0002-9947-1928-1501429-1.

[5] Athanasios T Alexiou, Maria M Psiha, and Panayiotis M Vlamos. "Combinatorial permutation based algorithm for representation of closed RNA secondary structures". In: *Bioinformation* 7.1 (Sept. 2011), pp. 91–95. ISSN: 0973-2063. DOI: 10.6026/97320630007091. URL: http://dx.doi.org/10.6026/97320630007091.

[6] V. Arnold. "Topological Invariants of Plane Curves and Caustics". In: *University Lecture Series* (July 1994). ISSN: 1047-3998. DOI: 10.1090/ulect/005. URL: http://dx.doi.org/10.1090/ulect/005.

[7] Vladimir I Arnol'd. "The geometry of spherical curves and the algebra of quaternions". In: *Russian Mathematical Surveys* 50.1 (1995), p. 1. DOI: 10.1070/RM1995v050n01ABEH001662. URL: http://stacks.iop.org/0036-0279/50/i=1/a=R01.

[8] J. Arsuaga et al. "Knotting Probability of DNA Molecules Confined in Restricted Volumes: DNA Knotting in Phage Capsids". In: *Proceedings of the National Academy of Sciences* 99.8 (2002), pp. 5373–5377. DOI: 10.1073/pnas.032095099. URL: http://dx.doi.org/10.1073/pnas.032095099.

[9] Ted Ashton, Jason Cantarella, and Harrison Chapman. *plCurve: Fast polygon library.* Available at http://www.jasoncantarella.com/wordpress/software/plcurve/.

[10] Edward A Bender and E.Rodney Canfield. "The asymptotic number of rooted maps on a surface". In: *Journal of Combinatorial Theory, Series A* 43.2 (1986), pp. 244–257. ISSN: 0097-3165. DOI: 10.1016/0097-3165(86)90065-8. URL: http://www.sciencedirect.com/science/article/pii/0097316586900658.

[11] Edward A. Bender, Zhi-Cheng Gao, and L.Bruce Richmond. "Submaps of maps. I. General 0-1 laws". In: *Journal of Combinatorial Theory, Series B* 55.1 (1992), pp. 104–117. ISSN: 0095-8956. DOI: 10.1016/0095-8956(92)90034-U. URL: http://www.sciencedirect.com/science/article/pii/009589569290034U.

[12] Olivier Bernardi and Éric Fusy. "Bijections for planar maps with boundaries". In: (2015). arXiv: 1510.05194v2 [math.CO].

[13] Béla Bollobás and Oliver Riordan. "A Polynomial Invariant of Graphs On Orientable Surfaces". In: *Proceedings of the London Mathematical Society* 83.3 (Nov. 2001), pp. 513–531. ISSN: 0024-6115. DOI: 10.1112/plms/83.3.513. URL: http://dx.doi.org/10.1112/plms/83.3.513.

[14] Béla Bollobás and Oliver Riordan. "A polynomial of graphs on surfaces". In: *Mathematische Annalen* 323.1 (May 2002), pp. 81–96. ISSN: 0025-5831. DOI: 10.1007/s002080100297. URL: http://dx.doi.org/10.1007/s002080100297.

[15] J. Bouttier, P. Di Francesco, and E. Guitter. "Geodesic distance in planar graphs". In: *Nuclear Physics B* 663 (July 2003), pp. 535–567. DOI: 10.1016/S0550-3213(03)00355-9. eprint: cond-mat/0303272.

[16] E. Brézin et al. "Planar diagrams". In: *Communications in Mathematical Physics* 59.1 (1978), pp. 35–51. ISSN: 1432-0916. DOI: 10.1007/BF01614153. URL: http://dx.doi.org/10.1007/BF01614153.

[17] G. Brinkmann and B.D. McKay. "Fast generation of some classes of planar graphs". In: *Electronic Notes in Discrete Mathematics* 3 (May 1999), pp. 28–31. ISSN: 1571-0653. DOI: 10.1016/s1571-0653(05)80016-2. URL: http://dx.doi.org/10.1016/s1571-0653(05)80016-2.

[18] Gregory R Buck and E Lynn Zechiedrich. "DNA Disentangling By Type-2 Topoisomerases". In: *Journal of Molecular Biology* 340.5 (2004), pp. 933–939. DOI: 10.1016/j.jmb.2004.05.034. URL: http://dx.doi.org/10.1016/j.jmb.2004.05.034.

[19] Grant Cairns and Daniel M. Elton. "The Planarity Problem for Signed Gauss Words". In: *Journal of Knot Theory and Its Ramifications* 02.04 (Dec. 1993), pp. 359–367. ISSN: 1793-6527. DOI: 10.1142/s0218216593000209. URL: http://dx.doi.org/10.1142/s0218216593000209.

[20] Jason Cantarella, Harrison Chapman, and Matt Mastin. "Knot probabilities in random diagrams". In: *Journal of Physics A: Mathematical and Theoretical* 49.40 (2016), p. 405001. DOI: 10.1088/1751-8113/49/40/405001. URL: http://stacks.iop.org/1751-8121/49/i=40/a=405001.

[21] Jason Cantarella, Tetsuo Deguchi, and Clayton Shonkwiler. "Probability Theory of Random Polygons from the Quaternionic Viewpoint". In: *Communications on Pure*

and Applied Mathematics 67.10 (Aug. 2013), pp. 1658–1699. DOI: 10.1002/cpa.21480. URL: http://dx.doi.org/10.1002/cpa.21480.

[22] Jason Cantarella et al. "The expected total curvature of random polygons". In: *American Journal of Mathematics* 137.2 (2015), pp. 411–438. DOI: 10.1353/ajm.2015.0015. URL: http://dx.doi.org/10.1353/ajm.2015.0015.

[23] A.L. Cauchy, Imprimerie royale, and Debure freres. *Cours d'analyse de l'Ecole royale polytechnique; par m. Augustin-Louis Cauchy ... 1.re partie. Analyse algébrique.* de l'Imprimerie royale, 1821. URL: https://books.google.com/books?id=UrT0KsbDmDwC.

[24] Harrison Chapman. "Asymptotic laws for random knot diagrams". In: *Journal of Physics A: Mathematical and Theoretical* (2017). DOI: 10.1088/1751-8121/aa6e45. arXiv: 1608.02638 [math.GT]. URL: https://doi.org/10.1088/1751-8121/aa6e45.

[25] Guillaume Chapuy, Michel Marcus, and Gilles Schaeffer. "A Bijection for Rooted Maps on Orientable Surfaces". In: *SIAM J. Discrete Math.* 23.3 (2009), pp. 1587–1611. DOI: 10.1137/080720097. URL: http://dx.doi.org/10.1137/080720097.

[26] Sergei Chmutov and Boris Pittel. "The genus of a random chord diagram is asymptotically normal". In: *Journal of Combinatorial Theory, Series A* 120.1 (2013), pp. 102–110. ISSN: 0097-3165. DOI: http://dx.doi.org/10.1016/j.jcta.2012.07.004. URL: http://www.sciencedirect.com/science/article/pii/S0097316512001288.

[27] Moshe Cohen and Sunder Ram Krishnan. "Random knots using Chebyshev billiard table diagrams". In: *Topology and its Applications* 194 (2015), pp. 4–21. ISSN: 0166-8641. DOI: 10.1016/j.topol.2015.07.018. URL: http://www.sciencedirect.com/science/article/pii/S0166864115003119.

[28] Robert Coquereaux and Jean-Bernard Zuber. "Maps, Immersions and Permutations". In: *J. Knot Theory Ramifications* 25.08 (2016), p. 1650047. DOI: 10.1142/s0218216516500474. URL: http://dx.doi.org/10.1142/S0218216516500474.

[29] Henry Crapo and Pierre Rosenstiehl. "On lacets and their manifolds". In: *Discrete Mathematics* 233.1-3 (Apr. 2001), pp. 299–320. ISSN: 0012-365X. DOI: 10.1016/s0012-365x(00)00248-x. URL: http://dx.doi.org/10.1016/S0012-365X(00)00248-X.

[30] Marc Culler and Nathan M. Dunfield. *PLink, a computer program for viewing and editing piecewise linear link projections*. Available at http://www.math.uic.edu/t3m/plink/doc/ (31/05/2016).

[31] Isabel Darcy and DeWitt Sumners. "Applications of topology to DNA". eng. In: *Banach Center Publications* 42.1 (1998), pp. 65–75. URL: http://eudml.org/doc/208826.

[32] Isabel Darcy and DW Sumners. "A strand passage metric for topoisomerase action". In: *Knots*. Vol. 96. 1997, pp. 267–278.

[33] A Das et al. "Unfolded protein ensembles, folding trajectories, and refolding rate prediction". In: *The Journal of chemical physics* 139.12 (2013), p. 121925. DOI: 10.1063/1.4817215.

[34] Max Delbrück. "Knotting Problems in Biology". In: *Mathematical Problems in the Biological Sciences*. Ed. by R. Bellman. American Mathematical Society, 1962. Chap. 5, pp. 55–63. DOI: 10.1090/psapm/014. URL: http://dx.doi.org/10.1090/psapm/014.

[35] P. Di Francesco, E. Guitter, and J.L. Jacobsen. "Exact meander asymptotics: a numerical check". In: *Nuclear Physics B* 580.3 (Aug. 2000), pp. 757–795. ISSN: 0550-3213. DOI: 10.1016/s0550-3213(00)00273-x. URL: http://dx.doi.org/10.1016/s0550-3213(00)00273-x.

[36] Yuanan Diao. "The Knotting of Equilateral Polygons in $\mathbb{R}^3$". In: *Journal of Knot Theory and Its Ramifications* 04.02 (1995), pp. 189–196. DOI: 10.1142/S0218216595000090. eprint: http://www.worldscientific.com/doi/pdf/10.

1142/S0218216595000090. URL: http://www.worldscientific.com/doi/abs/10.1142/S0218216595000090.

[37] Yuanan Diao, Claus Ernst, and Uta Ziegler. "Generating Large Random Knot Projections". In: *Physical and Numerical Models in Knot Theory*. World Scientific, 2012. Chap. 23, pp. 473–494. DOI: 10.1142/9789812703460_0023. URL: http://www.worldscientific.com/doi/abs/10.1142/9789812703460_0023.

[38] C.H. Dowker and Morwen B. Thistlethwaite. "Classification of knot projections". In: *Topology and its Applications* 16.1 (July 1983), pp. 19–31. ISSN: 0166-8641. DOI: 10.1016/0166-8641(83)90004-4. URL: http://dx.doi.org/10.1016/0166-8641(83)90004-4.

[39] Nathan Dunfield et al. *Random Knots: A preliminary report*. 2014. URL: http://www.math.uiuc.edu/~nmd/preprints/slides/random_knots.pdf.

[40] Bertrand Duplantier and Scott Sheffield. "Liouville quantum gravity and KPZ". In: *Inventiones mathematicae* 185.2 (Dec. 2010), pp. 333–393. ISSN: 1432-1297. DOI: 10.1007/s00222-010-0308-1. URL: http://dx.doi.org/10.1007/s00222-010-0308-1.

[41] Chaim Even-Zohar et al. "Invariants of Random Knots and Links". In: *Discrete & Computational Geometry* 56.2 (2016), pp. 274–314. DOI: 10.1007/s00454-016-9798-y. URL: http://dx.doi.org/10.1007/s00454-016-9798-y.

[42] Bruce Ewing and Kenneth C. Millett. "Computational algorithms and the complexity of link polynomials". In: *Progress in knot theory and related topics*. Vol. 56. Travaux en Cours. Hermann, Paris, 1997, pp. 51–68.

[43] Roger Fenn, Louis H. Kauffman, and Vassily O. Manturov. "Virtual Knot Theory–unsolved Problems". In: *Fundamenta Mathematicae* 188.nil (2005), pp. 293–323. DOI: 10.4064/fm188-0-13. URL: http://dx.doi.org/10.4064/fm188-0-13.

[44] Philippe Flajolet and Robert Sedgewick. *Analytic combinatorics*. cambridge University press, 2009.

[45] V. V. Fock and A. A. Rosly. "Moduli Space of Flat Connections as a Poisson Manifold". In: *International Journal of Modern Physics B* 11.26n27 (Oct. 1997), pp. 3195–3206. ISSN: 1793-6578. DOI: 10.1142/s0217979297001544. URL: http://dx.doi.org/10.1142/s0217979297001544.

[46] P. Di Francesco, O. Golinelli, and E. Guitter. "Meander, Folding, and Arch Statistics". In: *Mathematical and Computer Modelling* 26.8-10 (1997), pp. 97–147. DOI: 10.1016/s0895-7177(97)00202-1. URL: http://dx.doi.org/10.1016/S0895-7177(97)00202-1.

[47] P. Di Francesco, O. Golinelli, and E. Guitter. "Meanders: exact asymptotics". In: *Nuclear Physics B* 570.3 (2000), pp. 699–712. ISSN: 0550-3213. DOI: 10.1016/S0550-3213(99)00753-1. URL: http://www.sciencedirect.com/science/article/pii/S0550321399007531.

[48] P. Freyd et al. "A New Polynomial Invariant of Knots and Links". In: *Bull. Amer. Math. Soc.* 12.2 (1985), pp. 239–247. DOI: 10.1090/s0273-0979-1985-15361-3. URL: http://dx.doi.org/10.1090/S0273-0979-1985-15361-3.

[49] H. L. Frisch and E. Wasserman. "Chemical Topology 1". In: *J. Am. Chem. Soc.* 83.18 (Sept. 1961), pp. 3789–3795. DOI: 10.1021/ja01479a015. URL: http://dx.doi.org/10.1021/ja01479a015.

[50] J Hadamard. "Sur le rayon de convergence des séries ordonnées suivant les puissances d'une variable". In: *CR Acad. Sci. Paris* 106 (1888), pp. 259–262.

[51] J. M. Hammersley. "The number of polygons on a lattice". In: *Proceedings of the Cambridge Philosophical Society* 57 (1961), p. 516. DOI: 10.1017/S030500410003557X.

[52] Christine E Heitsch and Prasad Tetali. "Meander Graphs". In: *DMTCS Proceedings* 01 (2011), pp. 469–480.

[53] Allison Henrich and Sam Nelson. “Semiquandles and flat virtual knots”. In: *Pacific journal of mathematics* 248.1 (2010), pp. 155–170. DOI: 10.2140/pjm.2010.248.155.

[54] Jim Hoste, Morwen Thistlethwaite, and Jeff Weeks. “The First 1,701,936 Knots”. In: *The Mathematical Intelligencer* 20.4 (1998), pp. 33–48. DOI: 10.1007/bf03025227. URL: http://dx.doi.org/10.1007/BF03025227.

[55] David Hrencecin and Louis H. Kauffman. “On filamentations and virtual knots”. In: *Topology and its Applications* 134.1 (Oct. 2003), pp. 23–52. ISSN: 0166-8641. DOI: 10.1016/s0166-8641(03)00100-7. URL: http://dx.doi.org/10.1016/s0166-8641(03)00100-7.

[56] J. Jacobsen and P. Zinn-Justin. “A transfer matrix approach to the enumeration of knots”. In: *J. Knot Theory Ramifications* 11.5 (2002), pp. 739–758. ISSN: 0218-2165.

[57] Michal Jamroz et al. “KnotProt: a database of proteins with knots and slipknots”. In: *Nucleic Acids Research* 43.D1 (2015), pp. D306–D314. DOI: 10.1093/nar/gku1059. eprint: http://nar.oxfordjournals.org/content/43/D1/D306.full.pdf+html. URL: http://nar.oxfordjournals.org/content/43/D1/D306.abstract.

[58] Eric Jones, Travis Oliphant, Pearu Peterson, et al. *SciPy: Open source scientific tools for Python*. [Online; accessed 2017-02-11]. 2001–. URL: http://www.scipy.org/.

[59] Douglas Jungreis. “Gaussian Random Polygons Are Globally Knotted”. In: *Journal Of Knot Theory And Its Ramifications* 03.04 (1994), pp. 455–464. DOI: 10.1142/S0218216594000332. eprint: http://www.worldscientific.com/doi/pdf/10.1142/S0218216594000332. URL: http://www.worldscientific.com/doi/abs/10.1142/S0218216594000332.

[60] L. H. Kauffman and V. O. Manturov. “Virtual knots and links”. In: *Proceedings of the Steklov Institute of Mathematics* 252.1 (Jan. 2006), pp. 104–121. ISSN: 1531-8605. DOI: 10.1134/s0081543806010111. URL: http://dx.doi.org/10.1134/s0081543806010111.

[61] Louis H. Kauffman. *Knots and physics*. World Scientific, 2001. ISBN: 978-981-02-4111-7. URL: http://www.worldcat.org/oclc/225961005?referer=xid.

[62] Louis H. Kauffman. "State Models and the Jones Polynomial". In: *Topology* 26.3 (1987), pp. 395–407. DOI: 10.1016/0040-9383(87)90009-7. URL: http://dx.doi.org/10.1016/0040-9383(87)90009-7.

[63] Louis H. Kauffman. "Virtual Knot Theory". In: *European Journal of Combinatorics* 20.7 (1999), pp. 663–691. ISSN: 0195-6698. DOI: 10.1006/eujc.1999.0314. URL: http://www.sciencedirect.com/science/article/pii/S0195669899903141.

[64] Harry Kesten. "On the Number of Self-Avoiding Walks". In: *J. Math. Phys.* 4.7 (1963), p. 960. DOI: 10.1063/1.1704022. URL: http://dx.doi.org/10.1063/1.1704022.

[65] Harry Kesten. "On the Number of Self-Avoiding Walks. II". In: *J. Math. Phys.* 5.8 (1964), p. 1128. DOI: 10.1063/1.1704216. URL: http://dx.doi.org/10.1063/1.1704216.

[66] V.G. Knizhnik, A.M. Polyakov, and A.B. Zamolodchikov. "Fractal Structure of 2d-Quantum Gravity". In: *Modern Physics Letters A* 03.08 (1988), pp. 819–826. DOI: 10.1142/s0217732388000982. URL: http://dx.doi.org/10.1142/S0217732388000982.

[67] L.D. Landau, E.M. Lifshitz ; translated from the Russian by J.B. Sykes, and M.J. Kearsley. *Statistical physics.* Butterworth-Heinemann, 1991. ISBN: 978-0-7506-3372-7. URL: http://www.worldcat.org/oclc/230013014?referer=xid.

[68] S.K. Lando et al. *Graphs on Surfaces and Their Applications*. Encyclopaedia of Mathematical Sciences. Springer Berlin Heidelberg, 2003. ISBN: 9783540002031. URL: https://books.google.com/books?id=DMJKJdBLviwC.

[69] Nathan Linial and Tahl Nowik. "The Expected Genus of a Random Chord Diagram". In: *Discrete & Computational Geometry* 45.1 (2010), pp. 161–180. DOI: 10.1007/s00454-010-9276-x. URL: http://dx.doi.org/10.1007/s00454-010-9276-x.

[70] Rhonald C. Lua and Alexander Y. Grosberg. "Statistics of Knots, Geometry of Conformations, and Evolution of Proteins". In: *PLoS Comput Biol* 2.5 (2006), e45. DOI: 10.1371/journal.pcbi.0020045. URL: http://dx.doi.org/10.1371/journal.pcbi.0020045.

[71] N. Madras and G. Slade. *The Self-Avoiding Walk*. Probability and Its Applications. Birkhäuser Boston, 2013. ISBN: 9781461241324. URL: https://books.google.com/books?id=JsoFCAAAQBAJ.

[72] Christopher Manon. "Compactifications of character varieties and skein relations on conformal blocks". In: *Geometriae Dedicata* 179.1 (June 2015), pp. 335–376. ISSN: 1572-9168. DOI: 10.1007/s10711-015-0084-6. URL: http://dx.doi.org/10.1007/s10711-015-0084-6.

[73] V. O. Manturov. "Compact and long virtual knots". In: *Transactions of the Moscow Mathematical Society* 69 (2008), pp. 1–26. ISSN: 1547-738X. DOI: 10.1090/s0077-1554-08-00168-4. URL: http://dx.doi.org/10.1090/s0077-1554-08-00168-4.

[74] R. James Milgram and R. C. Penner. "Riemann's moduli space and the symmetric groups". In: *Contemporary Mathematics* (1993), pp. 247–290. ISSN: 0271-4132. DOI: 10.1090/conm/150/01294. URL: http://dx.doi.org/10.1090/conm/150/01294.

[75] Kenneth C. Millett. "Knots in knots: A study of classical knot diagrams". In: *Journal of Knot Theory and Its Ramifications* 25.09 (Aug. 2016), p. 1641013. ISSN: 1793-6527. DOI: 10.1142/s0218216516410133. URL: http://dx.doi.org/10.1142/s0218216516410133.

[76] Kenneth C. Millett. "Knots, Slipknots, and Ephemeral Knots In Random Walks and Equilateral Polygons". In: *Journal of Knot Theory and Its Ramifications* 19.05 (2010), pp. 601–615. DOI: 10.1142/S0218216510008078. eprint: http://www.worldscientific.com/doi/pdf/10.1142/S0218216510008078. URL: http://www.worldscientific.com/doi/abs/10.1142/S0218216510008078.

[77] Kenneth C Millett. "Physical knot theory: an introduction to the study of the influence of knotting on the spatial characteristics of polymers". In: *Introductory Lectures on Knot Theory: Selected Lectures Presented at the Advanced School and Conference on Knot Theory and Its Applications to Physics and Biology, ICTP, Trieste, Italy, 11-29 May 2009*. Vol. 46. World Scientific. 2012, p. 346.

[78] Kenneth Millett, Akos Dobay, and Andrzej Stasiak. "Linear Random Knots and Their Scaling Behavior". In: *Macromolecules* 38.2 (2005), pp. 601–606. DOI: 10.1021/ma048779a. eprint: http://dx.doi.org/10.1021/ma048779a. URL: http://dx.doi.org/10.1021/ma048779a.

[79] Ali R. Mohazab and Steven S. Plotkin. "Polymer Uncrossing and Knotting in Protein Folding, and Their Role in Minimal Folding Pathways". In: *PLoS ONE* 8.1 (2013), e53642. DOI: 10.1371/journal.pone.0053642. URL: http://dx.doi.org/10.1371/journal.pone.0053642.

[80] S K Nechaev, A Yu Grosberg, and A M Vershik. "Random walks on braid groups: Brownian bridges, complexity and statistics". In: *Journal of Physics A: Mathematical and General* 29.10 (1996), pp. 2411–2433. DOI: 10.1088/0305-4470/29/10/020.

[81] Tahl Nowik. "Complexity of plane and spherical curves". In: *Duke Math. J.* 148.1 (May 2009), pp. 107–118. DOI: 10.1215/00127094-2009-022. URL: http://dx.doi.org/10.1215/00127094-2009-022.

[82] Malik Obeidin. "Volumes of Random Alternating Link Diagrams". In: (2016). arXiv: 1611.04944 [math.GT]. URL: http://arxiv.org/abs/1611.04944v2.

[83] Kenneth A. Perko. "On the Classification of Knots". In: *Proceedings of the American Mathematical Society* 45.2 (1974), pp. 262–262. DOI: 10.1090/s0002-9939-1974-0353294-x. URL: http://dx.doi.org/10.1090/S0002-9939-1974-0353294-X.

[84] Nicholas Pippenger. "Knots in Random Walks". In: *Discrete Applied Mathematics* 25.3 (1989), pp. 273–278. DOI: 10.1016/0166-218x(89)90005-x. URL: http://dx.doi.org/10.1016/0166-218X(89)90005-X.

[85] Eric J. Rawdon, Kenneth C. Millett, and Andrzej Stasiak. "Subknots in ideal knots, random knots, and knotted proteins". In: *Sci Rep* 5 (Mar. 2015). 25753957[pmid], p. 8928. ISSN: 2045-2322. DOI: 10.1038/srep08928. URL: http://www.ncbi.nlm.nih.gov/pmc/articles/PMC4354144/.

[86] K. Reidemeister. *Knotentheorie*. Ergebnisse der Mathematik und Ihrer Grenzgebiete. Chelsea Pub. Co., 1948. URL: https://books.google.com/books?id=W8s-AAAAIAAJ.

[87] E. J. Janse van Rensburg. *The statistical mechanics of interacting walks, polygons, animals and vesicles*. Vol. 18. Oxford Lecture Series in Mathematics and its Applications. Oxford University Press, Oxford, 2000, pp. x+379. ISBN: 0-19-850561-2.

[88] E J Janse van Rensburg and A Rechnitzer. "On the universality of knot probability ratios". In: *Journal of Physics A: Mathematical and Theoretical* 44.16 (2011), p. 162002. URL: http://stacks.iop.org/1751-8121/44/i=16/a=162002.

[89] L.B. Richmond and N.C. Wormald. "Almost All Maps Are Asymmetric". In: *Journal of Combinatorial Theory, Series B* 63.1 (1995), pp. 1–7. ISSN: 0095-8956. DOI: 10.1006/jctb.1995.1001. URL: http://www.sciencedirect.com/science/article/pii/S0095895685710015.

[90] Dale Rolfsen. *Knots and links*. Vol. 346. American Mathematical Soc., 1976.

[91] Pierre Rosenstiehl and Robert E Tarjan. "Gauss codes, planar hamiltonian graphs, and stack-sortable permutations". In: *Journal of Algorithms* 5.3 (Sept. 1984), pp. 375–390. ISSN: 0196-6774. DOI: 10.1016/0196-6774(84)90018-x. URL: http://dx.doi.org/10.1016/0196-6774(84)90018-x.

[92] V V Rybenkov, N R Cozzarelli, and A V Vologodskii. "Probability of DNA knotting and the effective diameter of the DNA double helix". In: *Proceedings of the National Academy of Sciences* 90.11 (1993), pp. 5307–5311. eprint: http://www.pnas.org/content/90/11/5307.full.pdf. URL: http://www.pnas.org/content/90/11/5307.abstract.

[93] Gilles Schaeffer. "Bijective census and random generation of Eulerian planar maps with prescribed vertex degrees." eng. In: *The Electronic Journal of Combinatorics* 4.1 (1997), Research paper R20, Research paper R20, 14 p. URL: http://eudml.org/doc/119255.

[94] Gilles Schaeffer. "Random Sampling of Large Planar Maps and Convex Polyhedra". In: *Proceedings of the Thirty-first Annual ACM Symposium on Theory of Computing*. STOC '99. Atlanta, Georgia, USA: ACM, 1999, pp. 760–769. ISBN: 1-58113-067-8. DOI: 10.1145/301250.301448. URL: http://doi.acm.org/10.1145/301250.301448.

[95] Gilles Schaeffer and Paul Zinn-Justin. "On the asymptotic number of plane curves and alternating knots". In: *Experiment. Math.* 13.4 (2004), pp. 483–493. ISSN: 1058-6458.

[96] C. Soteros et al. "Signed Unknotting Number and Knot Chirality Discrimination via Strand Passage". In: *Progress of Theoretical Physics Supplement* 191 (Jan. 1, 2011), pp. 78–95. DOI: 10.1143/PTPS.191.78. URL: http://ptps.oxfordjournals.org/content/191/78.abstract. published.

[97] Richard P. Stanley. *Enumerative Combinatorics*. Springer Nature, 1986. ISBN: http://id.crossref.org/isbn/978-1-4615-9763-6. DOI: 10.1007/978-1-4615-9763-6. URL: http://dx.doi.org/10.1007/978-1-4615-9763-6.

[98] Joanna I. Sulkowska et al. "Conservation of complex knotting and slipknotting patterns in proteins". In: *Proceedings of the National Academy of Sciences* 109.26 (2012), E1715–E1723. DOI: 10.1073/pnas.1205918109. eprint: http://www.pnas.org/content/109/26/E1715.full.pdf. URL: http://www.pnas.org/content/109/26/E1715.abstract.

[99] De Witt Sumners and Stuart G. Whittington. "Knots in self-avoiding walks". In: *J. Phys. A: Math. Gen.* 21.7 (Apr. 1988), pp. 1689–1694. DOI: 10.1088/0305-4470/21/7/030. URL: http://dx.doi.org/10.1088/0305-4470/21/7/030.

[100] Morwen B. Thistlethwaite. "Knot tabulations and related topics". In: *Aspects of topology*. Aspects of topology. Cambridge University Press (CUP), nil, pp. 1–76. DOI: 10.1017/cbo9781107359925.003. URL: http://dx.doi.org/10.1017/CBO9781107359925.003.

[101] Sonia Trigueros et al. "Novel display of knotted DNA molecules by two-dimensional gel electrophoresis". In: *Nucleic acids research* 29.13 (2001), e67–e67.

[102] Kyoichi Tsurusaki and Tetsuo Deguchi. "Fractions of Particular Knots in Gaussian Random Polygons". In: *Journal of the Physical Society of Japan* 64.5 (1995), pp. 1506–1518. DOI: 10.1143/jpsj.64.1506. URL: http://dx.doi.org/10.1143/JPSJ.64.1506.

[103] Vladimir Turaev. "Curves on Surfaces, Charts, and Words". In: *Geometriae Dedicata* 116.1 (Nov. 2005), pp. 203–236. ISSN: 1572-9168. DOI: 10.1007/s10711-005-9013-4. URL: http://dx.doi.org/10.1007/s10711-005-9013-4.

[104] Vladimir Turaev. "Knotoids". In: *Osaka J. Math.* 49.1 (2012), pp. 195–223. ISSN: 0030-6126. URL: http://projecteuclid.org/euclid.ojm/1332337244.

[105] W. T. Tutte. "A census of planar maps". In: *Canad. J. Math.* 15 (1963), pp. 249–271. ISSN: 0008-414X.

[106] R. E. Tuzun and A. S. Sikora. "Verification Of The Jones Unknot Conjecture Up To 22 Crossings". In: *ArXiv e-prints* (June 2016). arXiv: 1606.06671 [math.GT].

[107] Guy Valette. "A Classification of Spherical Curves Based on Gauss Diagrams". In: *Arnold Mathematical Journal* (2016), pp. 1–23. ISSN: 2199-6806. DOI: 10.1007/s40598-016-0049-3. URL: http://dx.doi.org/10.1007/s40598-016-0049-3.

[108] Martinus Veltman. "Diagrammatica". In: (1994). DOI: 10.1017/cbo9780511564079. URL: http://dx.doi.org/10.1017/cbo9780511564079.

[109] Fugao Wang and D. P. Landau. "Efficient, Multiple-Range Random Walk Algorithm To Calculate the Density of States". In: *Phys. Rev. Lett.* 86.10 (2001), pp. 2050–2053. DOI: 10.1103/physrevlett.86.2050. URL: http://dx.doi.org/10.1103/PhysRevLett.86.2050.

[110] J B Wilker and S G Whittington. "Extension of a theorem on super-multiplicative functions". In: *Journal of Physics A: Mathematical and General* 12.10 (1979), p. L245. URL: http://stacks.iop.org/0305-4470/12/i=10/a=001.

[111] D. Zagier and J. Harer. "The Euler characteristic of the moduli space of curves." In: *Inventiones mathematicae* 85 (1986), pp. 457–486. URL: http://eudml.org/doc/143377.

[112] P. Zinn-Justin. "The General O(n) Quartic Matrix Model and Its Application to Counting Tangles and Links". In: *Communications in Mathematical Physics* 238.1 (July 2003), pp. 287–304. ISSN: 1432-0916. DOI: 10.1007/s00220-003-0846-0. URL: http://dx.doi.org/10.1007/s00220-003-0846-0.

[113] P. Zinn-Justin and J.-B. Zuber. "Knot theory and matrix integrals". In: *Random Matrix Theory*. Eds Akemann, Baik and Di Francesco. 2009.

[114] P. Zinn-Justin and J.-B. Zuber. "Matrix integrals and the counting of tangles and links". In: *Discrete Mathematics* 246.1-3 (Mar. 2002), pp. 343–360. ISSN: 0012-365X. DOI: 10.1016/s0012-365x(01)00267-9. URL: http://dx.doi.org/10.1016/s0012-365x(01)00267-9.

[115] Paul Zinn-Justin and Jean-Bernard Zuber. "Matrix Integrals And The Generation And Counting Of Virtual Tangles And Links". In: *J. Knot Theory Ramifications* 13.03 (2004), pp. 325–355. DOI: 10.1142/s0218216504003172. URL: http://dx.doi.org/10.1142/S0218216504003172.